# UNIVERSITY OF SALERNO

**Faculty of Mathematical, Physical and Natural Sciences**




## Physics Department


# Investigation of the groundwater-river interaction, using Radon-222 as a natural tracer, in a karst Mediterranean environment like in the case study of the Bussento river basin


Thesis by

**DAVIDE GUADAGNUOLO**


in partial Fulfillment of the Requirements
for the Degree of

PhilosophiæDoctor in Physics

*Thesis advisor:* Prof. Michele Guida

*Doctorate Coordinator:* Prof. Mario Salerno

**VIII ciclo II serie** (2006-2009)

# Contents

**Introduction** **1**

**1 Radon: Overview of Properties, Origin and Transport** **3**
1.1 Physical and chemical properties of Radon . . . . . 4
1.1.1 Radioactive decay chains . . . . . 5
1.1.2 The importance of prompt daughters . . . . . 10
1.1.3 Ranges of alpha particles and recoil nuclei . . . . . 10
1.1.4 Distribution of Radon between phases . . . . . 12
1.1.5 Diffusion . . . . . 13
1.1.6 Permeation . . . . . 13
1.2 Sources of Radon . . . . . 14
1.3 Release mechanisms . . . . . 15
1.4 Radon transport . . . . . 15
1.5 Radon daughters in air . . . . . 17
1.6 Radon indoor . . . . . 20
1.7 Health effects . . . . . 21

**2 Radon Occurrence and Geology** **26**
2.1 Radon in rocks and soils . . . . . 26
2.2 Formation and emanation of radon . . . . . 29
2.3 Radon concentration, emanation and water content . . . . . 33
2.4 Transport of radon through soil . . . . . 35

**3 Radon and Groundwater** **37**
3.1 The groundwater resource . . . . . 38
3.2 Groundwater movement . . . . . 38
3.3 The behavior of U- and Th-series nuclides in groundwater . . 39
3.4 Behavior of Radium in groundwater . . . . . 40
3.5 Radon as aqueous tracer . . . . . 41
3.6 Modeling aquatic pathways . . . . . 43
3.7 Groundwater mixing in karts systems . . . . . 44
3.8 Radon and Submarine Groundwater Discharges . . . . . 47
3.9 Radon in the mineral springs . . . . . 47

**4 The study area of the Bussento river basin** **50**
4.1 The karst topography . . . . . 51
4.2 Hydromorphology of the study area . . . . . 53
4.3 Bussento Radon Monitoring Station System . . . . . 60

**5 Instruments and methods** **66**
5.1 RAD7 . . . . . 66
5.1.1 RADH2O System . . . . . 69
5.1.2 Water Probe . . . . . 73
5.2 E-PERM: Electret Ion Chambers . . . . . 75

**6 Results and discussion** **81**
6.1 Segment scale analysis . . . . . 81
6.2 Reach scale analysis . . . . . 85
6.2.1 Sicilì Bridge reference reach . . . . . 86
6.2.2 WWF Oasis reference reach . . . . . 92
6.3 Upper Bussento Segment . . . . . 96
6.4 Radon gas exchange analysis . . . . . 98
6.5 Karst spring analysis . . . . . 105

**Conclusions** **109**

**A The recoil flux of alpha daughters to solution** **110**
A.1 Spatial distribution of alpha recoil daughters . . . . . 110
A.2 Flux of daughters to solution . . . . . 112
A.3 Effect of surface adsorption . . . . . 112
A.4 Relative recoil fluxes . . . . . 113

**References** **114**

# Introduction

More than 50% of the population depends upon groundwater as its primary source of drinking water. Groundwater is water that occurs in saturated non-consolidated geologic material (sand or gravel) and in fractured and porous rocks. These saturated strata are called aquifers. Groundwater comprises approximately 4% of the water contained in the hydrologic cycle, which consists of the movement of water between oceans and other bodies of surface water, the atmosphere, and the land.

In the past, and particularly for management purposes, groundwater and surface water have generally been treated as separate entities, i.e. hydrological connectivity of the water bodies has been neglected. However, growing evidence suggests that substantial water exchange occurs between most hydraulically connected surface water and groundwater bodies [Sop02], with exchange occurring in both directions, i.e. from the surface water into the aquifer and vice versa.

The EU Water Framework Directive (WFD) now requires an integrated approach to the management of water resources, placing even greater emphasis on the need to *understand* the underlying processes that govern groundwater/surface water interactions (GSI).

The sustainable exploitation of the Earth's water resources and the protection and future management of coastal and terrestrial environments require a comprehensive understanding of the processes related to GSI. Both disturbances of the natural water balance and advective material transport across the groundwater/surface water interface can cause detrimental environmental impacts. For example, intrusion of contaminated surface water into an aquifer may result in an unrecoverable contamination of a drinking water supply, or the overexploitation of coastal aquifers may cause seawater infiltration and salinisation of the groundwater [Zek05].

Alternatively, groundwater discharge can be a major source of nutrients and contaminants into surface waters, leading to problems such as eutrophication of lakes [Nak08] or harmful algal blooms in coastal waters [Hu06], and thus a degradation of water quality. In addition, the dynamic groundwater/surface water interface is a biogeochemically active zone, where transformations of nutrients and pollutants can occur [Gan07]. Finally, many aquatic ecosystems are sensitive to variability in GSI intensity [Bru97].

Despite a growing recognition of the importance of GSI, there is still a substantial lack of understanding of the individual drivers governing its intensity and of its role in dissolved material transport. An underlying reason for this deficiency is the heterogeneous nature of GSI; its spatial and temporal variability causes difficulties for quantifying rates of GSI and associated processes. *Direct* methods for the quantification of GSI rates rely

on measurements at discrete locations, and are often limited by the large number of single measurements that are needed to investigate a greater region of interest. In contrast, the use of natural and anthropogenic tracers to *indirectly* identify and quantify GSI allows a more in-depth understanding of the underlying processes, in many cases, due to the integrating nature of tracer-based methods.

Tracer can either be artificially into the water body or are ubiquitously present in the environment. Such environmental tracers are defined as natural and anthropogenic chemical and isotopic substances that are present in all natural waters and originate from defined sources. In contrast to artificially injected tracers, environmental tracers have the general advantage of not contaminating the study site by introducing chemicals into the environment that may prove persistent. In addition, due to their occurrence in nature, environmental tracers are also more suitable for large-scale long-term GSI studies.

A range of naturally occurring dissolved components are currently utilized as tracers for GSI studies. Conventionally, easily accessible dissolved chemical components have been employed, such as selected elements (e.g. Ca, Sr, Ba) or nutrients (phosphate, silica, ammonium, nitrate), as well as standard physico-chemical water parameters such as temperature and salinity, with the former more widely used in terrestrial and the latter in marine studies. Although these parameters are relatively easy to measure, they have significant constraints and most importantly do not yield any information about pathways and in particular about residence times of water volumes.

The naturally-occurring radionuclides have proven to be powerful tools for assessing the time dependency of GSI processes. The radionuclide $^{222}$Rn (referred to as radon) has the advantage of being a radioactive noble gas, i.e. a (short-lived) radionuclide that is chemically inert and can easily be detected on site. Since radon is produced in every mineral matrix and is soluble in water, it occurs ubiquitously in all natural waters. Radon concentrations that are usually found in groundwater are about three to four orders of magnitude higher than radon concentrations typical for surface waters.

The aim of this work is to use radon as a tracer to investigate the groundwater-river interaction, in particular to perform an useful methodology for the localization of the contributions of groundwater to the riverbed, in a typical karst environment, the Bussento river basin (Campania region, southern Italy). The Bussento river basin, located in the south-east of Campania region, shows interesting issues related to water assessment and management. Complex interactions and exchanges between surface and groundwater exist, influencing also on-shore and off-shore submarine springs. Therefore, gaining river segments from karst groundwater and losing river segments towards the aquifer are recognized. Groundwater protection for drinking domestic use, riverine wild-life conservation and coastal water quality require a progressively optimized knowledge of these interactions.

# Chapter 1

# Radon: Overview of Properties, Origin and Transport

Radon is a unique natural element in being a gas, noble, and radioactive in all its isotopes. Gases are of special interest, first, because they are mobile and can carry messages over significant distances within the earth and the atmosphere and, second, because inhalation can be a problem to health. The fact that radon is noble insures that it is not immobilized by chemically reacting with the medium that it permeates. As a result, free radon normally diminishes only by its radioactive decay as it moves from its source. Finally its radioactivity allows radon to be measured with remarkable sensitivity. For humans the greatest importance of the radioactivity of radon is that in high concentrations it can be a health hazard, a cause of lung cancer.

Radon's chemical inertness, like that of lighter noble gases, is not complete. In fact it can form a fluoride [Fi62], which by analogy with the behavior of xenon may be $RnF_4$. Radon can also be trapped by physical absorption on finely divided carbon, a behavior that is utilized in the charcoal canister type of radon measurements. In the earth, radon isotopes are born by the decay of radium, and radium production in turn comes from uranium or thorium decay - usually (but not always) from trace impurities in minerals. The possibilities of transport of radon within the earth, its waters, and atmosphere make it a useful tracer for a remarkable variety of geophysical, geochemical, hydrological, and atmospheric purposes. These applications range from exploration for resources such as uranium and hydrocarbon deposits, to studying gas flow and mixing in the atmosphere, to recognizing fluid transport within the earth, to attempting to predict seismic and volcanic events through premonitory changes in radon concentrations in the earth.

These desirable functions of radon are countered by destructive health effects: sustained exposure of humans to substantial concentrations of radon decay products can produce lung cancer. Radon measurements play a critical role in monitoring human health and safety, both in homes and in mines. Radon is a ubiquitous hazard - and radon problems are aggravated where it is naturally concentrated in certain geological materials or is sociologically intensified by undesirable home construction practices.

Because radium - the parent of radon - is found in all crustal materials, radon is ubiquitous in both indoor and outdoor air. Sources of radon include soil, water, outdoor air and building materials, but transport of radon-bearing gas from soil is generally the most predominant source of indoor radon, particularly in buildings with elevated concentrations.

## 1.1 Physical and chemical properties of Radon

Radon is the heaviest member of the noble gas family and is colorless, odorless, relatively chemically inert, naturally radioactive, and has the highest melting point, boiling point, critical temperature and critical pressure of noble gases [Cot87].

It is soluble in water, with solubility decreasing with increasing temperature, as shown in fig. 1.1. An important property of radon is its higher solubility in organic solvents compared to water, a property used in various analytical or field techniques [Sch07].

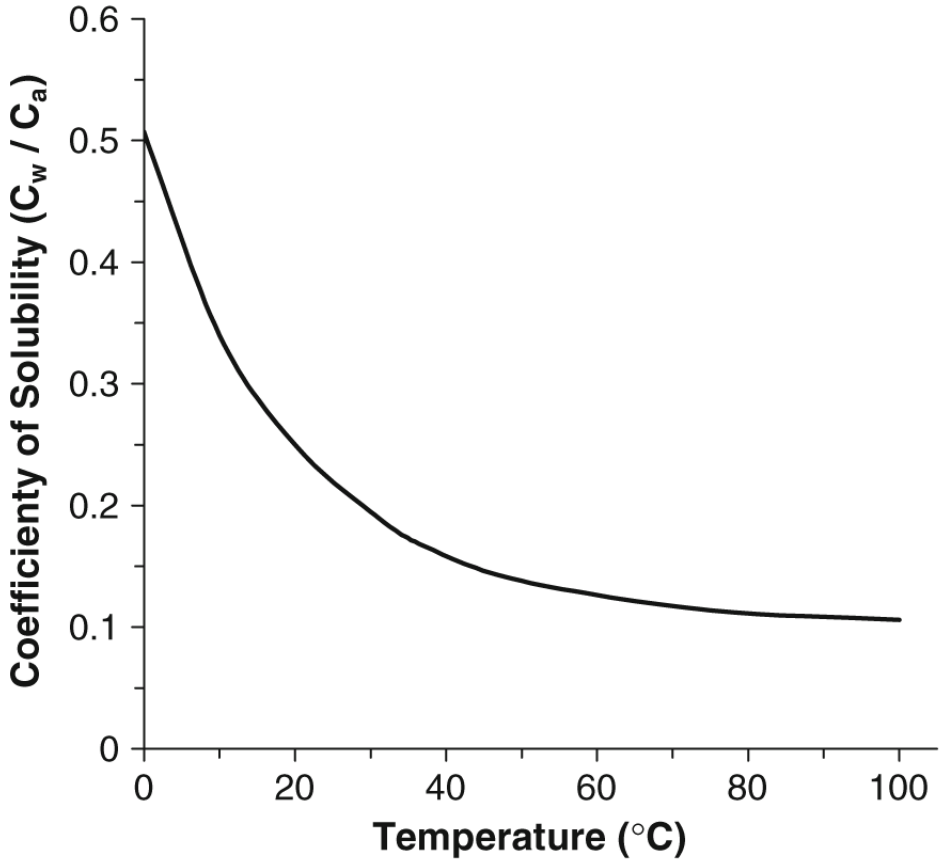


Figure 1.1: Solubility of radon in water with respect to temperature (where $C_W$ and $C_A$ are concentrations in water and air respectively) [Mud08].

In general, radon behaves as an inert gas, though it can form clathrates and complex fluorides (no successful formation of oxides or other halides is known) [Cot87].

The chemistry of radon remains relatively understudied compared to other noble gases [Mal01]. The element radon has 86 protons and a variable number of neutrons in its atomic nucleus, due to the radon being derived from a different parent radionuclide decay series. The three primary sources for natural radon are the parent isotopes of the two uranium series ($^{238}$U and $^{235}$U) and the thorium series ($^{232}$Th). These decay chains give rise to the specific radon isotopes of $^{222}$Rn (*Radon*), $^{220}$Rn (*Thoron*) and $^{219}$Rn (*Actinon*) respectively, and their decay products, commonly referred to as *progeny*.

The extent to which radon, actinon and thoron isotopes are present in a given situation will depend on whether the decay chain is in secular equilibrium (i.e. undisturbed) and the primary concentration of uranium and thorium.

### 1.1.1 Radioactive decay chains

Formed in the $^{238}$U decay chain from the decay of $^{226}$Ra, $^{222}$Rn is the most important radon isotope because it has the longest half-life, 3.8 days. This is long enough that much of the $^{222}$Rn formed either in building materials or in the ground within approximately a meter of building understructures can reach the indoor environment. Similarly, much of the $^{222}$Rn radon formed within a meter of the earth's surface reaches the outdoor atmosphere, although this has less radiological significance than that reaching indoor environments, which have relatively small volumes compared with the contributing source material.

In contrast, although about as much $^{220}$Rn (thoron, derived from the $^{232}$Th decay chain) activity is formed, substantially less reaches air because its short half-life (56s) limits the distance it can travel before decay. In fact, in air, for a constant diffusion, the mean distances of diffusive motion (i.e. the distance diffused over a mean life) are 2.2 m for $^{222}$Rn and 0.029 m for $^{220}$Rn.

Finally, very little of $^{219}$Rn is present in air because the $^{235}$U decay chain, of which it is a member, has a natural abundance that is a factor of 100 lower and because of actinon's short half-life (4s).

All radon isotopes give rise to progeny of polonium, bismuth, tellurium (actinium series only) and lead with half-lives ranging from fractions of a second (e.g. $^{214}$Po) to several years (e.g. $^{210}$Pb). These relatively short half-lives give rise to the progeny all having a very high specific radioactivity, and includes numerous alpha, beta and gamma decay steps (see later sections). The behavior of radon and progeny is therefore critical to understand in order to predict radiation exposures.

The equation describing the loss of atoms of a particular radionuclide by radioactive decay is:

$$\frac{dN}{dt} = -N\lambda \tag{1.1}$$

where $N$ is the number of radioactive atoms, $\lambda$ is the radioactive decay constant for that species and $t$ is the time.

The solution to this differential equation is given by

$$N(t) = N_0 e^{-\lambda t} \tag{1.2}$$

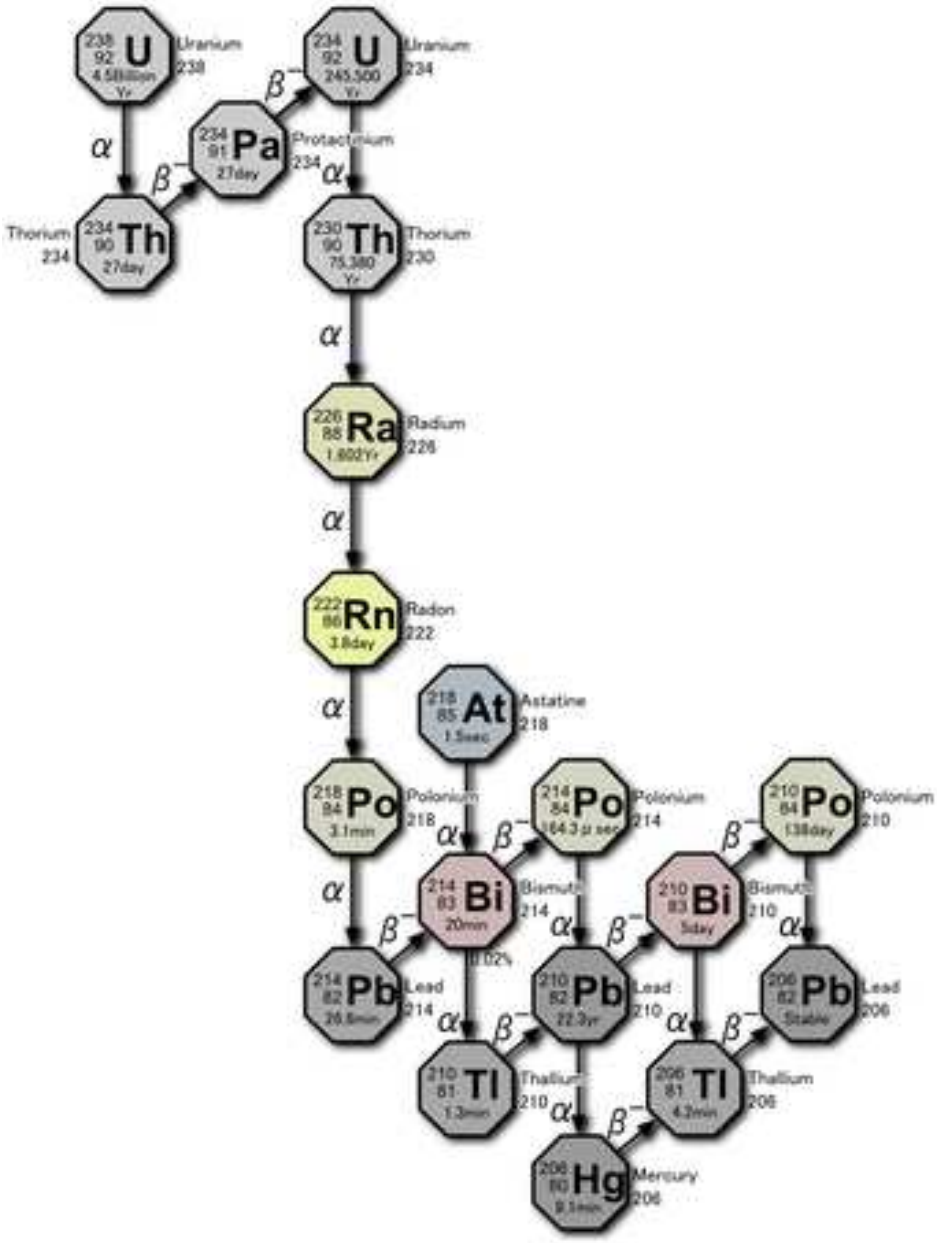


Figure 1.2: $^{238}$U decay series, including $^{222}$Rn and its decay products.

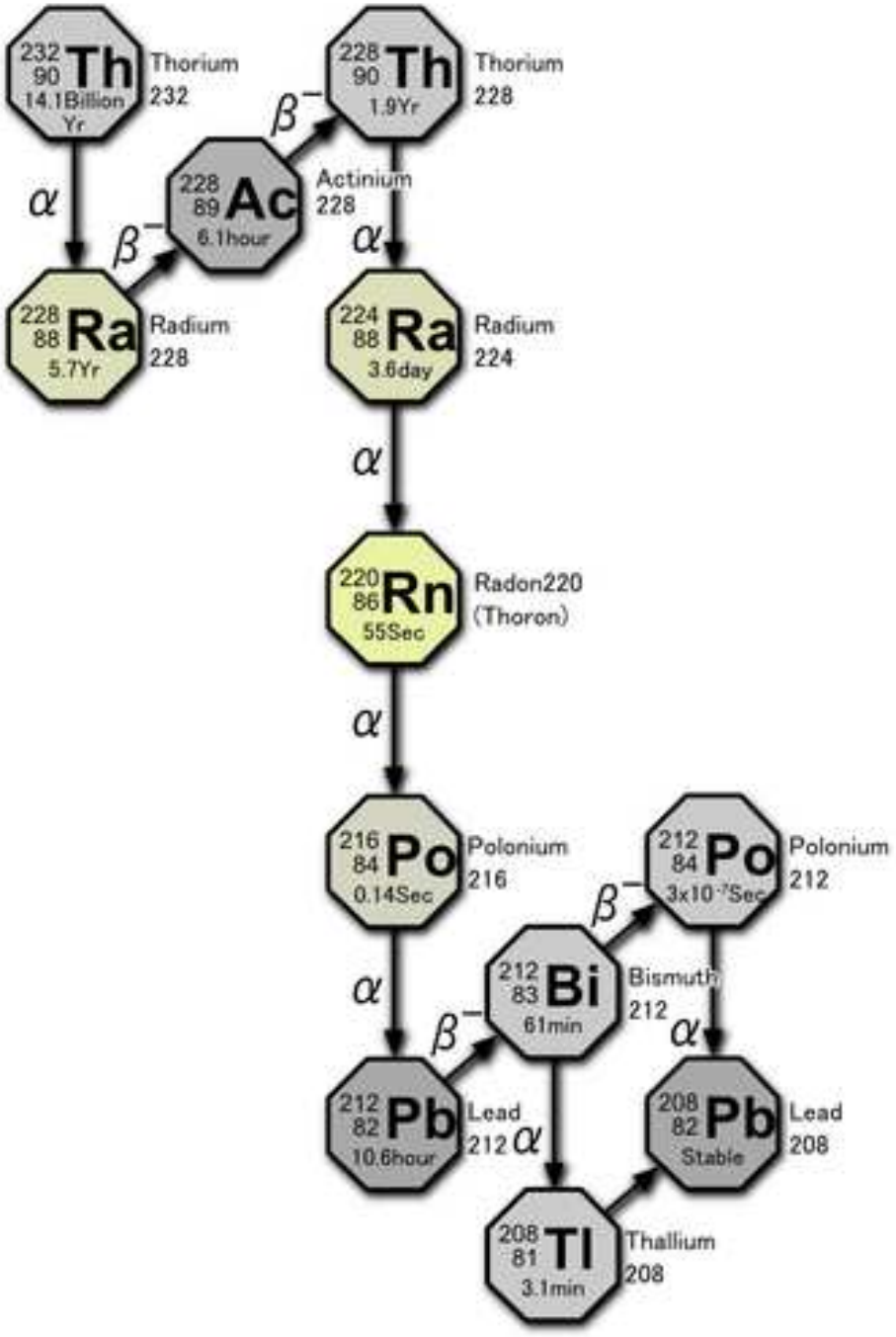


Figure 1.3: The decay series for $^{232}$Th, which includes $^{220}$Rn and its decay products.

| **Series** | Uranium | Thorium | Actinium |
|---|---|---|---|
| **Mass number code** | 4n + 2 | 4n | 4n + 3 |
| **Long-lived parent and half-life** | $^{238}$U 4.51 × $10^9$y | $^{232}$Th 1.39 × $10^{10}$y | $^{235}$U 7.13 × $10^8$y |
| **Radium parent and half-life** | $^{226}$Ra 1600 y | $^{223}$Ra 11.4 d | $^{224}$Ra 3.66 d |
| **Radon isotope and half-life** | $^{222}$Rn (radon) 3.82 d | $^{220}$Rn (thoron) 55.6 s | $^{219}$Rn (actinon) 4.0 s |
| **Potential alpha-energy in short-lived radon decay chain** | 19.2 MeV per atom | 20.9 MeV per atom | 20.8 MeV per atom |
| **Stable end product** | $^{206}$Pb | $^{208}$Pb | $^{207}$Pb |

Table 1.1: Some characteristics of the natural radioactive decay series.

where the decay constant, $\lambda$, is related to the half-life by

$$\lambda = \frac{ln2}{t_{1/2}} \tag{1.3}$$

and $N_0$ is the number of radioactive atoms present initially (at time t = 0). The quantity N$\lambda$ is often referred to as the activity, designated by $I$ (where $I_0 = N_0\lambda$).

The equations relating the radioactive growth and decay equilibrium between two or more radioactive species (as in the case of the equilibrium established between radon and its decay products) are based on the same principles, although they are functionally more complicated. For the general case of A → B, where both A and B are radioactive, the differential equation describing the production of B from the decay of A and the subsequent radioactive decay of B is

$$\frac{dN_B}{dt} = N_A\lambda_A - N_B\lambda_B. \tag{1.4}$$

Similar equations can be derived for successive parent-progeny relationships. These equations, known as the Bateman equations, can be simplified for specific cases where, for example, the half lives of parent and progeny species are quite different and where initial conditions can be specified. For $N_{B_0} = 0$ and $N_{A_0} = N_A$ at t = 0, the solution for the equation 1.4 is

$$N_B = \frac{\lambda_A}{\lambda_B - \lambda_A} N_{A_0} \left(e^{-\lambda_A t} - e^{-\lambda_B t}\right) \tag{1.5}$$

or using I = N$\lambda$ and equation 1.3

$$\frac{I_B}{I_{A_0}} = \frac{t_{1/2}\,(A)}{t_{1/2}\,(A) - t_{1/2}\,(B)} \left(e^{-\lambda_A t} - e^{-\lambda_B t}\right). \tag{1.6}$$

Using the Bateman equations for the production and decay of each of the radon decay products, the time-dependent activity concentration can

be calculated. The results are shown in fig 1.4 for the case of an initially pure sample of radon. This figure also illustrates a condition of radioactive equilibrium. In the case of $^{222}$Rn, radioactive equilibrium between radon and the radon decay products is achieved after approximately 3 hours. After that time, the activity concentrations of the short-lived decay products are essentially equal to that of the radon parent. This situation is referred to as *secular equilibrium*. As can be seen in fig 1.4, the activity concentration of $^{218}$Po increases rapidly in a pure $^{222}$Rn sample (as is also the case in a building in response to radon entry) so that approximately 50% of the equlibrium concentration is achieved within 4 minutes and almost 90% of the equilibrium between the radon parent and this first decay product is obtained within 10 minutes.

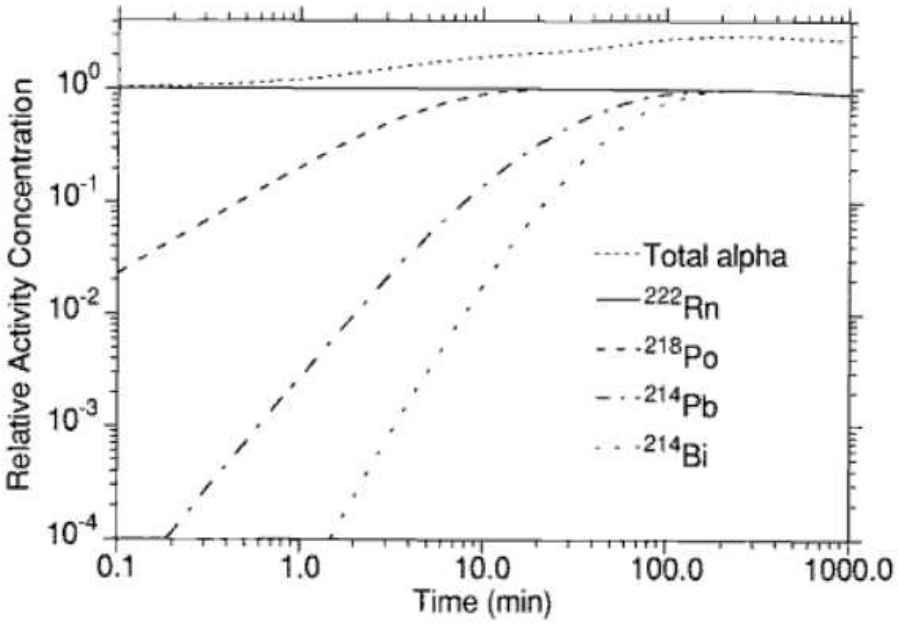


Figure 1.4: Relative activity concentration of $^{222}$Rn and its immediate radioactive decay products as a function of time. These concentrations assume that only $^{222}$Rn is present initially. The total alpha activity concentration as computed from equation 1.7 is also shown [Nag94].

For the $^{220}$Rn series, on the other hand, the initial concentration of $^{220}$Rn decays away quite quickly, and no equilibrium between the radon parent and the subsequent decay products exists. Instead, the total alpha activity observed for a sample of $^{220}$Rn for times greater than 10 minutes after collection is controlled by the decay of the 10.6 hours $^{212}$Pb isotope.

The equilibrium conditions in actual indoor environments are different than illustrated here, since the airborne radon decay product concentrations are affected by indoor aerosol concentrations, ventilation rates, and radon entry rates.

By combining the equations describing the concentrations of the alpha-active radionuclides, the total alpha activity as a function of time can be calculated. Using the decay constants or half-lives for radon and its respective decay products as summarized in table 1.2, the equation for the total

alpha activity is:

$$\frac{Total\ \ alpha\ \ activity}{I_{Rn-222(initial)}} = 3.010e^{-\lambda_{Rn-222}\cdot t} - 1.024e^{-\lambda_{Po-218}\cdot t} + \\ - 4.404e^{-\lambda_{Pb-214}\cdot t} + 3.418e^{-\lambda_{Bi-214}\cdot t}. \quad (1.7)$$

### 1.1.2 The importance of prompt daughters

Health hazards of radon and thoron are not primarily due to those isotopes directly, but to the short-lived daughters that can be inhaled. Because radon is a noble gas with a lifetime that is long relative to breathing times, most of it that is inhaled is exhaled again rather than decaying, or becoming lodged in the lungs and later decaying. In contrast, the immediate, promptly-decaying daughters of $^{222}$Rn ($^{218}$Po, $^{214}$Pb, $^{214}$Bi and $^{214}$Po), which wish to be part of a condensed phase, attach to surfaces, typically of aerosols, which can be inhaled; they then deposit on epithelial surfaces within the lung, and shortly decay. Since the longest lived of the four, $^{214}$Pb, has a half life of less than 27 minutes, the whole sequence of decays can be completed before the normal clearance processes of the lung can sweep them away. The result is that the sensitive surfaces of the bronchi are irradiated by these decays - the most energetic and destructive of which are the heavily ionizing, short-range alpha particles from the polonium isotopes $^{214}$Po and $^{218}$Po. A third alpha-active polonium isotope $^{210}$Po contributes relatively little to the radon measurements because its decay requires the prior decay of 22-year half-life $^{210}$Pb.

Thoron is somewhat different case. Its first daughter $^{216}$Po is so prompt (mean life 0.22 s) that it decays wherever $^{220}$Rn decays. There then follows 15.2 h mean life $^{212}$Bi, which lives on the average long enough that most of it will be transported from the bronchial portions of the lungs, except at points of stagnation that exist at bifurcations in the bronchial tree. Its primary health effect is likely to be at such points, where ultimately the daugther $^{212}$Po will alpha decay.

### 1.1.3 Ranges of alpha particles and recoil nuclei

For understanding the physical behavior of radon and its decay products, it is helpful to know the penetrating power of alpha particles that are emitted in decay and also those of the residual nuclei that recoil from the alpha decays. Table 1.3 lists ranges in air and water of alpha particles emitted by $^{220}$Rn and $^{222}$Rn and their prompt alpha-active daughters. Their alpha-decay energies are also given. Ranges in typical plastics are similar to those in water. For example, the range of the 5.49 MeV $^{222}$Rn alpha particle approximate values are 39 $\mu$m in water, 32 $\mu$m in polyethylene terephthalate (of density 1.2 g cm$^{-3}$), 31 $\mu$m in polyethylene, 37 $\mu$m in Lexan polycarbonate, but 23 $\mu$m in soda lime glass (density $\approx$ 2.5 g cm$^{-3}$).

Recoiling nuclei resulting from alpha decay have far lower energies ($\sim$ 100 keV) and consequently very short ranges ($\sim$ hundreds of atomic distances). Values computed by the method of Lindhard et al. [Lid63] are given in table 1.4 for $SiO_2$. Other common minerals will have similar values. For example,

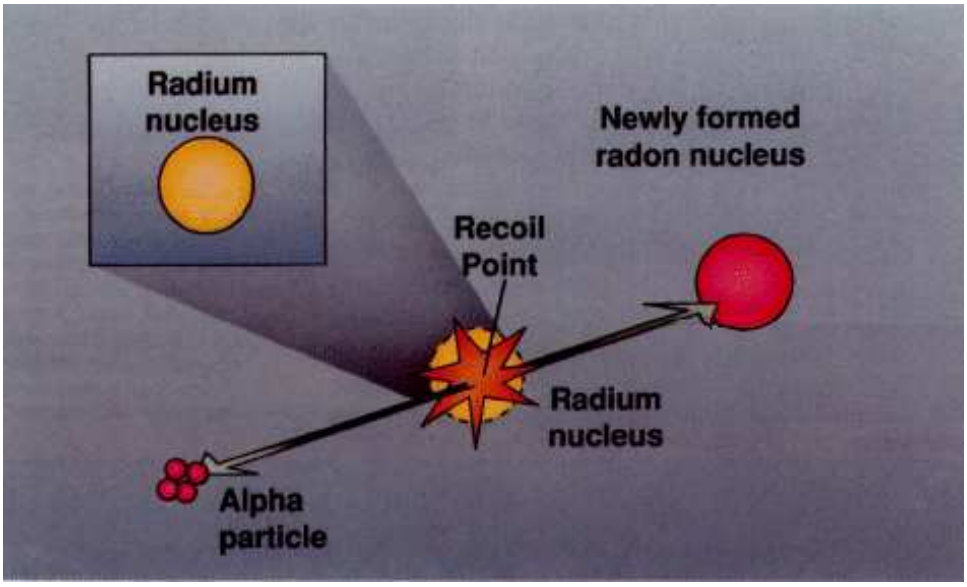


Figure 1.5: A radium atom decays to radon by releasing an alpha particle, containing two neutrons and two protons, from its nucleus.

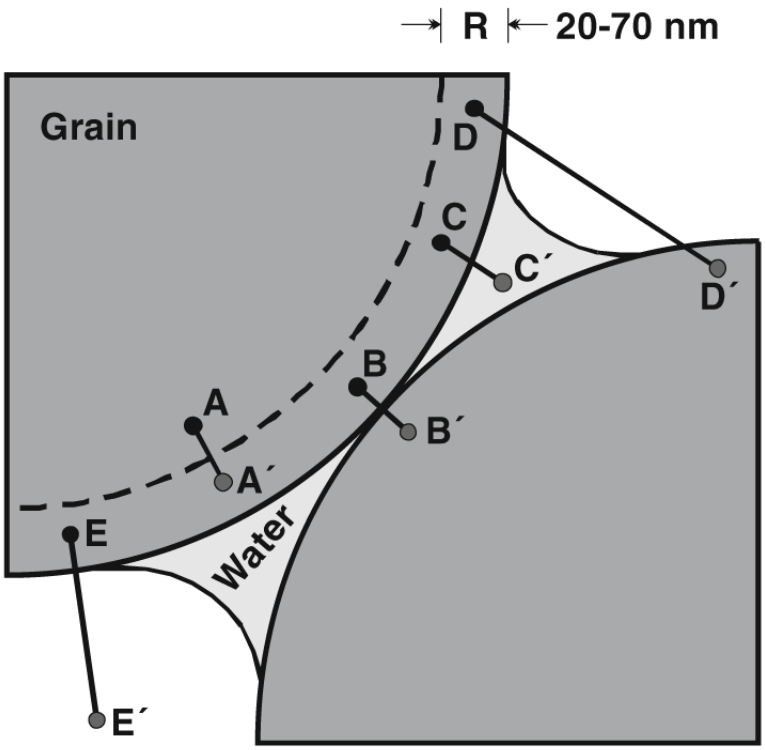


Figure 1.6: Radon atom recoils: A-A' inside same mineral grain; B-B' from one mineral to adjacent mineral; C-C' from mineral to water; D-D' from mineral through air to adjacent mineral; E-E' from mineral to air [Cot87; Law05; Mud08].

| | | | Major Radiation Energies | | Potential Alpha Energy Calculation | | |
|---|---|---|---|---|---|---|---|
| **Nuclide** | **Half Life** | **Decay Constant $\lambda$ ($s^{-1}$)** | **$E_\alpha$** (MeV) | **$E_\gamma$** (keV) | **N atoms** ($Bq^{-1}$) | **$\Sigma$ $E_\alpha$** (MeV $atoms^{-1}$) | **Fraction** |
| $^{226}$Ra | 1600 y | $1.37 \times 10^{-11}$ | 4.60 (6) | ... | $7.3 \times 10^{10}$ | ... | ... |
| | ... | ... | 4.78 (94) | ... | ... | ... | ... |
| $^{222}$Rn | 3.82 d | $2.10 \times 10^{-6}$ | 5.49 (100) | ... | $4.8 \times 10^{8}$ | ... | ... |
| $^{218}$Po | 3.04 m | $3.80 \times 10^{-3}$ | 6.00 ($\sim$ 100) | ... | 263 | 13.69 | 0.104 |
| $^{214}$Pb | 26.9 m | $4.29 \times 10^{-4}$ | ... | 242 (20) | 2329 | 7.69 | 0.517 |
| | ... | ... | ... | 295 (52) | ... | ... | ... |
| | ... | ... | ... | 352 (100) | ... | ... | ... |
| $^{214}$Bi | 19.7 m | $5.86 \times 10^{-4}$ | ... | 609 (100) | 1705 | 7.69 | 0.379 |
| | ... | ... | ... | 1120 (33) | ... | ... | ... |
| | ... | ... | ... | 1764 (35) | ... | ... | ... |
| $^{214}$Po | 164 $\mu$s | $4.23 \times 10^{3}$ | 7.69 (100) | ... | $2 \times 10^{-4}$ | 7.69 | 0 |
| $^{210}$Pb | 22.3 y | $9.86 \times 10^{-10}$ | ... | 47 (100) | ... | ... | ... |
| $^{210}$Bi | 5.01 d | $1.60 \times 10^{-6}$ | ... | ... | ... | ... | ... |
| $^{210}$Po | 138 d | $5.81 \times 10^{-8}$ | 5.30 (100) | ... | ... | ... | ... |
| $^{206}$Pb | stable | ... | ... | ... | ... | ... | ... |

Table 1.2: $^{222}$Rn decay series [Nag94].

if the range in $SiO_2$ is 30 nm, the expected value is 27 nm for muscovite mica and 21 nm for zircon, but 68 nm for polyethylene.

### 1.1.4 Distribution of Radon between phases

When radon is present in a gas such as air, nitrogen, or natural gas, it will, to some extent, penetrate water until it reaches an equilibrium concentration that decreases with increasing temperature [Fa54]. Some values for the ratio of radon in water to radon in gas (atoms per unit volume) are 0.53 (0°C), 0.43 (6°C), 0.28 (15°C), 0.22 (26°C), 0.16 (40°C), and 0.11 (100°C).

Where water is in direct contact with mineral particles that contain radium, radon can be implanted in water by alpha recoil [Ki71] to levels that far exceed the equilibrium with nearby gas. For example, Hess et al. [He82] found as much as $1.9 \cdot 10^6$ Bq $m^{-3}$ (52000 pCi $l^{-1}$) in water, while the corresponding air concentration was only 150 Bq $m^{-3}$ (4 pCi $l^{-1}$). Water with such supersaturation is prone to rapid outgassing when given sufficient agitation, as for example in washing machines or showers within homes. Such

| Nuclide | Alpha Energy (MeV) | Alpha Range ($\mu$m of water) | Alpha Range (cm of air) |
|---|---|---|---|
| $^{222}$Rn | 5.49 | 39 | 4.08 |
| $^{218}$Po | 6.00 | 44 | 4.67 |
| $^{214}$Po | 7.69 | 66 | 6.91 |
| $^{220}$Rn | 6.29 | 48 | 5.01 |
| $^{216}$Po | 6.78 | 41 | 5.67 |
| $^{212}$Po (64%) | 8.78 | 83 | 8.53 |
| $^{212}$Bi (36%) | 6.05 | 45 | 4.73 |

Table 1.3: Alpha particle energies and ranges, calculated for 6°C at sea level.

| Decaying Nuclide | Recoil Nuclide | Range in $SiO_2$ (nm) |
|---|---|---|
| $^{226}$Ra | $^{222}$Rn | 26 |
| $^{222}$Rn | $^{218}$Po | 30 |
| $^{218}$Po | $^{214}$Pb | 34 |
| $^{214}$PO | $^{210}$Pb | 45 |
| $^{224}$Ra | $^{220}$Rn | 31 |
| $^{220}$Rn | $^{216}$Po | 35 |
| $^{216}$Po | $^{212}$Pb | 38 |
| $^{212}$Po (64%) | $^{208}$Pb | 52 |
| $^{212}$Bi (36%) | $^{208}$Tl | 35 |

Table 1.4: Range of alpha recoil nuclei in silica.

emission can be a significant health hazard where groundwater comes from a radium-rich aquifer, as has been noted in parts of the state of Maine in the U.S.A. by Hess *et al.* [He82].

### 1.1.5 Diffusion

Radon diffusion rates in air and water are vastly different. As table 1.5 shows, the diffusion constant $D$ in water is lower by a factor of $10^4$. There is a mean distance of motion of a radon isotope before it disappears by decay, $\sqrt{D \cdot \tau}$, where $\tau$ is the mean life of the isotope. Thus the average $^{222}$Rn atom moves about 1.6 m in dry porous soil, but only 1.6 cm in water-saturated soil.

| Medium | Mean Distance (cm) | Diffusion Constant Assumed ($cm^2\ s^{-1}$) |
|---|---|---|
| Air | 220 | $10^{-1}$ |
| Porous soil | 155 | $5 \cdot 10^{-2}$ |
| Water | 2.2 | $10^{-5}$ |
| Saturated Porous Soil | 1.55 | $5 \cdot 10^{-6}$ |

Table 1.5: Mean Diffusion distances of $^{222}$Rn in different media. The values for the Diffusion Constant are taken from a compilation by Tanner [Tan64].

### 1.1.6 Permeation

The permeation characteristics for radon in various substances are of great interest for two primary reasons. One factor is the obvious need for barriers to seal homes against invasion by radon. Are walls and foundations tight?

What plastic sheet, caulks or sealing compounds are effective barriers? The second issue is less obvious - the use of membrane barriers to keep all other alpha emitting isotopes except $^{222}$Rn out of a detector air space, so that $^{222}$Rn can be measured by itself [War77]. This application is part of the established Terradex methodology that is standard in the United States for accurate long-term indoor radon measurements [Fle80].

Table ref, most of which comes from Fleischer [Fle88], gives permeabilities, $k$, for plastic sheets and caulking compounds. A delay time ref is given for $^{222}$Rn entering an air space of volume $V$ through a membrane of area $A$ and thickness $\delta$ for one set of assumed $\delta$, $A$ and $V$ values that is used in $^{222}$Rn detectors. For $^{222}$Rn detection systems, a delay time that is long relative to the 1.34 min mean life of $^{220}$Rn is desired (so that no thoron is counted) and which is not much larger than that of $^{222}$Rn (5.5 days). Polyethylene is one commonly used choice. For barriers against radon entering a home, thick tightly adhering low-permeability materials are desired. Amongst the caulks, acrylic latex is by far the most effective of the four that have been reported [Fle92].

## 1.2 Sources of Radon

Radon is most abundant in mineral grains, is 25x lower in soil gas in the ground, a further 1000x less in homes, still lower in the air over the ground (by 5x), and another 100x lower over oceans. The trends give a coherent picture: radon originates from radium decay in soil grains; a small fraction of it is freed to move through the pore spaces into the atmosphere over land; and much of that has decayed before being transported by the winds to over the oceans. Homes, because they lie at the interface between the soil and the continental atmosphere, have radon concentrations that are intermediate between those of the soil gas and the free atmosphere. Table 1.6 gives rough representative numbers for the concentrations of radon at various locations.

| **Location** | **Concentration** (atoms cm$^{-3}$) |
|---|---|
| Air over oceans | 0.04 |
| Air near the earth's surface | 4 |
| Typical home in the US | 20 |
| Soil Gas | $20 \cdot 10^4$ |
| Interior of typical mineral | $5 \cdot 10^5$ |

Table 1.6: Typical $^{222}$Rn concentration.

Radon isotopes are produced in minerals by the decay of Radium that itself is the product of a natural chain of decays that begins with $^{238}$U, $^{235}$U or $^{232}$Th. Although table 1.6 makes use of an average radon production rate, minerals vary widely in their contents of these progenitors of radon. Typical continental rocks have $\sim 10^{-6}$; sub-oceanic basalts $\sim 10^{-7}$. Granitic rocks and alum shales tend to be higher than the usual continental rocks. Within a given rock type the different minerals contain very different concentrations of uranium, which often is preferentially located in certain accessory minerals.

## 1.3 Release mechanisms

The heterogeneous distribution of uranium has implications for the processes responsible for the release of radon. These are aided by uranium and radium being close to mineral surfaces.

Table 1.6 implies that most radon that is produced by the decay of radium never escapes from the mineral in which it is born; rather usually it is wedged tightly in place within the crystal lattice for the few days until it in turn decays. The small fraction of radon that escapes is either released promptly as it is born or within the few days before it decays. One process is established in each of those alternatives.

The first possibility for escape is direct ejection of the radon atom by recoil from alpha emission, proposed and documented by Kigoshi [Kig71]. Conservation of momentum reveals that emission of an alpha particle with 4.78 MeV by $^{226}$Ra gives the residual $^{222}$Rn nucleus a recoil energy of 86 keV, which table 1.4 shows that is sufficient to move the recoiling radon through 26 nm of $SiO_2$. Alternatively, if the radium atom was within 26 nm of the surface of the mineral and the recoil properly directed, as in figure 1.7, the recoil can actually leave the grain and enter the interstitial space.

Two results can be imagined. If the pore space contains water, as Kigoshi imagined, the ejected recoil most often will be brought to rest in the liquid, as sketched in the upper part of figure 1.7. The radon atom is then free to diffuse from the water or be transported by it.

The second possibility, shown in the lower part of figure 1.7, is that the interstitial space is dry (i.e. filled only with soil gas) and not wide enough to stop the recoiling radon. In this case, it enters a neighboring grain - apparently immobilizing itself. It is, however, less isolated than if it failed to exit its grain of origin, the reason being that radiation damage extends to it from where it entered its new grain. Hence, if the originally dry grains become wet before the radon has decayed, it can be released into the interstitial space.

## 1.4 Radon transport

Radon moves by two basic means, diffusion and forced flow. Diffusion inevitably occurs, even though its extent may be limited. Hence diffusive migration sets a lower limit on the transport of radon. Forced flow depends on pressure gradients, which may or may not be present in a given situation.

The diffusive motion in the ground is controlled by the extent of open, connected porosity in soil and rock. In general, higher porosity enables more extensive diffusive transport; but it is critical to consider only that fraction of the pore space that allows through motion. Most porosity in soil is interconnected; but in rocks that is not necessarily true.

The forced flow of radon through soil and rock is due to pressure gradients. The ease of such flow is given by the hydraulic permeability,$K$:

$$K = [\eta(dV/dt)/A(dP/dx)] \tag{1.8}$$

where $\eta$ is the viscosity, $(dV/dt)/A$ the volume moved per unit time and per unit area, and $dP/dx$ the pressure gradient. Table 1.7 indicates the wide

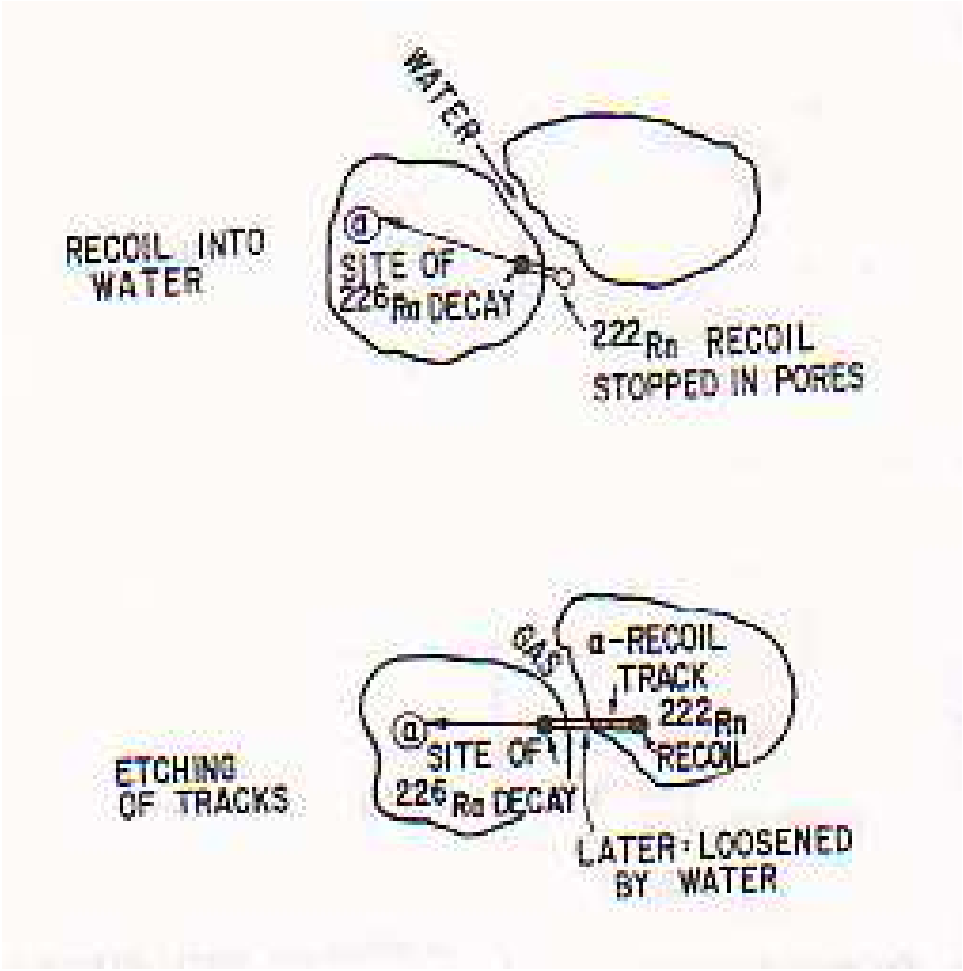


Figure 1.7: Models of two radon-release mechanisms: (top) the recoiling $^{222}$Rn nucleus is stopped by water in the intergranular material [Kig71]; (bottom) the nucleus recoils into an adjacent grain and the damage track is later removed chemically by the intergranular liquid, releasing the recoil nucleus [Fle80; Fle88]. The figure is from Durrani [Dur97].

spectrum of values that are found for hydraulic permeabilities $K$ [Scd60].

| **Substance** | **Permeability Range** ($cm^2$) |
|---|---|
| Black slate powder | $4.9 \cdot 10^{-10}$ - $1.2 \cdot 10^{-9}$ |
| Silica powder | $1.3 \cdot 10^{-10}$ - $5.1 \cdot 10^{-10}$ |
| Sand (loose beds) | $2.0 \cdot 10^{-7}$ - $1.8 \cdot 10^{-6}$ |
| Soils | $2.9 \cdot 10^{-9}$ - $1.4 \cdot 10^{-7}$ |
| Sandstone ("oil sand") | $5.0 \cdot 10^{-12}$ - $3.0 \cdot 10^{-8}$ |
| Limestone, dolomite | $2.0 \cdot 10^{-11}$ - $4.5 \cdot 10^{-10}$ |
| Brick | $4.8 \cdot 10^{-11}$ - $2.2 \cdot 10^{-9}$ |
| Bituminous concrete | $1.0 \cdot 10^{-9}$ - $2.3 \cdot 10^{-7}$ |
| Cork board | $3.3 \cdot 10^{-6}$ - $1.5 \cdot 10^{-5}$ |
| Fiber glass | $2.4 \cdot 10^{-7}$ - $5.1 \cdot 10^{-7}$ |

Table 1.7: Representative values of hydraulic permeability $K$ [Scd60].

For a non-uniform material the $K$ values depend on the scale of the measurement, since flow on a large enough scale between two measuring points may be facilitated by occasional easy-flow paths.

A number of observation of radon flow have been made and some models have been proposed. Although most of these processes occur at some times and places, it is difficult to prove for any single observation that in fact a particular mechanism was clearly responsible.

The mechanisms differ depending on the geophysical and geochemical phenomena - earthquakes, volcanic eruptions, oil prospecting and uranium prospecting.

Three main categories are gas emission, stresses and fluid convection. Gases can be released by oil deposits [Fle84], and they can be generated and pressurized by hot regions such as volcanoes. Stress can be generated by the build-up of strains that precede earthquakes [Dob79; Fle81] and volcanic eruptions, and the stress gradients in turn can encourage fluid flow in the earth. Fluid convection could produce flows if there were sufficiently steep geothermal gradients and high enough permeabilities [Mog77]. Such flows could deliver signals from uranium deposits from greater depths that would allow detection of ore solely by diffusion of radon. Here again volcanic effects (in this case thermal) could reveal impending activity.

A fourth contributor to pressure-induced flow is atmospheric pumping in the near-surface soil by the pressure fluctuations that are associated with weather systems [Cle74].

## 1.5 Radon daughters in air

Various parameters influence the concentration of radon and its decay products in the air. The basic processes involved are attachment to atmospheric aerosols, deposition (plate-out), recoil of radon and radon daughters from aerosols and surfaces, and decay.

Growth of the activity of the individual short-lived decay products, $A_i$, from a constant source of radon activity, $A_0$, is shown in fugure 1.8. From this figure it is evident that $^{218}$Po, owing to its short decay time ($\tau_{1/2} = 3$ min), relatively quickly ($\approx 20$ min) reaches equilibrium with $^{222}$Rn activity. Activities of $^{214}$Pb and $^{214}$Bi ($^{214}$Po) are close to equilibrium with $^{222}$Rn

after approximately 3 hours.

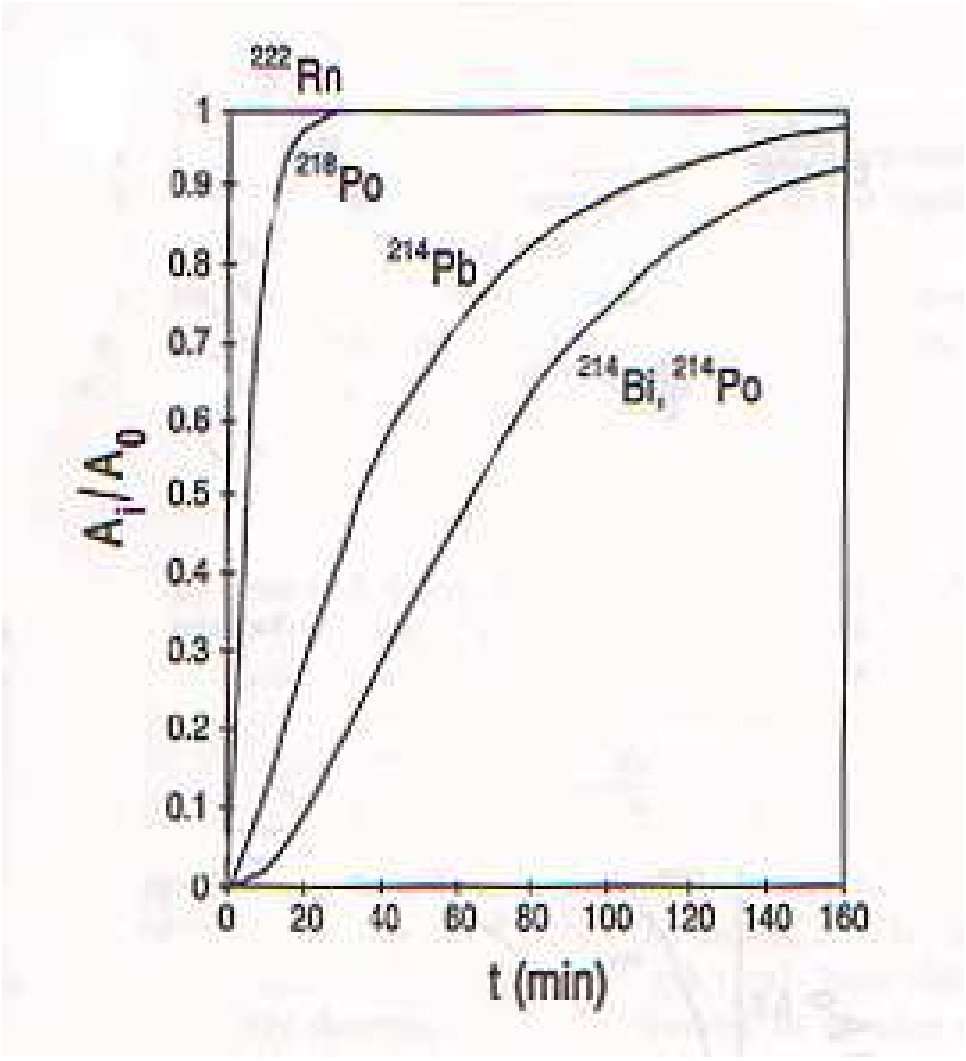


Figure 1.8: Growth of activity of individual short-lived radon decay products, $A_i$, from a constant source of radon activity, $A_0$ [Eva69; Dur97].

Other basic processes influencing the activity balance between radon and its progeny are illustrated in figure 1.9, in which the mechanisms shown are very simplified. Here ionization, electrostatic forces, gravity, air flow and other important processes influencing the transport of radon and its decay products in air are neglected. If such processes are neglected and when only steady-state molecular diffusion is taken into account, with the diffusion coefficient equal for $^{222}$Rn, $^{218}$Po and $^{214}$Po in air and being 0.06 cm$^2$ s$^{-1}$, we obtain a reduced activity concentration of radon decay products in the air near surfaces due to their progressive deposition on the surfaces.

Activity concentration profiles for unattached radon progeny are shown in figure 1.10 [Brg91]. It can be seen that their activity concentrations significantly decrease at distances less than about 10 cm from the walls.

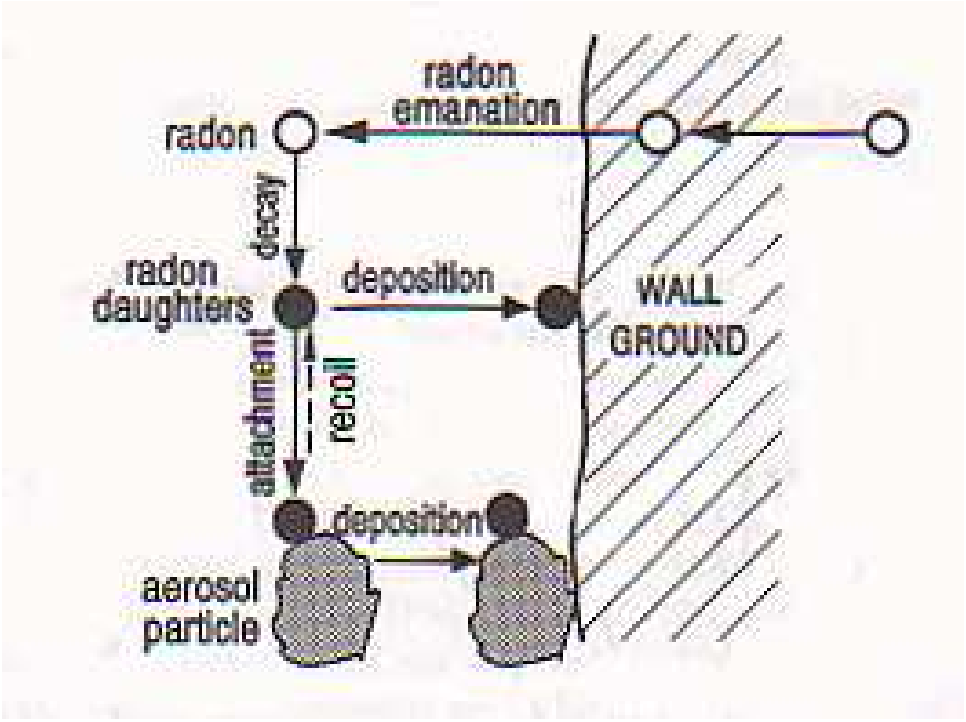


Figure 1.9: Basic processes influencing the activity balance of radon and its progeny [Pos84].

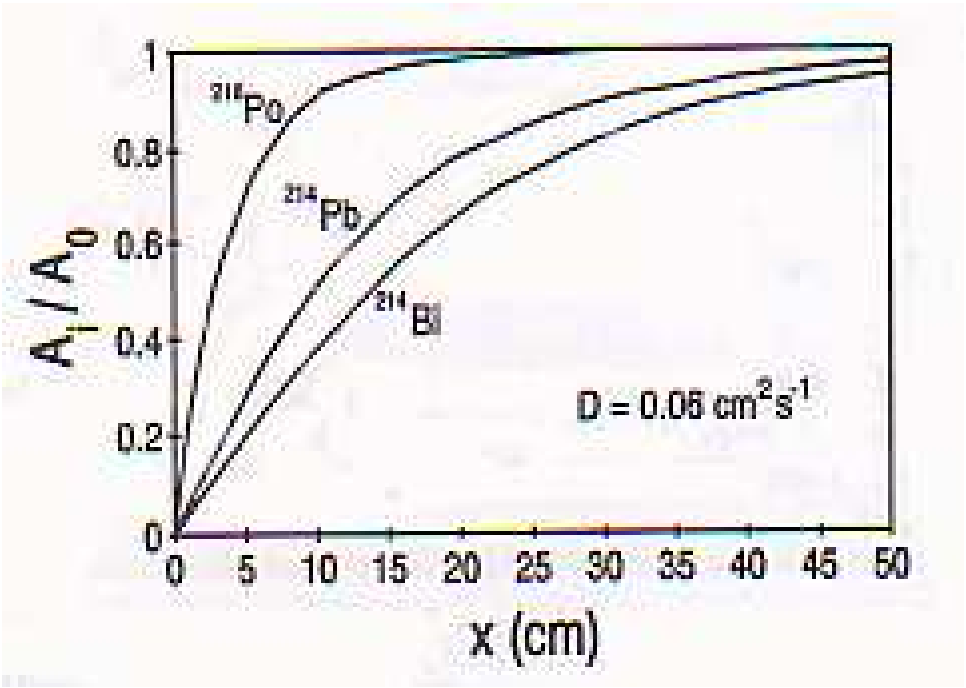


Figure 1.10: Activity concentration profiles for unattached radon decay products $A_i$. The distance from the surface is denoted by $x$. Radon activity and diffusion coefficient for radon in air are denoted by $A_0$ and $D$ respectively [Brg91].

## 1.6 Radon indoor

Radon is an ubiquitous contaminant in indoor air. It is also a significant source of radiation exposure for the general population, constituting more than half the annual effective dose equivalent, even at average indoor concentrations.

These average concentrations ($\sim$ 50 Bq/m$^3$) may result from contributions from several sources, such as outdoor air, diffusion from or through building materials, or indoor water use from private groundwater sources. The contribution of pressure-driven flow of soil gas bearing radon to such concentrations is unclear, though the magnitude of the estimated contribution from this source covers a wide range of values, and could easily account for all or part of the observed average concentrations.

For elevated indoor radon concentrations, advective flow of soil gas is the predominant source in almost all cases [Nag94].

Thoron may account for 10% or more of the annual effective dose equivalent. Outdoor air and emanation from building materials indoor may account for the indoor concentrations that have been observed; however, it is not known, in general, whether indoor $^{220}$Rn concentrations may increase with increasing $^{222}$Rn concentrations.

The indoor environment is very dynamic, with changes in ventilation rates and pollutant emissions occurring at several time scales, from hourly to seasonal effects. In part, these are a result of the interaction of the building with the external environment, where temperature differences or winds provide the driving force for both ventilation and for advective radon entry.

The operation of mechanical systems within the building shell can effect the ventilation rate of the structure, the radon entry rate, and mixing within the building. In actual buildings, these interactions are often complex. The resulting indoor radon and radon decay-product concentrations can also be highly variable over similar time periods.

According to to an extensive compilation presented by UNSCEAR [UNS00], given in tables 1.8 and 1.9, an indoor radon activity of between 30 and 40 Bq/m$^3$ is typical, with an apparent relationship to latitude shown in fig. 1.11. The data suggests that closer to the equator has lower ambient indoor radon, most likely due to greater ventilation associated with higher temperatures, although the scatter at higher latitudes suggests that other factors can also be important.

The accumulation of radon inside residential dwellings is a complex combination of factors and processes, sometimes competing against each other. The major factors involved in determining radon and progeny activities inside a residential dwelling include geology, climate, building materials, design and construction (especially single or multi-storey), building age, barometric pressure effects, and finally lifestyle.

Air pressure differences can suck radon into a dwelling or suppress it from entering. Lifestyle aspects often relate to how a dwelling is utilised and can exacerbate or minimise radon issues.

Some regions naturally contain elevated uranium and/or thorium in soils and rocks, such as granites up to 40 mg/kg uranium, and this can lead to significant radon emanating into and accumulating in dwellings. Based

| Region | Country | Arithmetic Mean | Geometric Mean | Maximum | Geometric SD |
|---|---|---|---|---|---|
| Africa | Algeria | 30 | | 140 | |
| | Egypt | 9 | | 24 | |
| | Ghana | | | 340 | |
| | South Africa (Paarl) | ∼37 - 132 | | 465 | |
| Northern America | Canada | 34 | 14 | 1720 | 3.6 |
| | United States | 46 | 25 | | 3.1 |
| Central America | Mexico | 83 | 75 | 448 | |
| Southern America | Argentina | 37 | 26 | 211 | 2.2 |
| | Chile | 25 | | 86 | |
| | Paraguay | 28 | | 51 | |
| Eastern Asia | China | 24 | 20 | 380 | 2.2 |
| | Hong Kong | 41 | | 140 | |
| | India | 57 | 42 | 210 | 2.2 |
| | Indonesia | 12 | | 120 | |
| | Japan | 16 | 13 | 310 | 1.8 |
| | Kazakistan | 10 | | 6000 | |
| | Malaysia | 14 | | 20 | |
| | Pakistan | 30 | | 83 | |
| | Thailand | 23 | 16 | 480 | 1.2 |
| Western Asia | Armenia | 104 | | 216 | 1.3 |
| | Iran | 82 | | 3070 | |
| | Kuwait | 14 | 6 | 120 | |
| | Syria | 44 | | 520 | |
| Oceania | Australia | 11 | 8 | 420 | 2.1 |
| | New Zealand | 20 | 18 | 90 | |

Table 1.8: Summary of indoor radon activities ($Bq/m^3$) in Africa, America, Asia and Oceania [UNS00], including additional Mexican data from Segovia et al. [Seg07] and Paarl, South African data from Lindsay et al. [Lin08].

on studies in the UK, Czech Republic, Germany and elsewhere, the most common geological situations giving rise to elevated U/Th are related to granites [Apt07]. Alternately, the earthen materials used in construction may contain elevated U/Th, leading to elevated radon (e.g. alum shale in Sweden).

## 1.7 Health effects

The link between radon and health impacts, however, has only been suggested since the early twentieth century-though not widely scientifically accepted until the 1960s [Jac93; NAS99].

By the 1930s, based on the lung cancer rates in German-Czech mines, radon was being suggested as the main cause of the health impacts, but the quantitative evidence was not sufficiently clear, especially the role of radon progeny. In the 1950s, work done by William F Bale and John Harley in the USA demonstrated that the major radiological dose was actually delivered

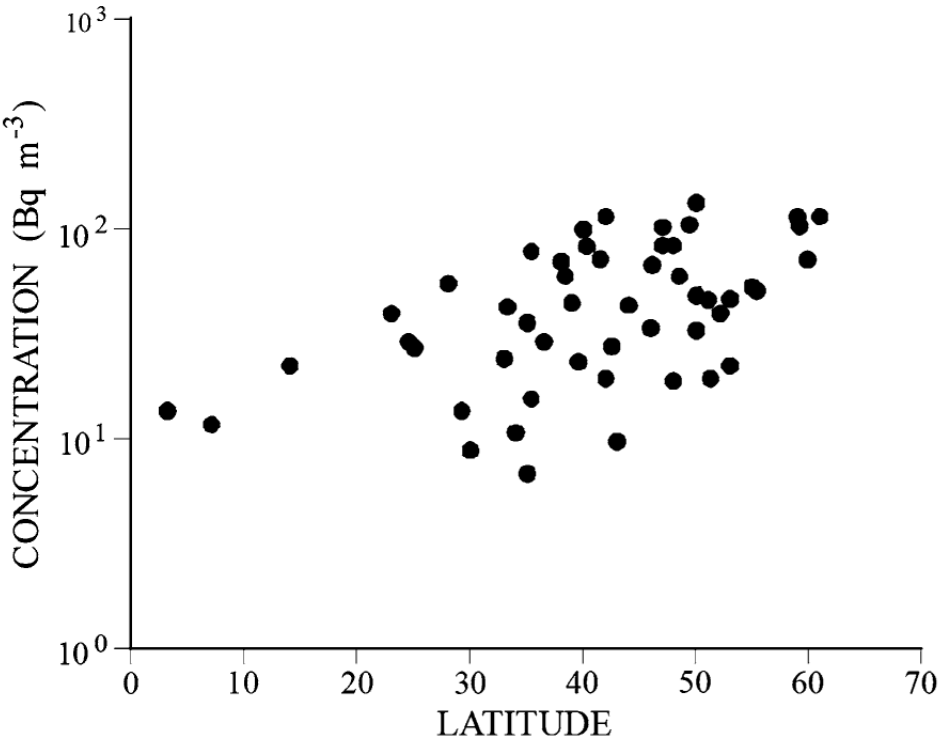


Figure 1.11: Average radon indoor activity versus latitude [UNS00].

to lung tissues by the progeny and not the radon gas [Jac93].

Combined with epidemiological studies emerging by the early 1970s, it became clearer that high radon and progeny activities were associated with impacts such as lung cancers. In the same decade it also became clear that residential dwellings could also allow radon and progeny to accumulate to exposures sometimes as high as uranium miners.

Lung cancer due to radon occurs as a result of the dose of alpha energy emitted by radon decay products, which is delivered to target cells in the lungs. Because alpha energy deposition in the lungs cannot be directly measured, modeling is used to simulate the sequence of events from inhalation of radon decay products to cellular injury. Such efforts in dosimetry provide valuable insights and enable research into various aspects of the cause-and-effect relationship such as the effect of long-term exposures to low levels of radon.

Epidemiologic studies or health studies of human population, whether specific segments of the population or the population in general, offer another avenue for assessing health effects of radon. Epidemiologic investigations, by their nature, have some constraints in yielding fully definitive conclusions because multiple causes of the same health effect, such as cigarette smoking and radon in the case of lung cancer, have to be carefully considered. Studies of lung cancer in the uranium miners have consistently shown increased lung cancer occurrence from exposure to radon decay products.

Studies of the general population are underway but are complicated by the fact that the history of exposure to radon is difficult to reconstruct,

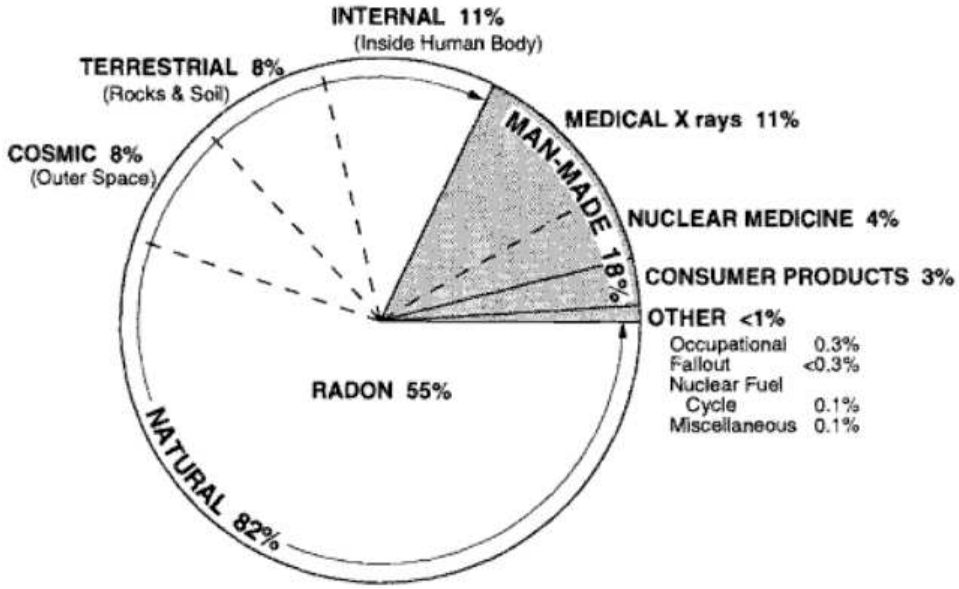


Figure 1.12: Sources of radiation exposure to U.S. population [NCRP87].

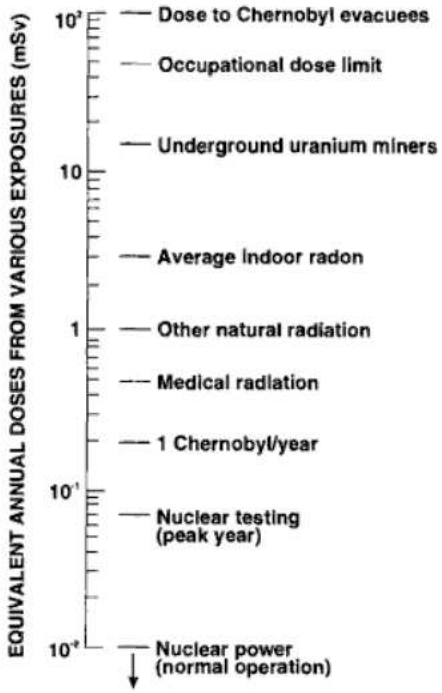


Figure 1.13: Comparison of radiation doses from different sources [Ner89].

particularly for people who have changed residences.

There are two principal exposure scenarios for radon: (i) high activities and exposure with good relationships to health impacts (e.g. uranium mining), or (ii) low activities and exposures and somewhat uncertain links between exposures and health impacts (e.g. natural background radon).

The evidence for radon's carcinogenic nature is derived from molecular, cellular, animal and human (epidemiological) studies accumulated over many decades [NAS99].

| Region | Country | Arithmetic Mean | Geometric Mean | Maximum | Geometric SD |
|---|---|---|---|---|---|
| Northern Europe | Denmark | 53 | 29 | 600 | 2.2 |
| | Estonia | 120 | 92 | 1390 | |
| | Finland | 120 | 84 | 20000 | 2.1 |
| | Lithuania | 55 | 22 | 1860 | |
| | Norway | 73 | 40 | 50000 | |
| | Sweden | 108 | 56 | 85000 | |
| Western Europe | Austria | | 15 | 190 | |
| | Belgium | 48 | 38 | 12000 | 2.0 |
| | France | 62 | 41 | 4690 | 2.7 |
| | Germany | 50 | 40 | > 10000 | 1.9 |
| | Ireland | | 37 | 1700 | |
| | Luxembourg | 110 | 70 | 2500 | 2.0 |
| | Netherlands | 23 | 18 | 380 | 1.6 |
| | Switzerland | 70 | 50 | 10000 | |
| | United Kingdom | 20 | | 10000 | |
| Eastern Europe | Bulgaria | | 22 | 250 | |
| | Czech Republic | 140 | | 20000 | |
| | Hungary | 107 | 82 | 1990 | 2.7 |
| | Poland | 41 | 32 | 432 | 2.0 |
| | Romania | 45 | | 1025 | |
| | Slovakia | 87 | | 3750 | |
| Southern Europe | Albania | 120 | 105 | 270 | 2.0 |
| | Croatia | 35 | 32 | 92 | |
| | Cyprus | 7 | 7 | 78 | 2.6 |
| | Greece | 73 | 52 | 490 | |
| | Italy | 75 | 57 | 1040 | 2.0 |
| | Portugal | 62 | 45 | 2700 | 2.2 |
| | Slovenia | 87 | 60 | 1330 | 2.2 |
| | Spain | 86 | 42 | 15400 | 3.7 |
| **Median** (Tab. 1.8 and 1.9) | | 46 | 37 | 480 | |
| **Population-weighted Average** (Tab. 1.8 and 1.9) | | 39 | 30 | 1200 | |

Table 1.9: Summary of indoor radon activities ($Bq/m^3$) in Europe [UNS00].

# Chapter 2

# Radon Occurrence and Geology

The geology of an area determines the concentration of radium and radon in the rock and soil as well as the ease with which radon can move through them. As $^{226}$Ra is one of the nuclides formed in the disintegration series from $^{238}$U, the amount of radon formed in rocks and soils depends on their uranium content. But it is not decisive in determining the radon concentration of air or water in the pores of the soil.

It is also determined by the extent to which the radon atoms formed actually emanate from the mineral grains and whether radon can leave the pore space either by diffusion or together with a flow of air or water. In addition, radon concentration in the soil air is significantly affected by the occurrence of water in the pores

Some rock types having high radon emanation potential include carbonaceous shales, glauconite sandstones, phosphorites, uranium-bearing granites, metamorphic rocks, and sheared or faulted rocks. The radon emanation potential of such rock types, combined with soil characteristics such as porosity, permeability to gas movement and moisture content, are important in determining radon potential, i.e. radon production and mobility.

## 2.1 Radon in rocks and soils

Uranium and thorium with their disintegration products, and the radioactive isotope of potassium, $^{40}$K, account for by far the greatest part of naturally occurring ionizing radiation in the human environment. Uranium, thorium and potassium are lithophile elements. This means that they occur primarily together with magmata rich in silica, i.e. the ones forming granites and syenites, and the hypabysal and volcanic rocks pegmatite and aplite and the volcanic rocks rhyolite and porphyry. Uranium and thorium can be mobilized and transported by geological processes such as metamorphosis and with hot hydrothermal solutions, to be precipitated in fissures and other permeable structures. Precipitation often takes place in a reducing environment. Examples of such environments are rocks rich in calcium and fracture filling, as well as magnesium, rocks rich in iron, and products of weathering. For instance, uranium often occurs in contact with basic rocks, in skarn in iron ores and in clay gouge. Uranium is easily leached even at normal pH

of around 5-7, and many of the large uranium ore deposits are formed by groundwater that has transported uranium which has been precipitated in a reducing environment. When the bedrock weathers and is exposed to water erosion, the heavy minerals bearing uranium and thorium are often separated. They can accumulate together with iron, titanium and zircon and form placer deposits. Areas with large recent deposits of heavy minerals include the coasts of Florida, Brazil, India and Australia, but they also occur as layers and deposits in sandstones and quartzites.

Thorium does not readily dissolve in water. The small quantity in streams and river water is precipitated almost immediately on reaching the sea. Uranium, on the other hand, has higher concentrations in sea-water than river-water. It is removed from sea-water by adsorption of clay particles and precipitation, e.g. with phosphate. Thus clays and shales nearly always have higher uranium and radium concentrations than other sedimentary rocks. Examples of sedimentary rocks with relatively high uranium concentrations are certain black shales (e.g. alum shale in Sweden and Norway, and Chattanooga shale in the USA) and sedimentary deposits of phosphate in Morocco, Jordan and Florida.

Soil consists of products broken down from the bedrock. The topsoil, or A-horizon, can be more or less mixed up with organic material. There are several different ways in which soil is formed:

- The bedrock is subjected to chemical and mechanical weathering (conditioned by temperature, running water and wind). Soil formed by chemical- and temperature-conditioned weathering remains directly on the surface of the bedrock. Examples are lateritic soils.

- The bedrock is subjected to downward crushing and wear from an immense covering of glacial ice. Till is formed in that way, as a direct product of the underlying bedrock.

- Eruption products from volcanoes form layers of ash and stone.

- Precipitation products from sea- and fresh-water. The precipitation may be chemical or biological. Examples of such soils are lime sludge, peat and diatomaceous earth.

- Loose soil is transported, sorted and redeposited by moving water, waves and wind, often with different means of transport combining. Examples of soils formed by water transport and sorting are river deposits of gravel, sand and clay. Examples of redeposited soils are sand along sea coasts, while examples of deposits formed by wind transport are loess and sand dunes.

Throughout the process of soil formation, changes take place in the original uranium and radium concentrations in the bedrock. Moreover, uranium and radium have different chemical properties and are affected to a different extent by chemical leaching. There is often a separation of uranium and radium.

Like radium, thorium is not readily dissolved and the disintegration period from $^{228}$Ra (the first decay product of $^{232}$Th) to $^{208}$Pb is about 20 years

(three half-lives of $^{228}$Ra). There is thus no time for any significant disintegration disequilibrium between $^{232}$Th and its daughter products. The relationship between the concentrations of $^{232}$Th and its daughters is not altered to any extent in chemical decomposition of the bedrock or soil horizon.

In chemical weathering, uranium can be released and removed by percolating or flowing water, to be precipitated once again in a reducing environment, e.g. soil horizons fairly rich in calcium, or at the water table. In podsol soils, uranium is depleted in the topsoil and deposited in the rust-coloured B-horizon at a depth of one, or a few, decimetres [Min83; Min90]. The B-horizon gets its pigmentation from precipitated iron and manganese hydroxide and organic matter, which act as a reducing environment for uranium and radium leached from the topsoil.

During mechanical transport by water, uranium, and to a certain extent radium, are leached from the material transported. In addition, uranium and radium are transported in the form of uranium-rich clay particles that were originally grains of uranium material. Uranium often occurs in the bedrock as very small grains of uranium mineral, e.g. coffenite $[U(SiO_4)_{1-x}(OH)_{4x}]$ and uraninite ($U_3O_8$), or absorbed on the grains or included in the lattice of zircon, apatite, titanite and other accessory minerals. Common to these is the fact that they are much smaller than the other mineral grains in the rock, in a granite mainly quartz, feldspar and glimmer. The uranium-bearing mineral grains are released during erosion and transport. The soft mineral grains are converted into clay particles and accompany the current of water, while hard grains such as zircon, monazite and titanite accompany the sand fraction. As these hard grains are heavier than most other minerals, they can be enriched by mechanical sorting and are often included in layers of heavy minerals, consisting otherwise of iron and titanium mineral.

| **Rock** | $^{226}$**Ra** (Bq kg$^{-1}$) | $^{232}$**Th** (Bq kg$^{-1}$) | $^{40}$**K** (Bq kg$^{-1}$) |
|---|---|---|---|
| Granite, normal | 25 - 80 | 20 - 80 | 620 - 1500 |
| Granite, uranium-thorium rich | 100 - 500 | 40 - 400 | 1200 - 1900 |
| Gneiss, sedimentary | 25 - 125 | 20 - 80 | 620 - 1500 |
| Gabbro, dolerite | 1 - 25 | 5 - 40 | 25 - 1000 |
| Sandstone | 1 - 60 | 5 - 40 | 100 - 1500 |
| Limestone | 5 - 40 | 0.5 - 10 | 30 - 160 |
| Shale | 10 - 125 | 5 - 60 | 300 - 1800 |
| Black Shale | 10 - 2000 | 10 - 50 | 300 - 1800 |
| Alum Shale | 125 - 4300 | 10 - 40 | 1000 - 1800 |
| Uranium ore | 12000 - 25·10$^5$ | | |
| Average | 35 | 38 | 775 |

Table 2.1: Range of concentrations of $^{226}$Ra, $^{232}$Th and $^{40}$K in some common rocks and uranium ores. Higher and lower concentrations occur occasionally. Averages from Kogan *et al.*, [Kog71].

An effect of sorting by water is that uranium and radium concentrations gradually decrease, and more so the greater the degree of sorting; so that they are very low in well-sorted, fine-grain soils such as quartz sand. Concentrations also increase with an increase in the clay mineral content.

| **Soil type** | $^{226}$**Ra** (Bq kg$^{-1}$) | $^{222}$**Rn** (Bq m$^{-3}$) |
|---|---|---|
| Till or residual soils with normal radium content | 15 - 65 | 5000 - 30000 |
| Till or residual soils with fragments of granite | 100 - 125 | 10000 - 60000 |
| Till with fragments of uranium - rich granite | 125 - 360 | 10000 - 200000 |
| Gravel | 30 - 75 | 10000 - 150000 |
| Sand | 5 - 35 | 2000 - 20000 |
| Silt | 10 - 50 | 5000 - 60000 |
| Clay | 10 - 100 | 10000 - 100000 |
| Soils containing fragments of alum shale | 175 - 2500 | 50000 - $>10^6$ |

Table 2.2: Normal concentrations of $^{226}$Ra and $^{222}$Rn in soils, measured at a depth of 1 meter.

As a result of the separation of uranium and radium that takes place when soil is formed, transported and sorted, radon concentrations in groundwater and soil air may differ substantially in different soil types. Thus they vary in different horizons in the same soil profile.

Table 2.1 gives the uranium concentrations in some typical rocks and uranium deposits and table 2.2 the concentrations of radium and radon in the soil air of some soils.

## 2.2 Formation and emanation of radon

There are three differing theories about how radon and thoron emanation takes place from the mineral lattice or molecule in which the radon or thoron atom is formed.

When $^{226}$Ra disintegrates, a radon atom and an alpha particle are formed, the latter being ejected from the decaying radium atom. When the alpha particle is ejected, a recoil effect arises. This dislodges the radon atom from the place in the mineral lattice or molecule where the radium atom was. The distance the radon atom can then move in a mineral grain of normal density is about 0.02 - 0.07 $\mu$m. It is this very movement of the radon atom that enables radon to emanate from a mineral grain [Fl80, Ki71, Ta80].

The radon atom could be ejected from the grain as a result of the movement, provided it was close to the surface, and was kicked in an outward direction. In the same way, the radon atom could be ejected to a micro-fissure in the mineral grain. Further transport in the micro-fissure is by diffusion. The process is illustrated in fig 2.1 [Dur97].

Other researchers have assumed that radon could emanate from the mineral grain by diffusion through the mineral lattice or by leaching by water through radiation damage in the mineral grain [Fle80; Fle82].

Radon and thoron concentrations in soil air or groundwater are determined by the radium concentration in surrounding soil and bedrock, how many of the radon atoms emanate to the pore space from the mineral grain in which they are formed, and the porosity and water content of the soil. In

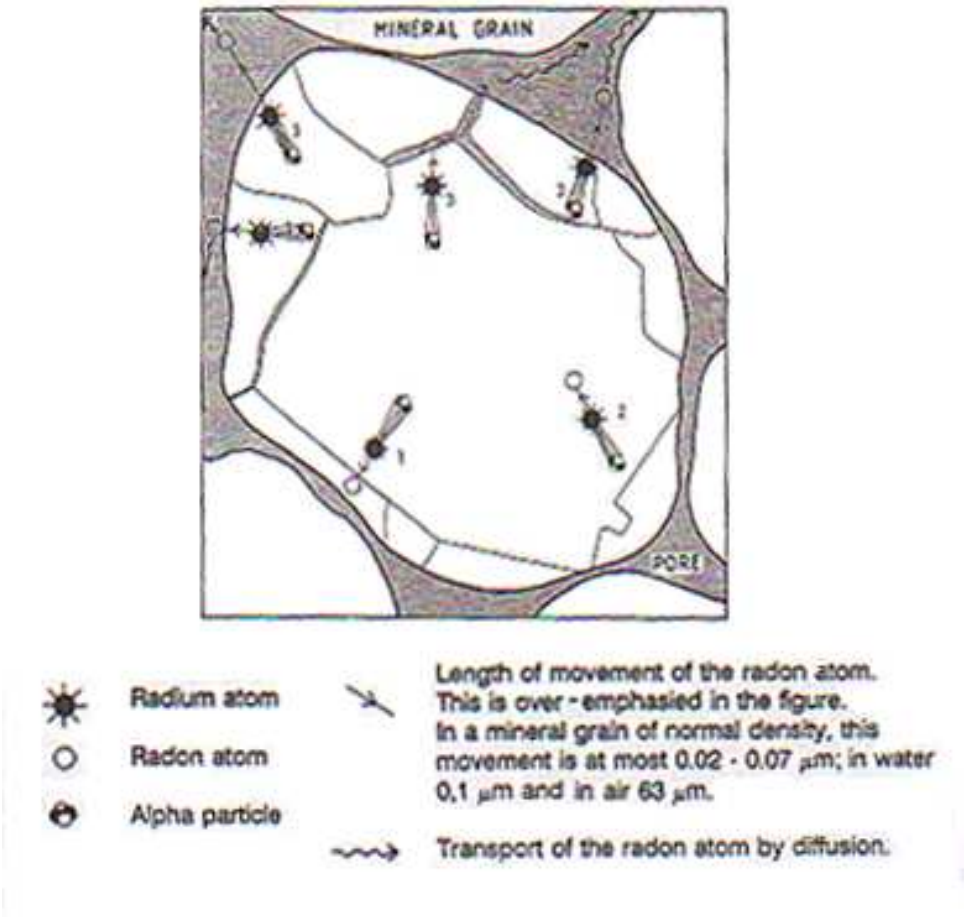


Figure 2.1: Principles of radon emanation from a mineral grain [Tan80]. *Case 1*: When radium decays, a radium atom and an alpha particle are formed. The radon atom is moved into an adjacent crystal by a recoil effect from the ejected alpha particle. *Case 2*: The radon atom is moved through the crystal. *Case 3 and 4*: The radon atom is moved from the crystal to a micro-fissure or the air in an adjacent pore. It is assumed that further transport is by diffusion.

addition, the radon concentration is affected by how much of the radon is removed or supplied by diffusion and transported by the movement of the soil air or water or of ascending gases such as CO2 and CH4. The permeability of the soil and the rock are of decisive importance for transporting radon.

If the radium concentration, porosity and emanation for a type of soil are known, the maximum radon concentration that can occur in the pore air can be calculated from equation 2.1 [And83].

Equation 2.1 is used to calculate the maximum radon concentration in the soil's pores when they are completely filled with either air or water

$$C_{max} = Aed\frac{(1-p)}{p} \tag{2.1}$$

where $C_{max}$ is the radon activity concentration (Bq $m^{-3}$) in pore volume with absolutely no ventilation (0 ach, air changes per hour); A is specific activity (Bq $kg^{-1}$); $e$ is the emanation (i.e. the fraction of all radon and thoron atoms formed that emanate to the pore space); $d$ is compact density (kg $m^{-3}$), (normal for mineral soils: 2700 kg $m^{-3}$); and $p$ is the porosity, ratio of pore volume to total volume. The value of $C_{max}$ increases as the value of $p$ falls.

This formula is not fully universal. When the concentration of radon atoms per unit of volume in the pore equals that in the surrounding mineral grain, passage by diffusion of radon atoms to the pore ceases if they cannot be transported further. In other words, the concentration of radon gas per unit of volume in the pore cannot be greater than the concentration in the mineral grains. This occurs when

$$p < e. \tag{2.2}$$

In soil above the water table, radon can be transported from the pore by diffusion, or by soil air or groundwater in motion. In soil below the water table, this possibility is strictly limited, as the radon in the water does not have a diffusion lenght greater than 5 cm. In practice, the concentration in soil horizons below the water table will continually maintain the same level, equal to the maximum that can be formed with the radium concentration, porosity and emanation for the soil in question.

The smaller the particle in which the radon atom is formed, the greater the chance of the atom escaping from it. The proportion of radon that emanates from a material is therefore greater the finer grained or more porous it is.

Radon emanation must be seen in relation to the distance the radon atom can be moved by the recoil effect (0.02-0.07 $\mu$m) and the grain size of the soil. Examples are:

As can be seen, the clay particles are so small that a large fraction of the radon atoms formed should emanate from them to ambient air or water in the pores when the radium atom disintegrates. This can explain why such high emanations as 40-70% of all radon formed, have been measured from clay.

It is more difficult to explain how emanation from dry sand and gravel can amount to 30%. Something other than the recoil effect is required to

| Type of Soil | Grain Size ($\mu$m) |
|---|---|
| fine clay | <0.6 |
| coarse clay | 0.6 - 2 |
| silt | 2 - 60 |
| sand | 60 - 2000 |
| gravel | 2000 - 60000 |

Table 2.3: Grain size of different type of soil.

| Type of Soil | e (%) |
|---|---|
| Gravel | 15 - 40 |
| Sand | 15 - 30 |
| Clay | 30 - 70 |
| Crushed rock | 5 - 15 |
| Crushed uranium-rich granite | 15 - 30 |

Table 2.4: Emanation of radon atoms to the pore air, e (expressed as a percentage), in various soils and crushed rocks.

explain such a high figure. Ek and Ek [Eks95] have studied the radon concentration in different particle sizes of gravel and coarse sand. They found two reasons for the enhanced emanation. One is that radium has been absorbed in the fine fractions of the soil (<0.15 mm), which have 3x to 8x higher radium concentrations than the coarser fractions. Another explanation is that radium atoms have been precipitated on the surface of the grains and fissures in them. Both these ways of occurrence facilitate high emanation. The conditions are results of the selective leaching, transport and precipitation of uranium and its daughter nuclides that takes place in weathering of the mineral grain.

Table 2.4 shows radon emanation in various soils and crushed rocks. The data are taken from tests reported in the literature [Bat75; Mak92; Rob95] and investigations undertaken by the Swedish Geological Co., the Swedish Geotechnical Institute, and the Swedish National Testing Institute [Hid83].

Thoron emanation from soil has been studied, among others, by Megumi and Mamuro [Meg74]. They found that about 10% of the thoron formed emanates from sand, silt and clay produced by the erosion of granite. As thoron and its daughter nuclides do not readily dissolve in water at a normal pH, and the nuclides have such short half-lives, chemical leaching and precipitation of thorium and its daughter nuclides is of little significance for radon emanation.

One of the factors affecting how large a part of the radon formed emanates from a rock or soil, is the manner in which the uranium or thorium occurs in the rock or rock fragments in the soil. If the uranium is found in the lattice of other minerals, e.g. feldspar, magnetite, apatite, allanite or zircon, radon emanation from the rock is relatively small. If, on the other hand, the uranium forms a uranium mineral such as uraninite ($U_3O_8$), uranothorite, or coffenite [$U(SiO_4)_{1-x}(OH)_{4x}$], radon emanation is substantially greater. The latter minerals often occur at the boundaries between larger grains of quartz and feldspar, or between strata in biotite, which facilitates radon emanation. It is also facilitated by the fact that uranium minerals

are relatively easily weathered, and many of them tend to be metamictized as a result of their own radioactivity over geological time periods. In granites with a normal uranium concentration of 4-10 ppm U (50-125 Bq $kg^{-1}$ $^{226}Ra$), it is most common for the uranium to be included in the lattice of other minerals, while it is more common for the uranium to occur in separate uranium minerals if the concentration is higher.

The chances of emanation from a rock or soil are greater the more porous the material is, which allows a greater diffusion of the radon gas. Emanation in relation to radium concentration is low, for instance, from an uncrushed, unweathered alum shale, which is a dense rock whose pores are filled with kerogen and sometimes oil. Emanation in relation to radium concentration can be large, on the other hand, from a coarse-grained granite. This is confirmed by measurements made by the Swedish Geological Survey from samples of unweathered alum shale and granite rich in uranium.

Radon emanation from a rock increases with crushing and weathering because the chances of emanation from the individual mineral grain increase. Emanation from a soil is thus considerably greater than from a coarsely crushed rock, provided they consist of the same type of material.

## 2.3 Radon concentration, emanation and water content

The concentration of radon gas in the air in soil pores increases with increasing water content in the pores. This is because of the equilibrium relationships between the ratio of radon in air to radon in water, which is dependent on the temperature. It is also due to the fact that the emanation of radon to the pore space increases with moisture.

In a closed volume with equal volumes of air and water, and at temperature of +15°C, the radon concentration is three times greater in the air than in the water [All76; Tan91]. As the number of radon atoms in the pore air in a soil is constant if the emanation in the soil is constant and no radon is supplied to or leaves the pore volume, an increase in the quantity of water in the pore volume means an increase in the radon concentration in the remaining air. If the pores were filled with 75% water and 25% air, for instance, the radon concentration in the pore air would be twice as great as when the pores were entirely filled with air.

A model incorporating temperature effects on $^{222}Rn$ concentration in the pore air at different water content is given by Washington and Rose [Wa90] for depths below which diffusional transport of radon to the surface is negligible, by the following expression:

$$C_{max} = \{Aed\,(1-p)\,/p\}\,[F\,(K_T - 1) + 1] \tag{2.3}$$

where $C_{max}$ is the radon activity concentration (Bq $m^{-3}$) in a pore volume with absolutely no ventilation; $e$ is the emanation fraction of all radon atoms formed that emanate to the pore space; $d$ is the compact density (kg $m^{-3}$) (normal for mineral soils: 2700 kg $m^{-3}$); $p$ is the porosity, ratio of pore volume to total volume; $F$ is the water fraction; and $K_T$ is the partition coefficient of $^{222}Rn$ between units of air and water.

$C_{water}/C_{air}$ values vary from 0.525 at 0°C to 0.226 at 25°C. Variations in the $^{222}$Rn concentration of up to a factor of about four can be accounted for as being due to effects of F and $K_T$. For warm (25°C) and very moist (F = 0.95) soil with A = 30 Bq kg$^{-1}$, $e$ = 0.2, and $d$ = 2700 kg m$^{-3}$, the $^{222}$Rn concentration is calculated to be 78.3 kBq m$^{-3}$; but when cold (0°C) and dry (F = 0.05), the $^{222}$Rn activity concentration is calculated to be 21.2 kBq m$^{-3}$.

The relationships between radon concentrations in pore water and pore air with different amounts of water in the pores and at different temperatures, can also be seen from figure 2.2. The closer they are to the water table, the more the pores are filled wuth water. It follows that radon concentration in the pore air increases the shorter the distance to the water table.

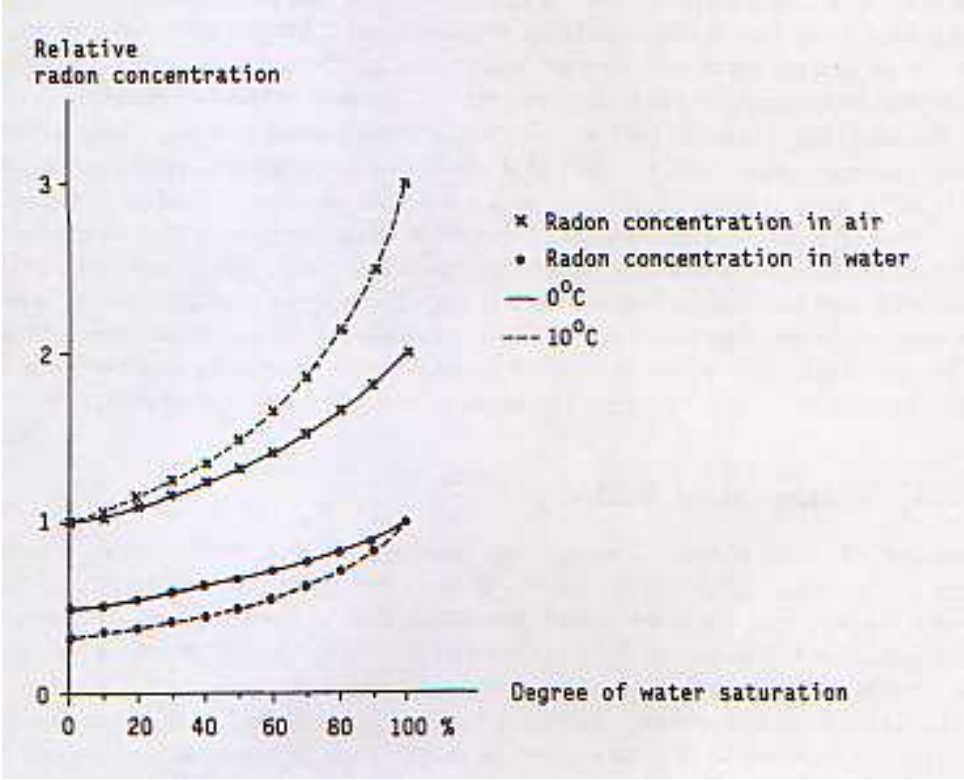


Figure 2.2: Radon concentrations in air and water in the pores with varying moisture content in the soil [Ake90].

In a soil horizon below the water table, all pores are filled with water. Therefore all the radon atoms emanating from the soil go into water. As the diffusion length of radon in water is small - the coefficient is $10^{-9}$ m$^2$ s$^{-1}$, compared to that for air of $10^{-5}$ m$^2$ s$^{-1}$ - only a small part of the radon can be moved by diffusion. Normally, there should be equilibrium in a water-filled pore between radon emanating to the pore and radon that disintegrates. This means that the concentration in a completely filled pore is equal to the maximum that can be formed in the soil's pores when they are completely filled with water and at the porosity in question. This is so, provided the water does not move more than a few centimeters, from the site where the radon was formed.

| Medium | D ($m^2s^{-1}$) |
|---|---|
| Air | $10^{-5}$ |
| Boulders - coarse gravel | $10^{-5}$ - $5 \cdot 10^{-6}$ |
| Dry sand | $10^{-5}$ |
| Moist sand | $2.5 \cdot 10^{-6}$ |
| Till | $5 \cdot 10^{-7}$ - $2.5 \cdot 10^{-6}$ |
| Clayey till | $8 \cdot 10^{-8}$ |
| Water | $10^{-9}$ |

Table 2.5: Diffusion coefficients, $D$, for $^{222}$Rn. Data from UNSCEAR (1982) and various reports.

Many researchers have shown that emanation and exhalation from a soil or crushed rock or a concrete slub increase as the pores get filled with water. The radon content of the pore is thus considerably lower in dry soil than in moist soil and radon exhalation lower from a dry than a moist concrete. Markkanen and Arvela [Mak92] have shown that there is an average emanation increase of 2-3 times in different soil samples if their water content is increased from 0% to 5%, with the various soils behaving differently.

Tanner [Tan80] suggests that the reason for increasing radon emanation with increasing water content ensues from the fact that the radon atom ejected on disintegration is retarded if there is water in the pore space and thus obstructed from penetrating into the lattice of a nearby mineral grain. Schery and Whittlestone [Scr89] have shown that sorption of radon occurs on the mineral grains in a dry soil. Of the materials studied, those with high external surface area such as clays had a larger sorption capacity, whereas the sorption values of certain coarse-grained materials such as quartz sands were too small to be measured. The effect of sorption decreases with increasing moisture, and at a moisture content of 10% by weight the sorption was below the limit of detection.

## 2.4 Transport of radon through soil

Transport of radon through the soil takes place by diffusion and/or with air ambient gases like $CO_2$ and $CH_4$ or water moving in the soil horizons. Moving air can be driven by wind, changes in air pressure and percolating rain or melted snow. Differences of temperature in the soil could be a further cause. The outflow of soil air which causes the snow to melt at certain places in gravel ridges such as eskers and above fractures in the bedrock, is assumed to result from the transport of warmer air through the soil or fractures. Owing to the stack effect in ridges, such transport of soil air can be a contributory cause of the high radon concentrations common in buildings on eskers. Soil air can also be transported and conducted to buildings along culverts and cable trenches. Often, the cause of the transport is lower pressure inside the building in relation to the atmosphere outside and in the ground.

The diffusion of radon through the ground is related to permeability, which is dependent on grain-size distribution, degree of compaction and the water content of the soil. Table 2.5 lists diffusion coefficients for radon in some soil types [UNS82]. It shows that radon diffuses through coarse gravel

about as easily as in the air, while there is very little diffusion through a water-saturated clay (ten thousand times less than in the gravel).

If the soil pores are completely filled with water, the soil has the same diffusion coefficient as water.

As radon has a limited life, the greater part of it will disintegrate after a certain diffusion distance: 90% of the radon emanated from a radon source, e.g. a deep-lying soil horizon, and transported by diffusion, will have decayed after a distance of 5 cm in water, about 2 m in sandy soil with a normal moisture content and 5 m in air [UNS82].

The transport distance for thoron is insignificant, as its half-life is no greater of 56 seconds.

Diffusion of radon through the soil up to the atmosphere above the surface of the ground is highly important in determining the radon concentration in the soil air at different depths.

# Chapter 3

# Radon and Groundwater

Groundwater has long been an active area of research driven by its importance both as a societal resource and as a component in the global hydrological cycle. Key issues in groundwater research include inferring rates of transport of chemical constituents, determining the ages of groundwater, and tracing water masses using chemical fingerprints. While information on the trace element pertinent to these topics can be obtained from aquifer tests using experimentally introduced tracers, and from laboratory experiments on aquifer materials, these studies are necessarily limited in time and space.

Regional studies of aquifers can focus on greater scales and time periods, but must contend with great complexities and variations. In this regard, the isotopic systematic of the naturally occurring radionuclides in the U- and Th- decay series have been invaluable in investigating aquifer behavior of U, Th, and Ra. These nuclides are present in all groundwaters and are each represented by several isotopes with very different half-lives, so that processes occurring over a range of time-scales can be studied. Within the host aquifer minerals, the radionuclides in each decay series are generally expected to be in secular equilibrium and so have equal activities [Bou03]. In contrast, these nuclides exhibit strong relative fractionations within the surrounding groundwaters that reflect contrasting behavior during release into the water and during interaction with the surrounding host aquifer rocks.

Radionuclide data can be used, within the framework of models of the processes involved, to obtain quantitative assessments of radionuclide release from aquifer rocks and groundwater migration rates. The isotopic variations that are generated also have the potential for providing fingerprints for groundwaters from specific aquifer environments, and have even been explored as a means for calculating groundwater ages.

Since radium is widely distributed in the earth's crust, it is found in minerals that come in contact with groundwater. Radon, which is soluble in water, is found in groundwater and, in some cases, significant concentrations have been observed. These concentrations appear to depend upon the structure of the aquifer and the distribution of the radium in the rock matrix. In many cases, these radon-in-water concentrations are *unsupported*, meaning that there is relatively little radium dissolved in the water giving rise to the radon. Rather, radon is transferred into water directly from the radioactive decay of radium in the solid materials in the aquifer, and the dissolved radon

is then transported with the water.

## 3.1 The groundwater resource

Groundwater may be defined as subsurface water that occurs beneath the water table in soils and geologic forms that are fully saturated [Fre79]. It is an integral part of the hydrologic cycle, and any approach to groundwater problems should recognize this. Groundwater is not only an important natural resource but also an essential part of the natural environment.

The global hydrologic cycle consists of the movement of water between the oceans and other surface water, the atmosphere and the land. A part of the precipitation, either as rainfall or melting snow, infiltrates the ground and percolates down through the unsaturated soil, known as the aerated zone, to the zone of saturation or the water-table level. Table 3.1, an estimate of the water balance of the world, shows the relative volumes of water contained in each part of the hydrologic cycle. Only 2.7% of all the water on the planet is fresh, and of that only 0.36% is easily available to users [Leo74].

The ability of an aquifer to store and transmit water is a function of its permeability and porosity [Fre79]. When the saturated substratum is sufficiently permeable to store and transmit significant quantities of water, the geological formation is called an aquifer. There are two main types of aquifers: confined and unconfined. An unconfined or water-table aquifer contains water under atmospheric pressure; the upper surface of the water is called the water table and may rise and fall according to the volume of water stored, which is dependent upon seasonal cycles of natural recharge. A perched aquifer is one in which a limited layer, or lens, of impermeable material occurs above the water table, forming a thin zone of saturation above it. It is a type of water-table aquifer. The second major category of aquifer is the confined, or artesian, aquifer. These are bounded top and bottom by layers of relatively impermeable geologic formations, termed aquitards or confining layers. The aquifer is completely saturated with water that is under greater than atmospheric pressure. An artesian aquifer is not recharged everywhere uniformly, but in one or more general recharge areas.

Aquifers can occur in unconsolidated materials such as sand and gravel or in consolidated material or bedrock. The latter may consist of carbonate rock, volcanic rock, or fractured igneous, metamorphic and sedimentary rocks. Sand and gravel aquifers usually contain the most groundwater, but high-yield wells can also occur in carbonate and volcanic rocks.

## 3.2 Groundwater movement

Groundwater moves in response to gravity, pressure and friction, the first two driving the water, the latter resisting to the motion. Due to the complexity of the channels through which groundwater flows, it is difficult to construct a model of the movement of groundwater at a microscopic level. The french engineer Darcy, however, formulated an empirical law in the mid-nineteenth century that effectively averages the microscopic complexities, providing a macroscopic model for groundwater movement. Darcy's law relates the rate at which groundwater flows across a surface to the rate of change of energy

| Parameter | Surface Area ($km^2$)$\times 10^6$ | Volume ($km^3$)$\times 10^6$ | Volume (%) | Equivalent Depth (m) | Residence Time |
|---|---|---|---|---|---|
| **Oceans and Seas** | 361 | 1370 | 94 | 2500 | $\sim$ 4000 yrs |
| **Lakes and Reservoirs** | 1.55 | 0.13 | $< 0.01$ | 0.25 | $\sim$ 10 yrs |
| **Swamps** | $< 0.1$ | $< 0.01$ | $< 0.01$ | 0.007 | 1-10 yrs |
| **River Channels** | $< 0.1$ | $< 0.01$ | $< 0.01$ | 0.003 | $\sim$ 2 wks |
| **Soil Moisture** | 130 | 0.07 | $< 0.01$ | 0.13 | 2 wks - 1 yr |
| **Groundwater** | 130 | 60 | 4 | 120 | 2 wks - 10000 yrs |
| **Icecaps and Glaciers** | 17.8 | 30 | 2 | 60 | 10 - 1000 yrs |
| **Atmospheric Water** | 504 | 0.01 | $< 0.01$ | 0.025 | $\sim$ 10 days |
| **Biospheric Water** | $< 0.1$ | $< 0.01$ | $< 0.01$ | 0.001 | $\sim$ 1 wk |

Table 3.1: Estimate of the water balance of the world [Fre79]. (The equivalent depth is computed as though storage were uniformly distributed of the entire surface of the Earth.

of the groundwater along the flow path. Under ideal homogeneous isotropic geologic groundwater conditions, the average linear groundwater velocity, $\bar{v}$, can be expressed by the Darcy relation:

$$\bar{v} = -\frac{K\,(dh/dl)}{n} \tag{3.1}$$

where $K$ is the hydraulic conductivity, $dh/dl$ is the hydraulic gradient and $n$ is the transport porosity.

For both granular and fractured media, the same equation is used to compare values for average linear groundwater velocity. The great difference is in the value of $n$. For granular media $n$ nearly represents the total porosity; in fractured rock or clay $n$ represents the total void space in connected fractures within a unit volume of media. The value of $n$ in granular material is usually between 0.3 and 0.45; in fractured material $n$ is usually very small, of the order of $10^{-2}$ or $10^{-4}$. When the values of $K$ and $dh/dl$ are similar in granular and fractured media, the average linear groundwater velocity may be orders of magnitude larger in fractured media than in granular media.

## 3.3 The behavior of U- and Th-series nuclides in groundwater

The highest activities, typically observed in groundwater, are for $^{222}$Rn, reflecting the lack of reactivity of this noble gas. Groundwater $^{222}$Rn activities are controlled only by rapid in situ decay and supply from host rocks, without the complications of removal by adsorption or precipitation.

The actinide U, which is soluble in oxidizing waters, is present in intermediate activities that are moderated by removal onto aquifer rocks. The

long-lived parent of a decay series, $^{238}$U, does not have a radioactive supplier, while $^{234}$U is a radiogenic nuclide; both of these nuclides have half-lives that are long compared to groundwater ages and so are generally not substantially affected by decay within aquifer systems.

The alkaline earth Ra, and to a greater extent the less soluble actinide Th, are readily removed from groundwater by water-rock interactions, and so are strongly depleted. Both of these elements have very short-lived as well as longer-lived isotopes, and so their isotope compositions reflect processes over a range of time-scales. Overall, since the set of nuclides in each decay series are tied by decay systematics, with daughter nuclide productions and distributions dependent upon parent distributions, combined studies of these elements can generate considerable information regarding radionuclide water-rock interactions and weathering release rates.

Research into the behavior of radionuclides continues to be active, greatly motivated by the necessities of understanding and predicting migration of contaminant actinides and related species.

In general, quantifying aquifer parameters that control trace element behavior are difficult at many sites by direct measurements, since the host rocks typically cannot be as readily sampled as groundwater, and average values for host rocks recovered from boreholes are difficult to obtain. However, decay series systematics of nuclides in groundwater provide the potential for quantifying some chemical parameters of water-rock interaction from direct measurements of waters alone. Various studies have attempted to model the transport of the range of U, Th, Ra, Rn and Pb radioisotopes in groundwaters by combining the systematics of the nuclides within the decay chains, and so providing a framework for calculating such critical parameters as retardation factors. These particular elements have the additional appeal of providing natural analogues for radioactive wastes, so that evaluations of the transport behavior of U and Th series nuclides can have predicting power for assessing the possible migration of low level anthropogenic waste nuclides in any environment. A key difference is in the supply functions; where the effects of the supply rate of naturally occurring nuclides within the aquifer can be distinguished, the controls on nuclides introduced only at the aquifer recharge boundary can be quantified. Many of the earlier advances in modeling naturally occurring nuclides have been summarized by Osmond and Cowart [Osm92], Ku et al. [Ku92] and Ivanovich et al. [Iva92]. While there are many different approaches that have been used to infer radionuclide behavior, these are all based on the fundamental connections between nuclides by radioactive decay, and simple modeling of known processes of input by weathering and recoil into groundwater as well as interaction with aquifer host rock surfaces by sorption and precipitation.

## 3.4 The behavior of Radium in groundwater

An important set of naturally occurring radiotracers is the radium quartet, including the two short-lived $^{223}$Ra ($t_{1/2}$ 11.4 d) and $^{224}$Ra ($t_{1/2}$ 3.66 d), and the two long-lived $^{226}$Ra ($t_{1/2}$ 1600 y) and $^{228}$Ra ($t_{1/2}$ 5.7 y).

The general behavior of radium has been examined under laboratory conditions and in various environments [Osm92]. A major goal of field studies

of Ra isotopes have aimed at obtaining bulk, in situ values of adsorption rates and so the retardation factors.

In low salinity solutions, Ra occurs as uncomplexed $Ra^{2+}$, while significant complexing as $RaSO_4$, $RaCO_3$ and $RaCl^+$ will only occur in brines with high concentrations of the respective inorganic ligand [Por03].

Adsorption exerts a strong control on Ra in dilute groundwater. Adsorption constants are strongly dependent upon the type of substrate, solution composition (e.g. Eh, pH and other cations) and temperature [Ben90]. Decreases in adsorption have been observed due to increases in salinity [Zuk87; Kri91; Stu01]. Reasons suggested for this include competition by other abundant cations for available adsorption sites, increases in mineral surface charge [Mah91], increases in the stability of inorganic complexes [Ham88], and the presence of strong organic complexes [Lan85]. Where there are strong changes in groundwater salinity, e.g. by mixing, Ra may be deposited on aquifer surfaces and so may be a local source of $^{222}Rn$ [Moi00].

Initial inputs to groundwater can occur due to weathering in the vadose zone. There are few data of Ra in natural soils (e.g. not impacted by mining wastes). Partitioning onto soil solids is quite strong, but it is not uniform and is hard to predict due to the effects of precipitation reactions, bioturbation, and varying distributions of organic matter and clays. Groundwater characteristics will reflect vadose zone inputs for some distance below the water table depending upon the half-life of the isotopes [Tri00].

Extensive use is made of the radium quartet by the marine community as tracers of submarine groundwater discharge and seawater re-circulation processes [Lov08; Moo96; Moo00; Moo08]. However, few studies have employed radium isotopes for groundwater/surface water interactions studies in freshwater environments. Whereas saline groundwater circulating though coastal aquifers has relatively high radium concentrations and even small inputs of that water into a coastal zone can be recognized as a strong positive radium signal, in freshwater aquifers radium is mainly adsorbed to the aquifer matrix, i.e. is not in solution in the groundwater.

However, a few studies have demonstrated applicability of radium isotopes as a freshwater tracer [Cut86; Eik01; Kra05], demanding further studies that specify the respective methodological advantages and limitations in order to establish innovative approaches using the radium quartet in terrestrial environments.

## 3.5 Radon as aqueous tracer

Radon is continuously produced via $\alpha$-decay of its parent nuclide radium, which is commonly found in soil and aquifer material. Hence, radon is a ubiquitously occurring natural component of groundwater, occurring as dissolved gas. The aquifer specific equilibrium radon concentration in groundwater ($C^\infty$) can be quantified as follows [Ans72]:

$$C^\infty = \frac{\epsilon A_{Ra} \rho_d}{n}. \tag{3.2}$$

Equation 3.2 shows that equilibrium radon concentration in groundwater is governed by just a few aquifer characteristics. The radium activity concentration of the aquifer matrix, $A_{Ra}$, determines the total amount of radon

produced in the mineral matrix. The dimensionless emanation coefficient, $\epsilon$, quantifies the share of the produced radon atoms that emanate into the pore space. The two matrix parameters, porosity $n$ and dry density $\rho_d$, are influential because a higher porosity at a given density results in a lower radon concentration in the pore space [Tan64]. Equilibrium radon concentrations in groundwater normally range between 10 and 100 Bq/L [Cot87].

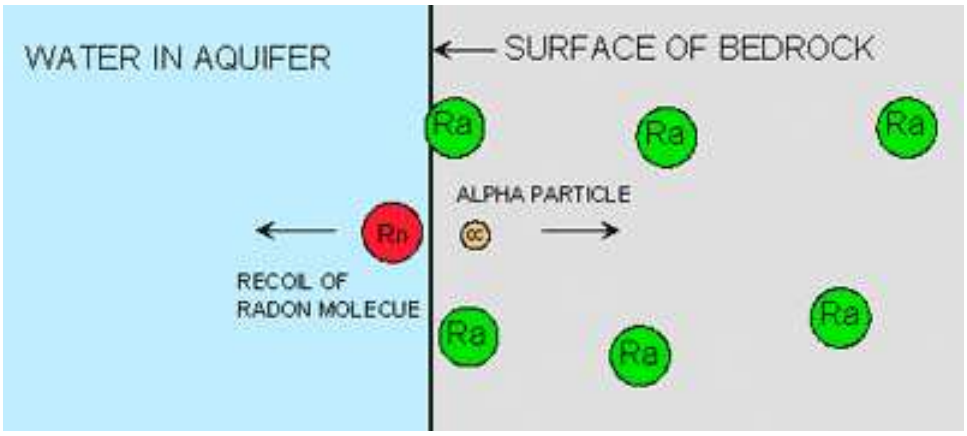


Figure 3.1: The injection of radon into the water will only occur as long as there is a fresh surface of radium next to the water.

The chemical and physical properties of radon and its behavior in the groundwater allow for its use as naturally occurring aqueous tracer.

As early as in 1918 Perret [Per18] reported that the radon concentration in a spring water may depend on the discharge. A generation later, during the hunt for uranium ores, this knowledge seems to have been lost [Pay53]. Sampling took place as if radon in spring water would be constant over time, depending only on the host rock. Still another generation later, in the wake of alarming news on adverse health effects of indoor radon, radon in water became fashionable again.

Later however, Hoehn and Von Gunten [Hon89] recognized radon's potential as a tracer to study river-water infiltration into a gravel bed. Claims about the importance of soil radon for the radon concentration in karst waters were published [Sur91], but Monnin et al. [Mon94] still considered deposits in karst channels and in fractures as a possible radon source.

Monthly sampling of 15 springs in western Switzerland [Eis95], most of them karst springs, during 1993 and 1994, showed large temporal variations and in general a positive correlation between radon concentration and discharge.

First continuous measurements [Sur93; Sur94] confirmed the claim that the radon produced in the soil covering a karst system is the most important source for radon peaks observed during storms [Eis95]. A new generation of radon monitors made it possible to start continuous measurements even in caves.

Besides the advantage that radon is a natural constituent of groundwater and has therefore not to be injected into the aquifer for the sake of a tracer experiment, the following characteristics make it generally suitable as aqueous tracer [Sch06]:

- Anthropogenic contamination of the groundwater with regard to radon, as it is possible with regard to many salt tracers, can be excluded.
- The radon concentration in the groundwater is not influenced by changing $pH/E_H$ conditions as it is observed for some fluorescent tracer dyes.
- The radon concentration in surface waters is not influenced by photolytic decomposition as observed for some fluorescence tracer dyes.
- As a result of its virtually inert behavior, radon retardation due to physical/chemical interaction with the aquifer matrix or due to flocculation/precipitation, as it is observed for many salt tracers or fluorescent tracer dyes, can be neglected.
- In contrast to many salt tracers, radon can be detected very precisely and selectively also at very low concentrations, due to its radioactive nature.

Because of the chemical inertness of radon, its transport in groundwater systems is controlled only by molecular diffusion and by the flow of groundwater itself. With a diffusion coefficient of $10^{-5}$ cm$^2$ s$^{-1}$ in water, diffusion is an important transport mechanism at scales on the order of $10^{-2}$ m.

Groundwater flow is the dominant mechanism by which radon is transported in aquifers. The limiting factor in the transport length of radon in groundwater is its half-life. In 30 days, the radon content of groundwater will be less than 1% of its original activity. The only other process that has any other significant effect on radon, once it is in solution in groundwater, is outgassing either by exposure to large air spaces, such as in caves and cavities in limestone, or by elevated temperature.

Radon is most soluble in organic liquid phases (when compared to gas and water phases) and has a strong affinity to non-aqueous phase liquids (NAPLs) [Sch07]. That property makes it applicable as naturally occurring partitioning tracer for assessing residual NAPL contamination of aquifers. In a NAPL contaminated aquifer, radon dissolved in the groundwater partitions preferably into the NAPL. The magnitude of the resulting radon deficit in the groundwater depends on the NAPL-specific radon partition coefficient and on the NAPL saturation of the pore space. Hence, if the partition coefficient is known, the NAPL saturation is attainable by determination of the radon deficit.

## 3.6 Modeling aquatic pathways

Practically useful models in radioecology must satisfy some key features that make them simple and reliable tools for environmental management:

- they must provide a good predictive power;
- they must be characterized by a relevant and simple structure, i.e., involve the smallest possible number of driving variables;
- the values of the necessary driving variables should be easy to access and/or to measure;

- the models must be validated for a variety of circumstances showing a wide range of environmental characteristics.

In broad terms, the variables used in environmental models may be divided into two categories:

1. variables for which site-specific data must be available such as lake volume, mean depth, water discharge, amount of suspended particulate matter in water, etc.;

2. variables for which generic (= general) values are used due to the lack of site-specific data, e. g., the sedimentation rate and/or rates for internal loading (like diffusion and advection rates).

The variables belonging to the first category are often called *site-specific variables*, or *environmental variables* or *lake/river specific variables*. They can generally be measured relatively easily and their experimental uncertainty should not significantly affect the overall uncertainty of the model predictions of the target variable(s). The second category, the *model variables* or *model constants*, are often difficult to access for each specific system, such as the transfer rates from the sediment to the water, the deposition velocity of X from water to sediments, the migration rate from catchment to lake, etc. The model variables may contribute significantly to the model uncertainty unless validated and reliable sub-models for their generic values have been established from critical tests.

## 3.7 Groundwater mixing in karts systems

Karst systems are an interesting example of groundwater mixing where a dual porosity generally exists. Connected porosity occurs in small-scale fissures and the porous matrix that provide much of the storage in the system and which contribute to baseflow. A second porosity can be identified in the high-velocity conduits through the system, which are more active during storm events. Stable isotopes can serve to serve to distinguish flow through these two systems.

Rank *et al.* [Ran92] have measured the $^{18}O$ contents of local precipitation and the discharge from two karst springs. Tritium contents in the groundwaters are used in a dispersion model to show that mean circulation times in the fissure/matrix porosity are on the order of 4.5 years (Wasserlamquelle spring) and 2.5 years (Siebenquellen spring). However, estimating the transit time and contribution to discharge for flow in the high-velocity conduits requires high-frequency sampling program. This can be provided by the seasonal variations in $^{18}O$. The authors used these data in a tracer mass balance to examine the contributions of high-velocity conduit flow to discharge from the karst. They found that this flowpath has a mean transit time of 2 months.

Despite the attenuation of seasonal variations in these two groundwater systems, inputs from storm flow through channels and conduits can have a short-term but significant effect on isotope contents. This is typical of groundwater in karst and other unconfined aquifers. As a groundwater enters confined conditions, it is isolated from further seasonal and storm con-

tribution and its isotopic composition is attenuated to a value representing the weighted mean of meteoric water inputs.

Where variations occur, a principal component separation is possible. Such analyses (based on chemical and isotopic data) were undertaken for a perennial karst spring in Indiana, USA, by Lakey and Krothe [Lak96]. Surprisingly, it turned out that only 20 to 25% of the discharge could be attributed to the storm event and that the bulk discharged from groundwater storage (fissure/porous matrix network). Typical phreatic and vadose storage may have contributed to discharge with the onset of the storm flow, while water from soil moisture and epikarst may have contributed at the onset of the discharge recession.

Some very good aquifers in the world host groundwaters many thousand of years old. The *age* of a groundwater has important implications for water resource management. Using groundwaters that are not actively recharged is mining. On the other hand, groundwater that is part of the modern hydrological cycle is continuously renewed. Its exploitation is potentially sustainable. Deep and/or regional groundwaters can be mixtures of modern and older inputs. However, the presence of even a minor component of modern recharge is important because it indicates a hydraulic connection with an active flow system. Increased pumping may then increase the proportion of the modern contribution.

The age of a groundwater can be a misleading term for two reasons. Firstly, only tritium is part of the water molecule and can thus actually *date* the water. All other dating methods rely on dissolved constituents whose abundance in water is controlled by physicochemical and biological processes. Secondly, hydrodynamic mixing and convergence of groundwater flow paths integrate a variety of recharge origins and ages. Only in well-defined and usually regional artesian aquifers will age gradients along the flow path be preserved. As a consequence, one should not talk about the age of a water but about *groundwater mean residence times* (MRT).

In practical terms, *modern* groundwater are those recharged within the past few decades and so are part of an active hydrological cycle. Classical methods are often the best indication of whether groundwaters are actively recharged. Evidence from hydrogeological mapping, seasonal fluctuations in water level, temporal variations in geochemistry or stable isotopes, and anthropogenic pollution (e.g. nitrate) are indications of active recharge. However, isotopes are used when such hydrogeological information is ambiguous, and more importantly, to constrain the age of recently recharged water.

Tritium has become a standard for the definition of modern groundwater. The era of thermonuclear bomb testing in the atmosphere, from May 1951 to 1976, provided the tritium input signal that defines modern water. Its decay from natural, pre-bomb levels is such that it cannot normally be detected in groundwaters recharged before 1950. Modern groundwaters are then younger than about 45 years relative to the mid-1990s. Tritium-free groundwaters are considered *submodern* or older.

A number of isotope method can be used to assess mean residence times. Seasonal variations in stable isotope provide a measure of age. The more routinely applied techniques are based on the decay of radionuclides. Those

with a long half-life ($^{14}$C, $^{36}$Cl, $^{39}$Ar and $^{81}$Kr) can be used to date paleogroundwaters. Short-lived radioisotopes ($^{3}$H, $^{32}$Si, $^{37}$Ar, $^{85}$Kr and $^{222}$Rn) and those produced by man's nuclear activities over the past decades ($^{3}$H, $^{14}$C, $^{36}$Cl and $^{85}$Kr) indicate modern recharge.

While the methods for analysis of $^{3}$H and $^{14}$C are now routine, other radioisotopes require complicated sampling and/or analytical techniques. The *submodern* period in the dating range between modern waters and paleogroundwaters is problematic. While this $>$ 45 to $\sim$ 1000 year range can potentially be filled by $^{39}$Ar dating ($t\frac{1}{2}$ =256 yr), this method requires rather ideal aquifers, very large samples, complicated sample preparation techniques and special counting facilities. Very few laboratories can afford this and, therefore, $^{39}$Ar dating has not developed into a routine tool.

Two other isotopes of the $^{238}$U decay series that can yield age information are $^{226}$Ra and its daughter $^{222}$Rn. Groundwaters gain $^{226}$Ra through two principal mechanisms including dissolution (rock-etch) of the rock matrix and alpha-recoil of $^{226}$Ra into solution on decay of $^{230}$Th. The solubility of $Ra^{2+}$ increases with salinity due to complexation [Her88], but can coprecipitate with $Ca^{2+}$ or $Ba^{2+}$ in carbonate saturated waters. Ingrowth of $^{226}$Ra approaches a secular equilibrium activity controlled by its production rate and half-life, and becomes constant after about 8000 years [An89]. High concentrations are then a reflection of long residence time. Data from the Stripa granite in Sweden shows that $^{226}$Ra activities increase from about 0.02 Bq/kg in shallow groundwaters to 0.3 at intermediate depths and reaching over 5 Bq/kg at the deepest levels (400 to 900 m)of the site. Deriving quantitative age information requires accurate estimation of dissolution rates, but offers good possibilities for dating in the 1000 to 5000 year period [Hil97].

The presence of radon in groundwater is a clear indication that its parent $^{226}$Ra is not far removed. Thus, it is an indicator for actively circulating groundwater and can identify groundwater discharges in surface systems that are otherwise free of radon. With information on the distribution of uranium and radium in rock and fracture minerals, it is possible to derive hydraulic information on rock permeabilities and fluid movements. A collection of case studies has been assembled by Graves [Grv88].

Whereas most studies look at the discharge of radon, its in-growth has been used to estimate residence times for artificial groundwater recharge. The water supplies of the city of Dortmund in Germany rely on artificially recharged groundwater with water from the Ruhr River as the primary source. Artificial tracing of drinking water supplies is not permitted, and so a method developed by Hoehn and Gunten [Hon89] was adopted. The ingrowth of $^{222}$Rn will reach a secular equilibrium after about 5 half-lives i.e. after 15 days - provided the input from $^{226}$Ra decay is constant in time. In the Dortmund study, it was indeed possible to identify water with different residence times, to show mixing of recharge water with water which infiltrated from a nearby lake, and recognize contributions from underground leaky pipes [Ho92].

## 3.8 Radon and Submarine Groundwater Discharges

Groundwater discharge to coastal waters and estuaries has been of interest for centuries. Several studies have utilized U- and Th- decay series nuclides to assess groundwater inputs to the coastal ocean (e.g. $^{228}$Ra, $^{226}$Ra and $^{222}$Rn) as well as the short-lived isotopes ($^{224}$Ra, $^{223}$Ra) to assess coastal mixing [Cab96; Moo96; Cor00; Moo00]. More recently, a renewed interest in submarine groundwater discharge has emerged from studies on coastal eutrophication and contamination [Gib90; Rea92; Bun96].

The complex interactions amongst geological, biological and geochemical processes at the land-sea margin control the delivery and fate of radionuclides, contaminants, and other natural elements in coastal environments [Swa03].

Theoretically, submarine groundwater discharge can occur wherever a coastal aquifer is hydrogeologically connected to the sea. Artesian or pressurized aquifers can extend for considerable distances from shore, and where the confining units are breached or eroded away, groundwater can flow directly into the sea [Man81; Moo98]. While the magnitude of this submarine groundwater discharge is often less than direct riverine runoff, recent studies have shown that coastal aquifers may contribute significant quantities of fresh water to coastal bottom waters [Moo96; Bur01; Bur03].

An ideal submarine groundwater discharge tracer should be highly enriched in groundwater relative to seawater, behave conservatively (i.e. reactive) or at least predictably and also be easy to measure. The four isotopes of Ra and $^{222}$Rn follow these constraints reasonably well and have recently been utilized to identify and quantify submarine groundwater discharge to various coastal oceans [Bol93; Kre00]. One strong advantage of these radiotracers over seepage meters is that the coastal water column effectively integrates the submarine groundwater discharge signal over a broad area and time period.

Recent studies of submarine groundwater discharge into estuaries indicate that select long-lived and short-lived U/Th series isotopes show great promise as new tools to directly examine exchange processes and rates across the sediment-water interface. As new detection techniques and field validation methods develop, e.g. *in situ* $^{222}$Rn monitors [Bur01], coastal scientists will for the first time be able to realistically identify and quantify submarine groundwater discharge.

Ideally, a thorough submarine groundwater discharge study should include direct measurements (e.g. seepage meters) and numerical modeling efforts to calibrate the geochemical tracers for quantifying groundwater discharges at the particular estuary. In concert, such an approach provides a powerful diagnostic tool for regional scale submarine groundwater discharge investigations.

## 3.9 Radon in the mineral springs

It has long been known that many mineral springs contain relatively high concentrations of radium and radon, and in many places in the world the

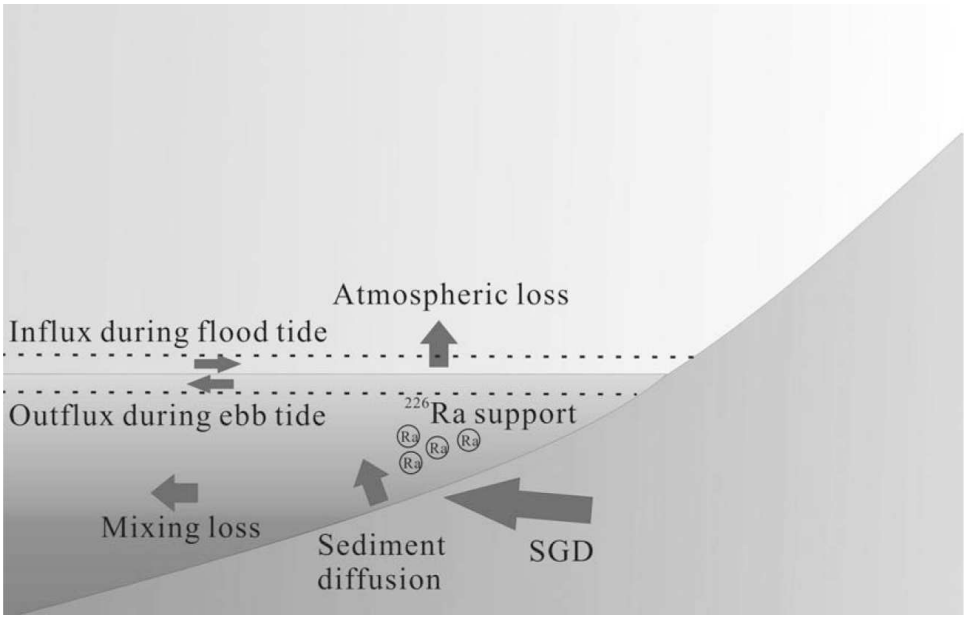


Figure 3.2: Sources and sinks of $^{222}$Rn in coastal waters [Lam03; Tse08].

radioactivity of springs has been exploited for their alleged curative powers. Mineral waters were perceived as being beneficial to health in Roman times, many centuries before any knowledge of radioactivity existed. When the phenomenon of radioactivity was discovered, high levels were found to exist in the mineral waters. This resulted in the following fallacy: the waters are good for health, the waters are radioactive, hence radioactivity is good for health. Spas in South America, Europe, Japan, and elsewhere have commercialized the high radioactivity content of local waters, and in some places research laboratories are operated in which the physiological basis for the alleged curative effects is studied. Visitors are encouraged not only to drink and bathe in the radioactive waters but also to sit in *emanatoria*, where they can breathe $^{222}$Rn emanating from surrounding rocks.

Published values of $^{226}$Ra in mineral waters [UNS94] ranged to more than 100 pCi l$^{-1}$ (3.7 kBq m$^{-3}$), which is several hundred times greater than the values normally reported for public water supplies. However, to illustrate the fact that the values reported for spring waters are not typical of the drinking water of the region, the $^{226}$Ra concentration in tap water of Bad Gastein, Austria, is reported to be 0.62 pCi l$^{-1}$ (23 Bq m$^{-3}$) compared to 100 pCi l$^{-1}$ (3.7 kBq m$^{-3}$) for some of the local springs [Mut57].

About 5 million liters of water that contain high concentrations of $^{222}$Rn are discharged daily from hot springs in Bad Gastein. The water is conveyed to hotels and bathhouses, where 58 Ci y$^{-1}$ (2.1 TBq y$^{-1}$) are released to the atmosphere. Uzinov et al. [Uzi81] described the manner in which $^{222}$Rn emanations from this water result in exposure to city residents, tourists who visit the spas, and employees of the many bathhouses. They estimate that exposure of some of the attendants is as high as 40 WLM y$^{-1}$. A cytogenetic survey of persons subject to a gradient of $^{222}$Rn exposure, including residents of Bad Gastein and several groups of employees of the spas, demonstrated

dose-dependent increases in the frequency of chromosomal aberrations in the white blood cells [Poh79].

One of the most popular mineral springs localities in the United States is at Saratoga, New York, where reports of the medicinal value of the water go back to the early eighteenth century. It is known that many of the springs contain $^{226}$Ra in amounts that exceed the EPA limit of 5 pCi $l^{-1}$ (185 Bq $m^{-3}$) by a factor of 100. A survey has been made of the persons using one spring, Hathorn No. 1 [Aul76], which attracts many visitors and contains an average of about 200 pCi $l^{-1}$ (7.4 kBq $m^{-3}$). Twenty-seven long-time users of the water from this spring who were selected for study stated that they consumed the water for 5 to 65 years, in amounts that ranged from about 0.2 to 3 $Ld^{-1}$. Based on the information obtained in this way, it was calculated that the $^{226}$Ra body burdens of the 27 individuals questioned ranged from slightly above normal to a high of 0.11 $\mu$Ci (4.1 kBq), which is slightly above the limit of 0.1 $\mu$Ci (3.7 kBq) for industrial workers. More comprehensive surveys are needed to evaluate the public health significance of mineral springs such as these. There are few studies of the extent to which the radioactivity contained in mineral spring waters has been absorbed by human beings.

# Chapter 4

# The study area of the Bussento river basin

The study shown in this thesis work has been started, in the framework of a multi-year strategic Interdepartment operating Research Program named RAD-CAMPANIA, carried out, since 2006, by researchers of the University of Salerno, in order to deal with the problem of the Radon prevention and the assessment of its impact on natural and anthropic environments, occurring in Campania Region.

The Program involves interdisciplinary skills and professional competences, like those ones from Environmental Physics, Geology, Geomorphology, Hydrogeology, Hydrology and Building Engineering, applied to interdisciplinary research projects and sub-projects and it is realized in very close collaboration and coordination with Academic Institutions like the Consortium inter-University for the prediction and prevention of Great RIsks (C.U.G.RI.), between the University of Salerno and the University Federico II of Naples, and the Regional Agency for the Environmental Protection of Campania (A.R.P.A.C.) and its facilities operating on the territory [ARP08].

The Program, in general, develops interdisciplinary researches, concerning the role and utility of the Radon in environmental and building studies; in particular, focusing on the human interrelations and impacts in life sites and styles.

These researches are based on the scientific background acquired at international and national level about Radon and are aimed, in particular, on their implementation in the territorial planning, the water protection and the safeguarding of people from environmental risks. Therefore, the Program deals with the main themes of operative research in environmental studies for the improvement in the actions and activities of the institutionally competent Authorities and Agencies of Campania Region in the soil, water and human health monitoring and protection, according to the national and regional regulations concerning the *Radon Risk*.

In the RAD-CAMPANIA program the investigation activities whose results are going to be reported in this thesis work have been performed in the framework of the Project Water and Sub Projects Marine, Springs and Rivers.

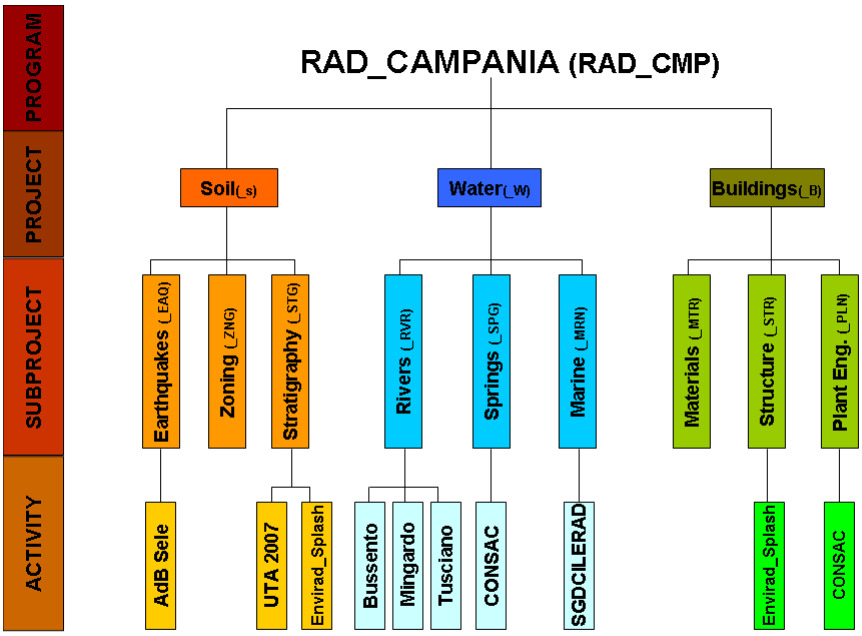


Figure 4.1: RAD_CAMPANIA Program Scheme.

## 4.1 The karst topography

Karst topography is a landscape shaped by the dissolution of a layer or layers of soluble bedrock, usually carbonate rock such as limestone or dolomite.

Due to subterranean drainage, there may be very limited surface water, even to the absence of all rivers and lakes. Many karst regions display distinctive surface features, with sinkholes or dolines being the most common. However, distinctive karst surface features may be completely absent where the soluble rock is mantled, such as by glacial debris, or confined by a superimposed non-soluble rock strata. Some karst regions include thousands of caves, even though evidence of caves that are big enough for human exploration is not a required characteristic of karst. Various karst landforms have been found on all 6 major continents.

Karst topography is characterized by subterranean limestone caverns, carved by groundwater.The geographer Jovan Cvijic (1865-1927) was born in western Serbia and studied widely in the Dinaric Kras region. His publication of Das Karstphänomen (1893) established that rock dissolution was the key process and that it created most types of dolines, *the diagnostic karst landforms*. The Dinaric Kras thus became the type area for dissolutional landforms and aquifers; the regional name kras, Germanicised as *karst*, is now applied to modern and paleo-dissolutional phenomena worldwide. Cvijic related the complex behaviour of karstic aquifers to development of solutional conduit networks and linked it to a cycle of landform evolution. He is recognized as *the father of karst geomorphology*.

Karst landforms are generally the result of mildly acidic water acting

on soluble bedrock such as limestone or dolostone. The carbonic acid that causes these features is formed as rain passes through the atmosphere picking up $CO_2$, which dissolves in the water. Once the rain reaches the ground, it may pass through soil that may provide further CO2 to form a weak carbonic acid solution. Recent studies of sulfates, in karst waters, suggests sulfuric acid and hydrosulfuric acid may also play an important role in karst formation.

This mildly acidic water begins to dissolve the surface along with any fractures or bedding planes in the limestone bedrock. Over time, these fractures enlarge as the bedrock continues to dissolve. Openings in the rock increase in size, and an underground drainage system begins to develop, allowing more water to pass through the area, and accelerating the formation of underground karst features.

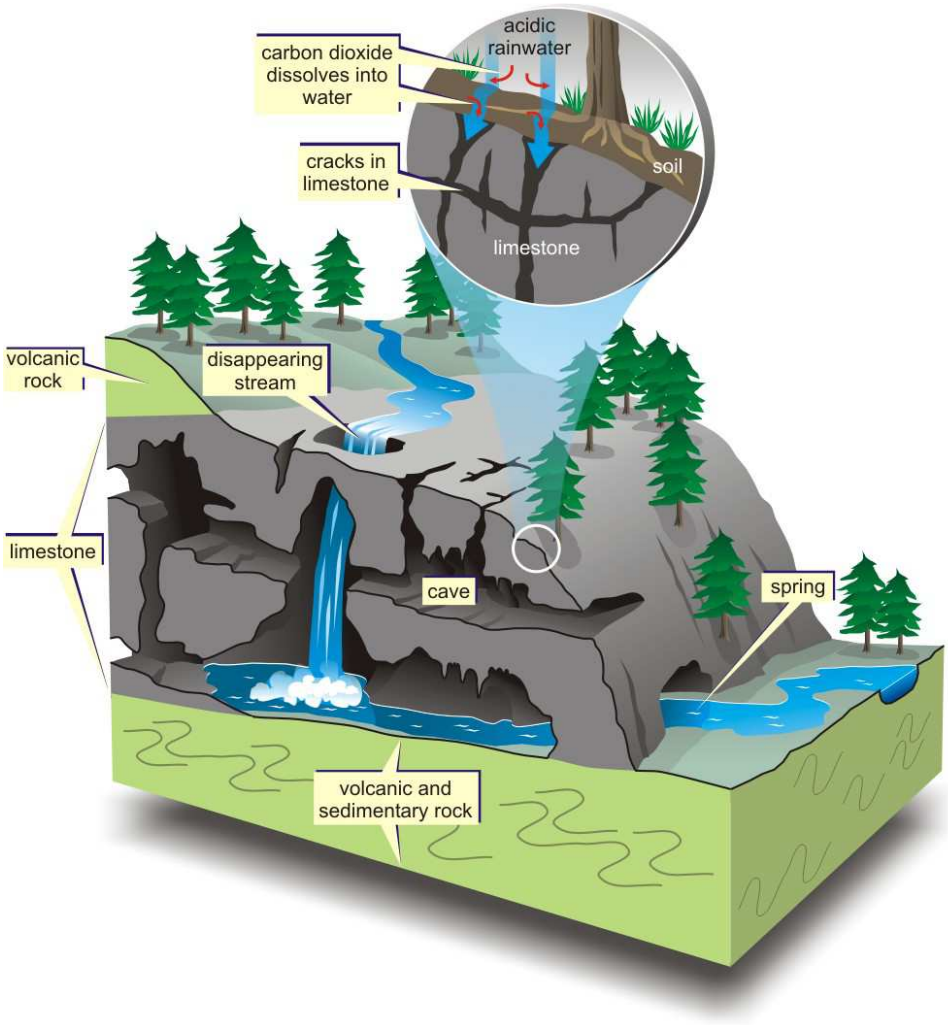


Figure 4.2: A simple scheme of a karst landscape.

The karstification of a landscape may result in a variety of large or small scale features both on the surface and beneath. On exposed surfaces, small features may include flutes, runnels, clints and grikes, collectively called karren or lapiez. Medium-sized surface features may include sinkholes or

cenotes (closed basins), vertical shafts, foibe (inverted funnel shaped sinkholes), disappearing streams, and reappearing springs. Large-scale features may include limestone pavements, poljes and blind valleys. Mature karst landscapes, where more bedrock has been removed than remains, may result in karst towers or haystack/eggbox landscapes. Beneath the surface, complex underground drainage systems (such as karst aquifers) and extensive caves and cavern systems may form.

Calcium carbonate dissolved into water may precipitate out where the water discharges some of its dissolved carbon dioxide. Rivers which emerge from springs may produce tufa terraces, consisting of layers of calcite deposited over extended periods of time. In caves, a variety of features collectively called speleothems are formed by deposition of calcium carbonate and other dissolved minerals.

Water supplies from wells in karst topography may be unsafe, as the water may have run unimpeded from a sinkhole in a cattle pasture, through a cave and to the well, bypassing the normal filtering that occurs in a porous aquifer. Karst formations are cavernous and therefore have high rates of permeability, resulting in reduced opportunity for contaminants to be filtered out.

Groundwater in karst areas is just as easily polluted as surface streams. Sinkholes have often been used as farmstead or community trash dumps. Overloaded or malfunctioning septic tanks in karst landscapes may dump raw sewage directly into underground channels.

The karst topography itself also poses difficulties for human inhabitants. Sinkholes can develop gradually as surface openings enlarge, but quite often progressive erosion is unseen and the roof of an underground cavern suddenly collapses. Such events have swallowed homes, cattle, cars, and farm machinery.

## 4.2 Hydromorphology of the study area

The Bussento river drainage basin is one of the major and more complex drainage river systems of the southern sector of Campania region, in Southern Italy (figure 4.3). This complexity is due to the highly hydrogeomorphological conditioning induced by the karst landforms and processes (figure 4.4).

In fact, it is characterized by widely and deeply karst features, like summit karst highlands with dolines and poljes, lowlands with blind valleys, streams disappearing into sinkholes, cave systems, karst-induced groundwater aquifers and gravitational karst-induced *sackungs* [Del87; Bis96]. The main stream originates from the upland springs of Mt. Cervati (1,888 m asl), one of the highest mountain ridges in Southern Apennines. Downstream, the river flows partly in wide alluvial valleys (i.e., Sanza valley) and, partly, carving steep gorges and rapids, where a number of springs, delivering fresh water from karst aquifers into the streambed and banks, increase progressively the river discharge. Near the Caselle in Pittari village, the Bussento river and adjacent neighbour minor creeks flow, respectively, into *La Rupe* (Bussento Upper Cave), Orsivacca and Bacuta-Caravo sinkholes, channelling the entire fluvial surface flow drained in the upper Bussento basin into the

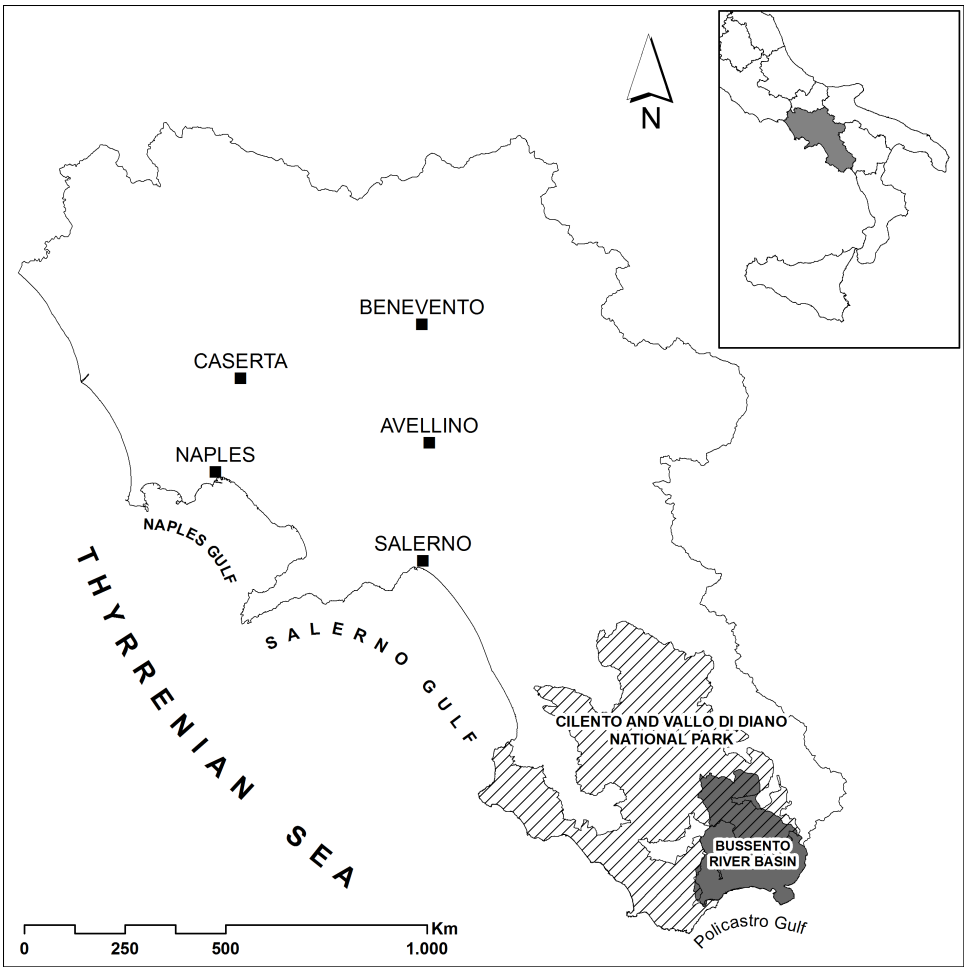


Figure 4.3: Location of the study area in Campania region and inside the Cilento and Vallo di Diano National Park.

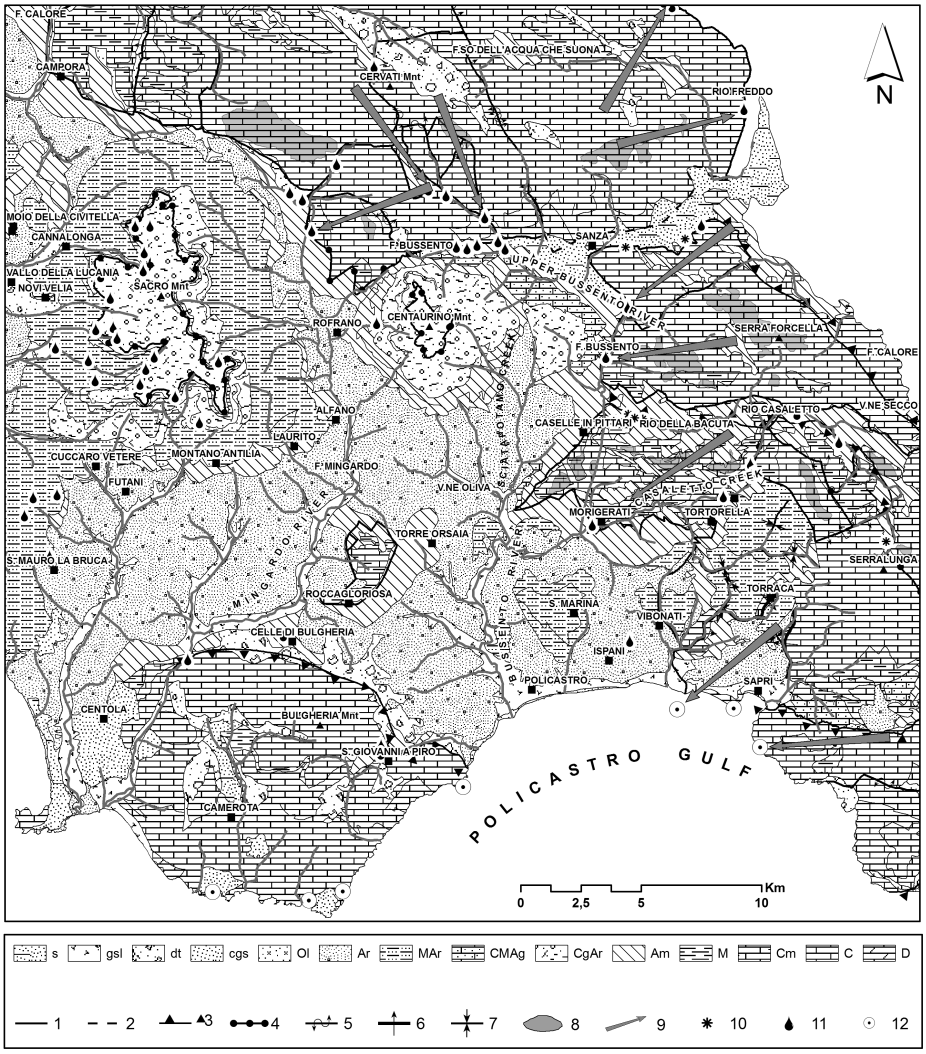


Figure 4.4: Hydro-geomorphological map of Bussento river and surrounding. **Legend**: *Hydrogeological Complex: s)Sand and gravelly sand; gsl) Fluvial sandy gravelly; dt) Slope debris; cgs) Sandy conglomerate; Ol) clayey Olistostrome; Ar) Sandstone and marls; MAr) Marl and Sandstone; CMAg) Marl and Conglomerate; CGAr) Conglomerate and Sandstone; Am) marly shale;M) Silty marl fogliarina; Cm) Marly limestone; C) Limestone; D) Dolostone. Symbology:1) Fault; 2) Hypotisized fault; 3) Overthrust; 4) Permeability limit; 5) Groundwater exchange; 6) Losing river; 7) Gaining river); 8)Karst summit; 9) Probable groundflow direction;10) Sinkhole; 11) Main spring; 12) Coastal and submarine spring.*

hypo-karst cave system and re-emerging a few kilometers downstream, in the neighbourhood of the Morigerati town, from the resurgence,called *Bussento Lower Cave*.

Downstream the resurgence, the Bussento river merges with Bussentino creek, originating from the eastern sector of the drainage basin and flowing along deep canyons and gorges, carved into the meso-cainozoic litho-stratigraphic sequences, prevalently constituted of limestone and marly limestone, referred to the Alburno-Cervati Unit [Dar73]. In the western and southern sectors of the basin (Sciarapotamo creek sub-basin), marly-argillaceous successions of the Liguride and the *Affinità Sicilide Complex* or *parasicilides* [Bon88; Cam00; Cam04] dominate the hilly landscape, whereas they underlie the arenaceous-conglomerate sequences at Mt. Centaurino (Guida D. et al., 1988). Downstream the confluence with Sciarapotamo creek, the Bussento river flows as a meander stream in a terraced floodplain and, finally, in the Policastro coastal plain.

In particular, the river drainage sector, which this paper concerns about, refers to the *Morigerati Hydrogeological Structure* [Iac88], comprising the Middle Bussento river Karst System (MBKS). This karst system develops within the carbonate ridge of Mt. S. Michele - Mt. Pannello - Mt. Zepparra , between the four sinkholes located to East of Caselle in Pittari and the final fluvial reach of the gorge located to SE of the Sicili village (Sicili bridge), up to the Bussento hydropower plant, just downstream the confluence with Sciarapotamo creek.

In figure 4.5 the detailed hydro-geomorphological map of the study area, with the hydrogeological complexes and main springs, the hypothesized palaeo- and present-day sink-cave-resurgence system, and the river segments and reference reaches of interest,are graphically drawn.

The Middle Bussento segment, comprising the Oasis WWF reach, is located in the Morigerati gorge, a typical epigenetic valley [Las80; Del87], along which groundwater inflows from epikarts spring, conduit spring (Old Mill Spring) and cave spring (Bussento Resurgence) supply a perennial streamflow in a step-and-pool river type [Mot98]. The Middle-lower segment, comprising the Sicilì bridge reach, is located more downstream.

Along the first one, beginning at the end of the Morigerati gorge and stretching to the Sciarapotamo creek confluence, three reaches can be recognized from downvalley: the more downstream, in correspondence of the Bussento Hydropower Plant results a typical riffle-pool river [Mot98], as a meander entrenched in fluvial and strath terraces [Bub01]; the second upstream reach, called Bottelli House reach, results in a riffle-pool river along low order alluvial terraces and, finally, the third, the above cited Sicilì Bridge reach, a plane bed river slightly entrenched in alluvial terrace and bedrock.

The hydro-geomorphological setting, above briefly illustrated, induces a very complex surface-groundwater interaction and exchanges. Therefore, groundwater inflows from outside of the hydrological watershed and groundwater outflows towards surrounding drainage systems, frequently occur, influencing the basin water budget and streamflow regime.

The Bussento river regime is also affected by a very complex hydropower plant system, which retains and diverts the river discharge in the Sabetta reservoir and the Casaletto weirs, respectively, from the upper Bussento river

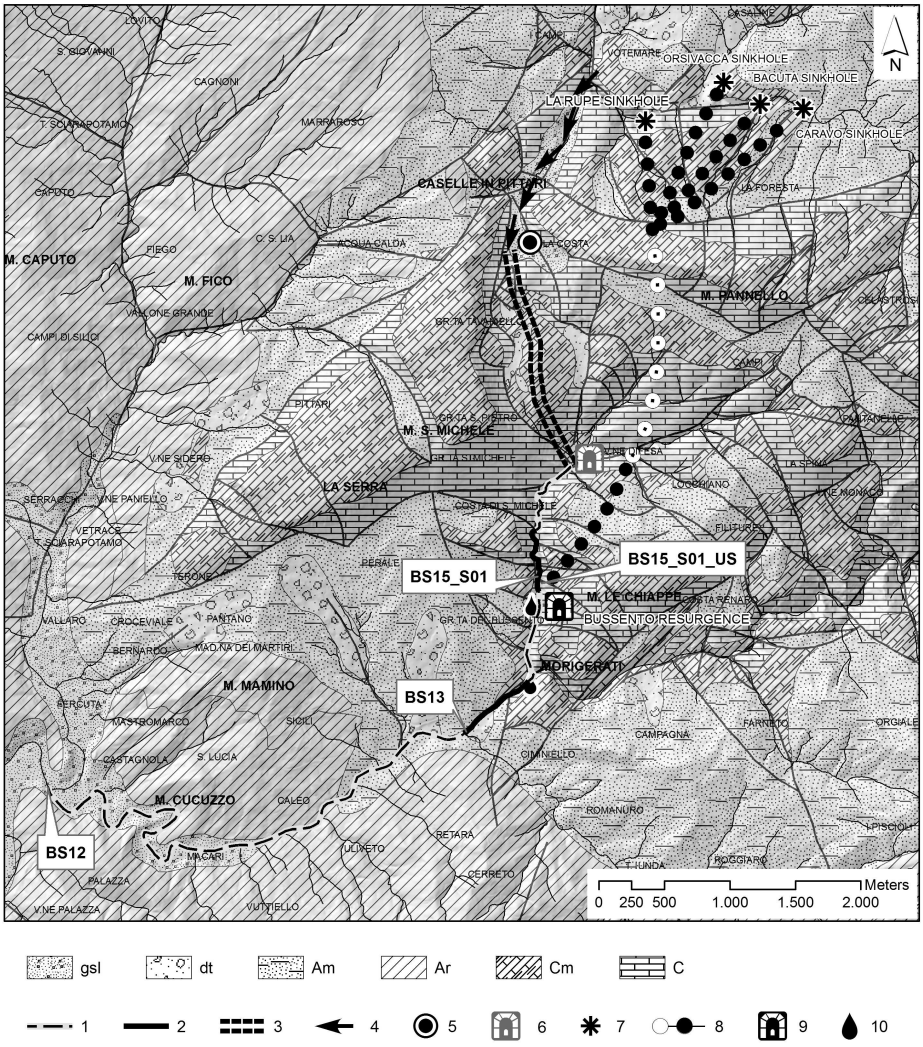


Figure 4.5: Detailed hydro-geomorphological map of the study area and related features. **Legend**: *Hydrogeological complexes: gsl) Fluvial sandy gravel; dt) Slope debris; Am) marly shale; Ar) Sandstone and marls; Cm) Marly limestone; c) Limestone. Symbology: 1) Location of fluvial segment of interest; 2) Location of the fluvial reaches of interest; 3) Abandoned subterranean flowpath of the Palaeo-Bussento River ; 4) Abandonned surface floepath of the Palaeo-Bussento river; 5) Abandoned sinkhole of the Palaeo-Bussento river; 6) Abandoned resurgence of the Palaeo-Bussento river ; 7) Upper Bussento active sinkhole; 8) Explored (grey circle) and no-explored (withe circle) subterranean flowpath of present-day Bussento river; 9) Active resurgence of the Bussento river; 10) Main karst spring.*

and the Bussentino creek reaches segment to the Lower Bussento fluvial segment.

In order to provide a physical scheme of the complex recharge, storage and routing system of the Middle Bussento karst area, a preliminary, physically-based, conceptual model has been built-up, accounting for an interconnected sequence of geologic substrates, structural discontinuities, type and rate in permeability distribution, recharge areas and discharge points, that collectively attempt a conceptualization of the karst aquifers-river interactions [Whi69; Whi77; Whi88; Whi03], focusing on the variety of hydrogeomorphologic settings and their influences on the streamflow regime. With reference to the work done by G. Iaccarino et al. [Iac88] and by D. Guida et al. [Gui06] , the conceptual hydro-geomorphological model of the MBKS, contains three nested hydrological domains (figure 4.6): i) a hydrogeologic domain; ii) a hydrogeomorphological domain and iii) an aquifer-river domain.

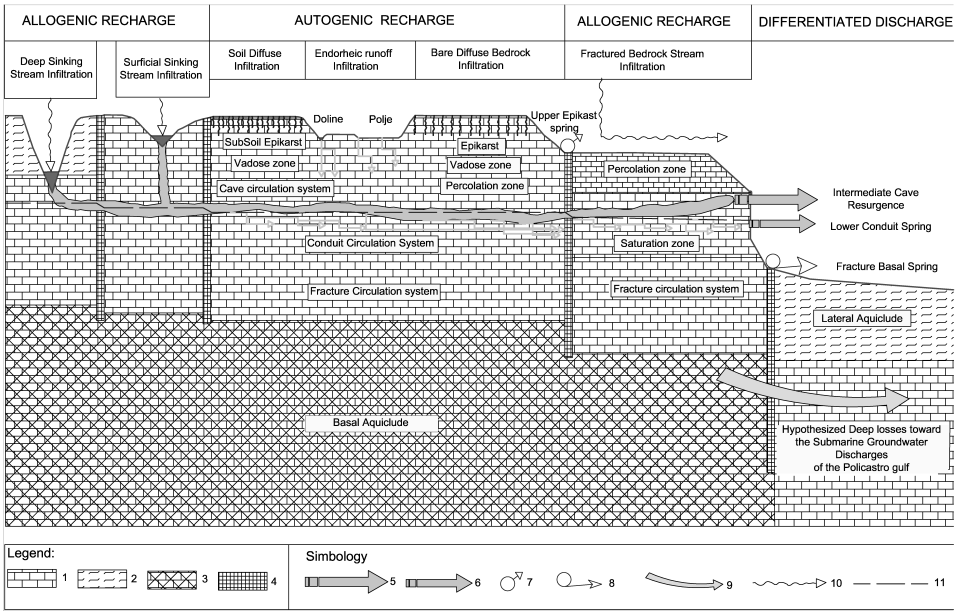


Figure 4.6: Conceptual hydro-geomorphological model of the Middle Bussento river Karst System (MBKS); **Legend**: *1) Limestone aquifer; 2) Marly shale aquiclude; 3) Basal highly fractured limestone aquitard; Lateral fractured faultinduced aquitard; 5) Intermediate cave resurgence; 6) lower conduit spring; 7) Upper epikarst spring; 8) Basal fracture spring; 9) Probable groundwater losses toward marine spring; 10) Infiltration of streamwater along the river bed; 11) Water table.*

The hydrogeological domain represents the 3-D structure of aquifer, aquitard and aquiclude, conditioning the groundwater circulation and storage, vertically differentiated in the classic subdivision of karst hydrostructures (Bakalowicz M., 1995): epikarst, vadose, percolation and saturated or phreatic zones [For89]. The last one is hydrodynamically subdivided in cave, conduit and fracture routing system [Whi69].

The hydro-geomorphological domain comprises karst and fluvial landforms and processes, conditioning groundwater recharge (*karst input control* [For07], by means of the infiltration and runoff processes, including: a) allo-

genic recharge from surrounding impervious drainage basins into deep and shallow sinking stream infiltration points, and fractured bedrock stream infiltration; b) autogenic recharge, including sub-soil and bare diffuse epikarst infiltration, endorheic runoff infiltration in dolines and poljes; c) groundwater discharge (*karst ouput control* [For07]), differentiated in the groundwater-river interactions within the aquifer-river domain.

This last comprises the complex interactions between the streambed-springs system, which generally results in a downstream river discharge increase, occurring generally in typical bedrock streams, flowing in gorge and canyons carved in enlarged fractured limestone sequences. Following the routing karst system, the springs inflowing into streamlow can be characterized in: i) upper epikarst springs, ii) intermediate cave resurgence springs, iii) lower conduit springs and iv) basal fracture springs. Figure 4.6 highlights, also, the hypothesized deep losses toward the Submarine Groundwater Discharges (SGD), emerging in the Policastro gulf [Gum07a], as reported in figure 4.4.

Each of the mentioned components corresponds, in the modeling conceptualization of the scheme, to a linear storage, which releases streamflow as a function of the water storage and of a characteristic delay time. The characteristic time indicates that there is a delay between the recharge to the system and the output from the system itself, and this delay is greater for deeper aquifers. The number of storages, each representing, thus, a different process, contributes to the total streamflow through a recharge coefficient, that is a measure of the magnitude of the single storage.

The application of a conceptual model, such as the one briefly described, requires the calibration of the model parameters, and in particular of the characteristic delay time and of the recharge coefficient of each single storage. In complex catchments, such as the Bussento River System, characterized by a large impact of karstic phenomena, raw streamflow data are not sufficient to the quantification of the contribute and magnitude of the single storage, and, therefore, are not sufficient to calibrate the model. To this aim, the use of Radon activity concentration measurements could represent a valuable future perspective.

The study area is characterized by a typical Mediterranean climatic regime, tending to temperate from the coast to the mountain reliefs. The 50-years (1921-1977) mean annual rainfall and mean annual temperature for historical meteorological stations of Morigerati, Caselle in Pittari, Casaletto Spartano and Sanza, located within the Bussento River watershed, are shown in table 4.1 [Gui80].

Since streamflow gauging stations, with long and high quality recorded data, are not available, a characterization of the hydrometric low flow regime is given, in the table 4.2, through data from G. Iaccarino et al. [Iac88], and D. Guida et al. [Gui06], and through discharge data collected during several field campaigns along the river segments of interest (fig 4.5) and from connected groundwater inflows.

| **Station** | **Elevation** (mts a.s.l.) | **MAP** (mm) | **MAT** (°C) | **MAPE** (mm) | **EP** (mm) |
|---|---|---|---|---|---|
| **Morigerati** | 300 | 1439 | 15.9 | 820 | 619 |
| **Caselle in Pittari** | 315 | 1657 | 15.3 | 788 | 869 |
| **Casaletto Spartano** | 310 | 1811 | 15.3 | 789 | 1022 |
| **Sanza** | 569 | 1596 | 12.2 | 668 | 928 |

Table 4.1: Climatic characterization of the study area. MAP is the Mean Annual Precipitation, MAT is the Mean Annual Temperature, MAPE is the Mean Annual Potential Evapotraspiration and EP is the Effective Precipitation.

## 4.3 Bussento Radon Monitoring Station System

In this section there is the description of the main monitoring stations established in the Bussento river basin:

- **BS00**, *Bussento Mouth*. It has been established at the mouth of the Bussento river to estimate the radon concentration in correspondence of the river, where the mixing of the marine water and the river sediments takes place.
- **BS01**, *Bussento Mouth Bridge*. It is important to check the radon concentration in a hydraulically definite, geologically characterized and easily accessible section.
- **BS02**, *Bussento Railway Bridge*. It is localized in proximity of the orographic right bottom threshold of Bussento river (transition transept between Middle-Lower and Lower Bussento).
- **BS03**, *Vallonaro Creek*. It has been established to evaluate the radon concentration above the inflow of the Vallonaro creek into the Bussento river.
- **BS04**, *Sciarapotamo Creek*. It is localized just below the homonymous bridge, and allows to evaluate the radon concentration immediately above the confluence of the creek in the Bussento river.
- **BS12**, *Bussento Hydropower*. It is localized immediately above the inflow of the water coming from the turbines of the hydroelectric plant of the Sabetta reservoir.
- **BS13**, *Sicilì Bridge*. It is localized under the homonymous bridge, and it has been established to evaluate the radon concentration below the inflow of the Cillito springs group.
- **BS14**, *Casaletto Creek*. It is localized downstream the Capello springs group, which is partially picked up.
- **BS15**, *WWF Oasis Bridge*. It is localized in correspondence of the bridge between the old watermill spring and the Bussento resurgence.

| River Section | 1985-1987 ($m^3/s$) | 1989-1990 ($m^3/s$) | 1999-2001 ($m^3/s$) | 2002-2005 ($m^3/s$) | 2007-2009 ($m^3/s$) |
|---|---|---|---|---|---|
| **Upper epikarst springs** | 0.08 | 0.12 | 0.06 | 0.04 | 0.05 |
| **Upstream Gorge reach** | 0.08 | 0.12 | 0.06 | 0.04 | 0.05 |
| **Lower conduit springs** | 0.25 | 0.31 | 0.22 | 0.20 | 0.21 |
| **Intermediate gorge reach** | 0.33 | 0.43 | 0.28 | 0.24 | 0.26 |
| **Intermediate cave resurgence spring** | 0.35 | 0.44 | 0.28 | 0.23 | 0.25 |
| **Downstream Gorge reach** | 0.68 | 0.88 | 0.56 | 0.47 | 0.51 |
| **Basal fracture springs** | 0.45 | 0.38 | 0.41 | 0.37 | 0.39 |
| **MBKS Total Minimum streamflow** | 1.13 | 1.25 | 0.97 | 0.84 | 0.90 |

Table 4.2: Annual minimum streamflow data from river discharge measurements along the cited reference reaches. Data in column 2 (1985-1987) are from Iaccarino et al. [Iac88], data in column 3 (1989-1990) are courtesy of Domenico Guida, data in column 4 (1999-2001) are courtesy of the National Park of Cilento, data in column 5 (2002-2005) are courtesy of CUGRI and data in column 6 (2007-2009) are from this study.

- **BS16**, *Ciciniello Creek*. It is localized under the bridge of the Bussentina road, and it is important to evaluate the radon concentration in the water coming from the homonymous basin.
- **BS17**, *Sabetta Resrvoir*. It is localized at the right side of Bussento, in correspondence of the entrance of the plant.
- **BS18**, *Acquevive Bridge*. It is localized at the river dike, and has been established to estimate the radon concentration in the river water below the Farnetani springs group.
- **BS19**, *Farnetani Bridge*. At about 100 m from the homonymous bridge, it has been established to estimate the radon concentration above the inflow of the Farnetani springs group and below all the inflows coming from the mountain creeks and the piedmont springs.
- **BS20**, *L'Abate Bridge*. Localized under the homonymous medieval bridge, it is an intermediate station the BS19 and the piedmont ones, which are influenced by the inflows of the Fistole di Sanza springs group.
- **BS21**, *Inferno Creek Bridge*. It is localized under the little bridge of the Varco del Carro muletrack, and it is important to evaluate the radon concentration in the water coming from the Inferno creek which

collects the water, prevalently spring water, coming from the southern side of Mount Cervati.

- **BS22**, *Persico Bridge*. Is is localized under the homonymous bridge and it has been established to estimate the incidence of Persico creek which drains both the water from the carbonatic side of Mount Cervati and the water coming from northern side of Mount Centaurino.
- **BS23**, *Bussentino Bridge*. Localized under the medieval bridge of the Morigerati-Vibonati road, it is useful to evaluate the radon concentration above the confluence between the Bussentino creek and the Bussento reach coming from the resurgence.
- **BS24**, *Melette Bridge*. It is localized under the Melette bridge (eastern Bussento) and it is useful to estimate the radon concentration in correspondence of the Melette springs group.
- **BS25**, *Bacuta Sinkhole*. It is localized immediately above the sinkhole and it is useful to evaluate the radon concentration in the water coming from Bacuta creek basin.


Figure 4.7: Map of the Bussento Radon Monitoring Station System (BRMSS). **Legend**: *BS) Bussento river station; PG) Policastro gulf station; 1) Bussento river basin; 2) Watershed.*

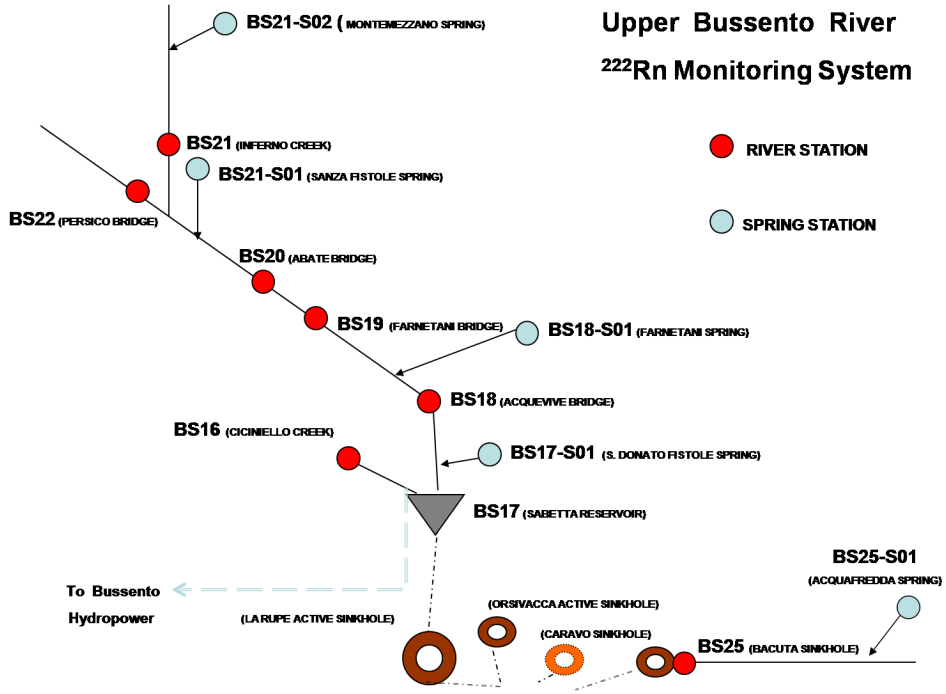


Figure 4.8: Scheme of the upper Bussento monitoring stations system.

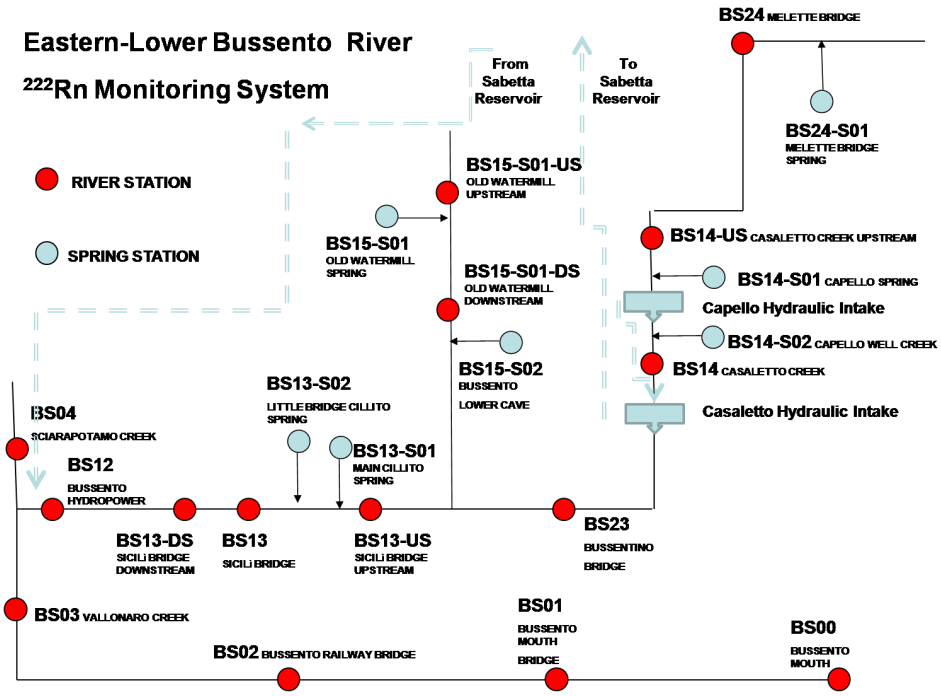


Figure 4.9: Scheme of the eastern-lower Bussento monitoring stations system.

| Station Name | Code | X-Coord. | Y-Coord. | Distance from the coast (m) |
|---|---|---|---|---|
| **Bussento Mouth** | **BS00** | 543605.3366 | 4435295.3874 | 0 |
| **Bussento Mouth Bridge** | **BS01** | 543365.5730 | 4435974.7175 | 1740 |
| **Bussento Railway Bridge** | **BS02** | 542247.8301 | 4438272.0435 | 3680 |
| **Vallonaro Creek** | **BS03** | 541834.8402 | 4440099.9059 | 6200 |
| **Sciarapotamo Creek** | **BS04** | 543412.8693 | 4442664.5218 | 10930 |
| **Bussento Hydropower** | **BS12** | 543583.6737 | 4442368.8007 | 10246 |
| **Sicilì Bridge** | **BS13** | 546446.5601 | 4442939.8484 | 14100 |
| **Casaletto Creek** | **BS14** | 553475.0352 | 4445318.3639 | 22717 |
| **Old Watermill Spring** | **BS15_S01** | 546915.6349 | 4444081.9437 | 15580 |
| **Ciciniello Creek** | **BS16** | 545934.8916 | 4449803.4248 | 22300 |
| **Sabetta Reservoir** | **BS17** | 547207.9202 | 4449424.2903 | 20900 |
| **Acquevive Bridge** | **BS18** | 548000.0954 | 4451699.0969 | 23534 |
| **Farnetani Bridge** | **BS19** | 546973.6582 | 4452744.0284 | 25550 |
| **L'Abate Bridge** | **BS20** | 544406.0243 | 4453604.0162 | 28460 |
| **Inferno Creek Bridge** | **BS21** | 543083.6774 | 4454695.1836 | 30300 |
| **Persico Bridge** | **BS22** | 543049.7711 | 4454630.4533 | 30095 |
| **Bussentino Bridge** | **BS23** | 548065.3782 | 4443510.8961 | 15995 |
| **Melette Spring** | **BS24_S01** | 557102.7175 | 4446756.1804 | 28734 |
| **Bacuta Sinkhole** | **BS25** | 548948.4602 | 4447695.8382 | 20500 |

Table 4.3: Radon Monitoring Stations along the Bussento river basin - Bussento Radon Monitoring Station System (BRMSS).

# Chapter 5

# Instruments and methods

Various factors need to be considered in selecting methods and instruments for measurement of radon or radon decay products. Example of such factors include measurement objectives, type of desired output and sampling duration.

Methods for measuring radon and its decay products are based on the detection of radioactive emissions. Such methods can include detection of alpha particles, gamma rays or, less commonly, beta rays. A variety of instruments based on such principles is commercially available.

Devices such as alpha track detectors, activated carbon monitors and passive electret ion chambers are widely used to provide time-integrated measurements of radon over a period of days (activated carbon, electrets) or months (alpha track detectors, electrets). Scintillation cells are commonly used for continuous monitoring or for instantaneous or grab sampling of radon.

There are different continuous $^{222}Rn/^{220}Rn$ monitors on the market, and most of these are based on detection of alpha particles. There are currently three types of alpha particle detectors being used as electronic $^{222}Rn/^{220}Rn$ monitors, namely, scintillation cells (or Lucas cells), ion chambers and solid state alpha detectors.

The instruments used in this study fall in the last two categories and will be described in the following sections.

## 5.1 RAD7

The RAD7 radon detector by the american Durridge uses a solid state detector. The semiconductor material converts the alpha radiation from the decay of the radionuclide (e.g. $^{218}Po$ and $^{214}Po$) into an electrical signal. One advantage of a solid state detector in radon or radon progeny detection is the fact that it can electronically determine the energy associated with the incoming alpha particle. In this way, the specific radionuclide can be identified.

RAD7 has an internal sample cell of a 0.71 hemisphere, with a solid state ion-implanted planar silicon alpha detector at the center. The inside of the hemisphere is coated with an electrical conductor which is charged to a potential of 2-5 kV relative to the detector, so that positively charged progeny decayed from $^{222}Rn$ and $^{220}Rn$ are driven by the electric field towards the

detector. When a progeny atom reaches the detector and subsequently decays and emits an alpha particle, the alpha particle has a 50% probability of being detected by the detector. As a result, an electrical signal is generated with the strength being proportional to the alpha energy. RAD7 will then amplify and sort the signals according to their energies.

The RAD7 spectrum is a scale of alpha energies from 0 to 10 MeV, which is divided into 200 channels each of 0.05 MeV width. The alpha energies associated with $^{222}$Rn and $^{220}$Rn are in the range of 6-9 MeV. These 200 channels are grouped into eight energy windows (labeled as A-H). Windows A-D are the functional ones.

- *Windows A* records 6.00 MeV alpha particles from $^{218}$Po, which has a half-life of 3 min, and it is thus the window for $^{222}$Rn sniff mode or "new" $^{222}$Rn.
- *Windows B* records 6.78 MeV alpha particles from $^{216}$Po, which has a half-life of 0.15 s, and it is thus the window for $^{220}$Rn sniff mode or "new" $^{220}$Rn.
- *Windows C* records 7.69 MeV alpha particles from $^{214}$Po, which has a half-life of nearly an hour, amd it is thus the window for "old" $^{222}$Rn.
- *Windows D* records 8.78 MeV alpha particles from $^{212}$Po, which has a half-life of about 10 h, and it is thus the window for "old" $^{220}$Rn. For every 66 counts in window D, there should be 34 counts (6.05 and 6.09 MeV) in window A due to the two-way split from $^{212}$Bi, so the counts in window A are automatically corrected for counts in window D by RAD7.

RAD7 adds windows E-H together to form window O (for "other"), which is mainly for diagnostic purposes.

RAD7 allows different modes of measurements, such as the normal mode and the sniff mode. In the sniff mode, RAD7 uses only $^{218}$Po signals to determine the $^{222}$Rn concentrations and $^{216}$Po signals to determine the $^{220}$Rn concentrations, ignoring subsequent and long-lived progeny.

Before making a measurement the RAD7 must be free of radon and dry. To achieve this, it should be purged for some time. In fact, after performing a water, soil gas or air measurement, the RAD7's internal sample cell will continue to contain the radon that was measured. If this radon is still present when a new measurement starts, it will erroneously influence the next measurement. This is of special concern when the radon concentration of the last measurement was high relative to the next measurement. To prepare for the next water measurement, the radon should be removed from the RAD7 and its air conducting accessories, including the aerator head, tubes and desiccant. This procedure is known as *purging the system.*

To purge the system a source of radon-free (or relatively radon-free) air is needed. The RAD7 must be put into a purge cycle allowing its pump to flush the clean air through the entire system for about 30 minutes. In this mode, the inlet of the RAD7 is connected to a desiccant column. The desiccant acrylic column is 6 cm in diameter and 28 cm in length. The purpose of the granules in the column is to absorb moisture, since the detection efficiency


Figure 5.1: RAD7 by Durridge.

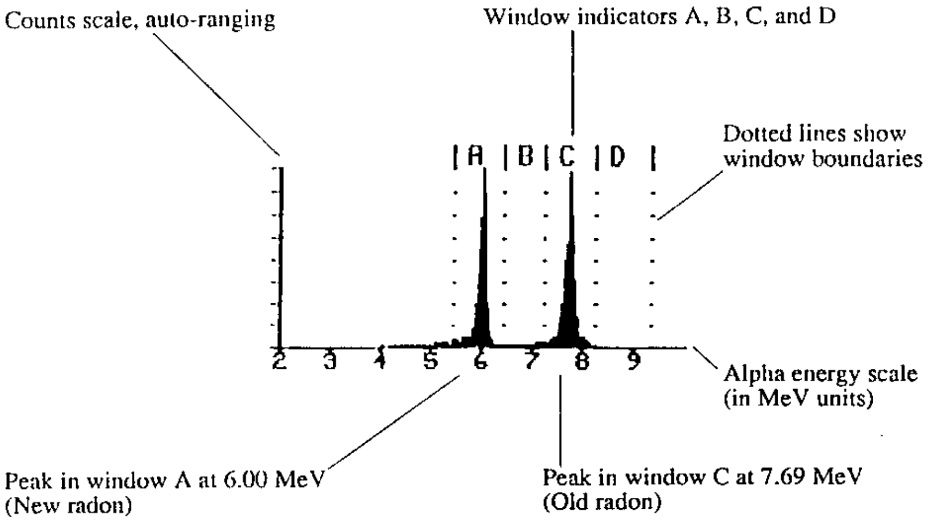


Figure 5.2: Alpha energy spectrum given by RAD7.

Figure 5.3: Aerating a 250 mL water sample [DUR09b].

of the RAD7 decreases as humidity increases due to the neutralization of polonium ions by water particles. An air filter at the entrance of the RAD7 prevents dust particles and charged ions from entering the radon chamber, which would contaminate the alpha detector.

The RAD7 has an RS232 serial port that can be used for transfer of data into a file on a personal computer. A computer software (Capture 1.2.0) is provided by the manufacturer for this purpose.

### 5.1.1 RADH2O System

The RADH2O is an accessory of the RAD7 that allows to measure radon in water with high accuracy over a range of concentrations from less than 50 pCi/L to greater than $10^5$ pCi/L. The lower limit of detection is less than 10 pCi/L. It gives results in 30 minutes with a sensitivity that matches or exceeds that of standard laboratory methods.

The RADH2O method employs a closed loop aeration scheme whereby the air volume and water volume are constant and independent of the flow rate. The air recirculates through the water and continuously extracts the radon until a state of equilibrium develops. The RADH2O system reaches this state of equilibrium within about 5 minutes, after which no more radon can be extracted from the water.

Usually Radon concentrations are measured with respect to the typical expected values in diluted waters, through either sampling (batch sampling)

measurements, performed on fixed volume samples of collected waters from springs or along the riverbed and followed by laboratory analysis or through continuous monitoring measurements directly in the waters [Sur05]. In the last case, in order to better implement such an approach, it is required the use of simple and not expensive, field usable Radon-in-water monitors with temporal resolutions of hours or less.

Another method to measure radon activity concentration in water consists in making an air circuit coupled to the water sample. The coupling can be realized by a very old method [Goc14], which exploits the Radon solubility into water and consists in bubbling air, from the closed circuit, directly through the water. The bubbling technique is very efficient in enabling fast exchange of Radon between water and air but its use on the field can turn out to be quite uncomfortable as efficient bubblers consume a lot of power. The RADH2O system is based on this last method.

A sample bottle is connected to the RAD7 in a closed air-loop mode, with a desiccant column before the air inlet of the counter. The specially designed screw-on cap of the sample bottle has two ports; one port is connected to the outlet of the RAD7, with a bubble stone connected at the other hand, and the other port is connected to a desiccant column. The radon from the water sample continuously circulates through the desiccant column, then through the RAD7's chamber, and then back to the water sample so that it reaches an equilibrium between the water and the air. Then, the activity of the $^{222}$Rn is determined by counting its alpha-emitting daughters in the monitor.

The internal air pump in the RAD7 re-circulates the air at a flow rate of about 1 L min$^{-1}$, purging radon in water to achieve a rapid equilibrium of radon between water and air. After the radon air-water equilibration is obtained, the radon in the air loop is measured by the RAD7.

The activity concentration of radon in water is calculated from the distribution factor of radon concentration between water and air. According to Weigel [Wei78], the distribution ratio at equilibrium, $k_w$ is governed by the water temperature as follows:

$$k_w = 0.105 + 0.405e^{-0.0502 \cdot T} \tag{5.1}$$

where $T$ is the temperature of the water in °C. The actual activity concentration of radon in a water sample is the sum of radon activity concentrations in the air loop, $C_{air}$, and water in the sample bottle, $C_{water}$, where radon is partitioned by Weigel's equation:

$$C_{water}V_{water} = C_{air}V_{air} + k_w C_{air}V_{water}. \tag{5.2}$$

Therefore, the original activity concentration of radon in the water sample can be represented as:

$$C_{water} = \frac{C_{air}V_{air} + k_w C_{air}V_{water}}{V_{water}} \tag{5.3}$$

where $V_{water}$ and $V_{air}$ are the water volume and the air volume in the loop (sample bottle, detection chamber, desiccant and tubes). As the volumes are fixed, the RAD7 gives automatically the result of the radon activity concentration in the water sample.

Figure 5.4: Aeration in progress of a 250 mL water sample [DUR09b].

The extraction efficiency, or percentage of radon removed from the water to the air loop, is very high, typically 99% for a 40 mL sample and 94% for a 250 mL sample. The exact value of the extraction efficiency depends somewhat on ambient temperature, but it is almost always well above 90%. Since the extraction efficiency is always high, little or no temperature effect is seen on the overall measurement.

After the measurement operations, the radon activity concentration can be measured. The value given by the instrument, C(t), must be corrected to get the activity concentration at the sampling instant, $C_0$, which is given by:

$$C_0 = C(t)e^{\lambda \cdot t} \tag{5.4}$$

where $\lambda$ is the radon decay constant. Remembering the radioactive decay law, $N(t) = N_0\ e^{-\lambda t}$, and knowing that radon has a half-life of 3.82 days, it has consequently a mean lifetime:

$$\tau = \frac{t_{1/2}}{ln2} \tag{5.5}$$

and so it has a decay constant:

$$\lambda = \frac{1}{\tau} = 2.08 \cdot 10^{-6} s^{-1} = 0.1814 days^{-1}. \tag{5.6}$$

The RAD7 gives an error on the activity concentration measurement, $\Delta C(t)$, which allows to get the error on the estimation of the value of $C_0$:

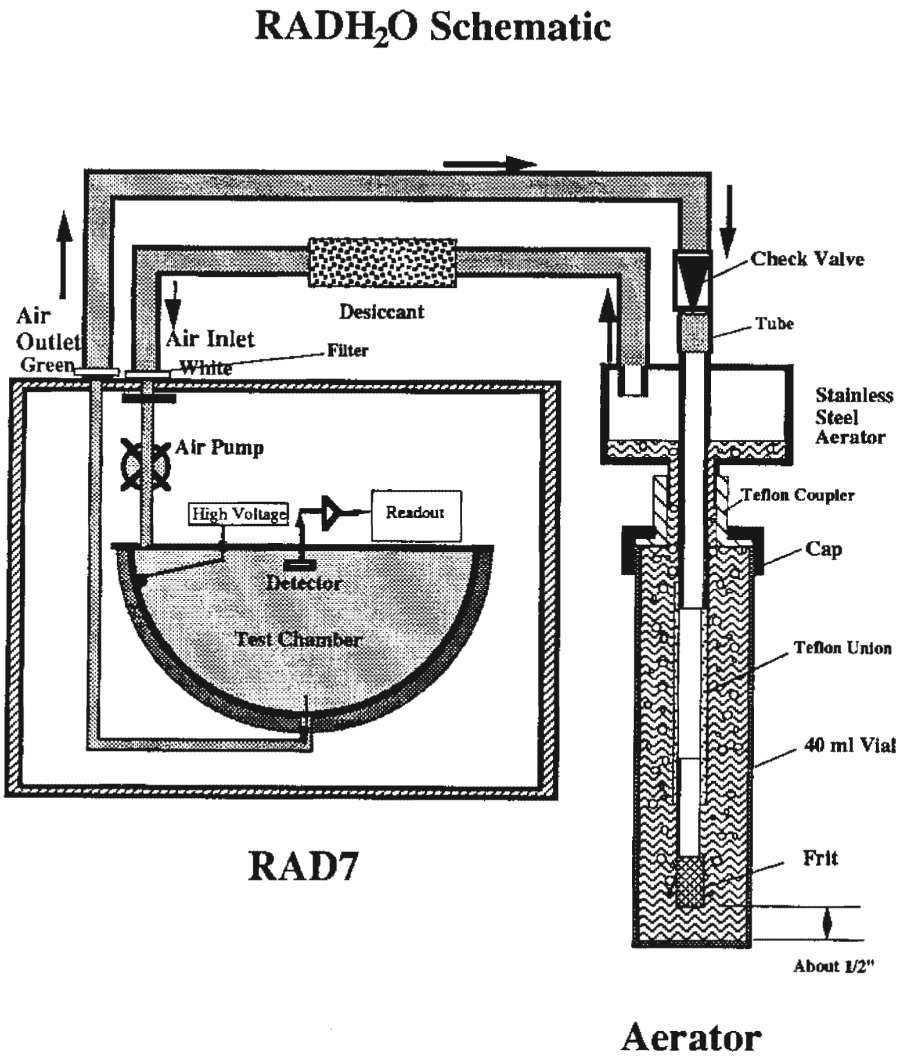


Figure 5.5: Scheme of the RADH2O system [DUR09b].

| Method | RADH2O | RADH2O | Liquid Scintillation | Lucas Cell |
|---|---|---|---|---|
| Sample size (mL) | 40 | 250 | 10 | 10 |
| Sensitivity (cpm/pCi/L) | 0.008 | 0.05 | 0.09 | 0.05 |
| Background (cpm) | 0.1 | 0.1 | 15 | 0.25 |
| **2-sigma error at 300 pCi/L (in pCi/L)** | | | | |
| 20-minute count | 88 | 35 | 32 | 35 |
| 60-minute count | 51 | 20 | 19 | 20 |
| **2-sigma error at 300 pCi/L (in pCi/L)** | | | | |
| 20-minute count | 53 | 20 | 24 | 20 |
| 60-minute count | 31 | 12 | 14 | 12 |
| **Detection Limit** (pCi/L) | | | | |
| 20-minute count | 40 | 6 | 28 | 9 |
| 60-minute count | 19 | 3 | 16 | 4 |
| 300-minute count | 7 | 1 | 7 | 2 |
| **Lower Limit of Detection** | | | | |
| 20-minute count | 60 | 10 | 41 | 13 |
| 60-minute count | 29 | 5 | 23 | 6 |
| 300-minute count | 11 | 2 | 10 | 3 |

Table 5.1: Comparison of RADH2O with other methods [DUR09b].

$$\Delta C_0 = \Delta C(t) e^{\lambda \cdot t} \tag{5.7}$$

### 5.1.2 Water Probe

An other way to make an air circuit coupled to water in order to extract radon from it, is to separate, instead, water and air through a diffusion membrane and then measuring radon in the gaseous phase. Thin plastic foils for such membranes usually show a slow response due to the small exchange surface and also they are pretty delicate from the mechanical point of view.

A solution can be to realize thick-walled membranes, mechanically much more stable and made of watertight membrane tubes developed for microfiltration, which show pretty good diffusion of radon through them. A good compromise is to have a membrane long (few meters) and thick (around 1.5 mm) enough to achieve the best possible time resolutions (below 1 hour) when used together with a flow-through radon-in-air detector [Sur96; Sch08].

A suitable experimental set-up consists of the Durridge RAD7 radon monitor in closed loop with a Radon-in-Water Probe (recently commercialized by Durridge), made of a Accurel for continuous measurements a commercially available permeable polypropylene tube, developed for microfiltration. The probe consists of a semi-permeable membrane tube mounted on an open wire frame. The tube is placed in a closed loop with RAD7.

When the probe is lowered into water, radon passes through the mem-

Figure 5.6: Water Probe by Durridge.

brane until the radon concentration in the air in the loop is in equilibrium with the radon concentration in the water. The equilibrium ratio of radon in the air to radon in the water is given by Weigel's equation (eq. 5.1), and depends on temperature which must be measured. The air stream is then fed to radon-in-air monitor that determines the concentration of $^{222}$Rn by collection and measurement of the alpha-emitting daughters, Polonium-218 and Polonium-214, in sequence.

The probe has an advantage in that it does not need a pump for the water. It will, however, take more than two hours to make a spot measurement or to respond to a step-change in radon concentration. It has a detection limit of 0.4 Bq/L and can also be used to monitor the radon concentration at a specified depth in open water.

In figure 5.7 it is shown the result of a measurement made with the probe at the BS13 (Sicilì Bridge) monitoring station on the 21st November 2009. The duration of the measurement is of 5 h and 30 m. After that time, an equilibrium between the radon activity in water and in the air loop is reached. The final result for radon activity concentration is 23000 ± 600 Bq/m$^3$ in air, $C_{air}$. Then, the radon activity concentration in water, $C_{water}$, is given by $k_w \cdot C_{air}$. Being the temperature of the water 13.4 °C (at the time of the measurement), the partition coefficient is 0.312, so $C_{water}$ = 7.2 ± 0.5 Bq/L, which is consistent with the measurement made at laboratory, with the RADH2O system, of a sample collected at the same time: $C_{water}$ = 7.5 ± 0.9 Bq/L.

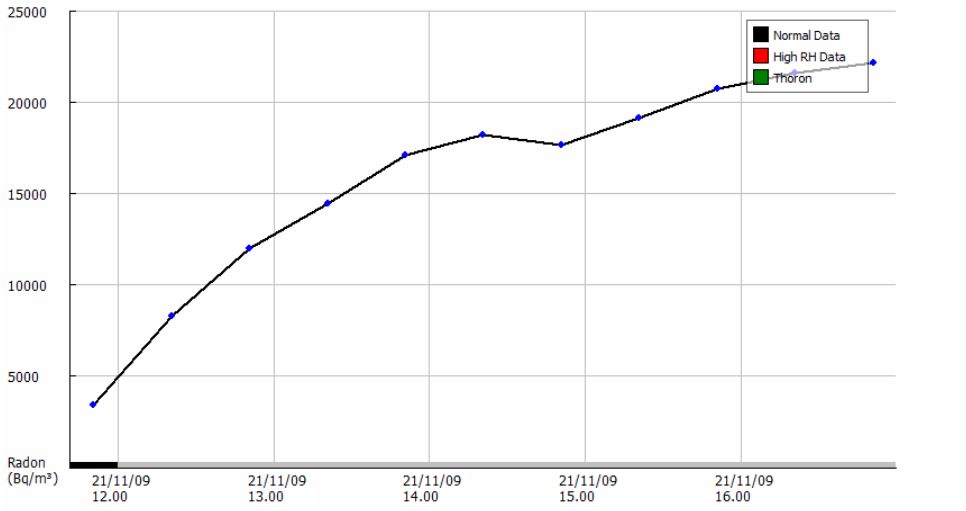


Figure 5.7: Radon activity concentration measured at the BS13 monitoring station with the probe. This graph is obtained through the Durridge's software Capture.

## 5.2 E-PERM: Electret Ion Chambers

E-PERM is a trade name for the Electret Ion Chambers manufactured by Rad Elec Inc. (USA). They are passive integrating ionization chambers requiring no batteries or power. This technology provides a unique, single-integrated solution for measuring short-term, long-term radon/thoron concentrations in air, radon in water, radon in soil and radon flux from surfaces and mill tailings.

Electret ion chamber for monitoring radon [Kot90; Kot96] consists of a stable electret (electrically charged Teflon disc) mounted inside an electrically conducting chamber. The electret serves both as a source of the electric field and as a sensor. The ions produced inside the chamber are collected by the electret. The reduction in charge of the electret is related to total ionization during the period of exposure. This charge reduction is measured using a battery operated electret reader.

The electret ion chambers have some similarities with alpha track detectors. In alpha track detectors, alpha particles from radon hit the special plastic and create a defect that will become visible when chemically processed. The number of tracks formed in the plastic over a time is related to integrated radon concentration over that period. In EIC, ions produced by alpha particles from radon are collected by electrets. The change in charge of the electret over a time is related to the integrated radon concentration over that time. Unlike alpha track detectors, no chemical processing is needed for EIC.

Using appropriate calibration factors and the exposure time, the desired parameters such airborne radon concentration in air, $C_{air}$ (in $Bq/m^3$) is calculated with the following equation:

$$C_{air} = \left( \frac{V_I - V_F}{CF \times t_{exp}} - BG \right) \times H \tag{5.8}$$


Figure 5.8: E-PERM System.


Figure 5.9: E-PERM System.

where $V_I$ and $V_F$ are the electret's initial and final voltage; $t_{exp}$ is the exposure time (in days); $BG = C \times R_\gamma$ is the equivalent radon concentration due to the environmental gamma radiation, in which $R_\gamma$ is the environmental gamma radiation (in nGy/h) and C is constant due to the particular electret-chamber configuration (table 5.4); H is a correction factor for the altitude (table 5.3).

CF is a calibration factor defined by the following equation (in $\frac{V \times m^3}{Bq \times days}$):

$$CF = \left( A + B \times \frac{V_I + V_F}{2} \right) \times 1/37 \tag{5.9}$$

where A and B are constants due to the particular electret-chamber configuration (table 5.4).

| **Chamber** | **Electret** | **A Constant** | **B Constant** | **C Constant** |
|---|---|---|---|---|
| S | ST | 1.6978 | 0.000542 | 0.35 |
| S | LT | 0.1400 | 0.0000525 | 0.35 |
| L | ST | 0.2613 | 0.0001386 | 0.59 |
| L | LT | 0.2383 | 0.0000112 | 0.59 |
| H | ST | 7.2954 | 0.004293 | 0.33 |

Table 5.2: Constants for the different electret-chamber configurations [MIAM05].

| **Altitude** (m) | **Correction Factor** (S Chamber) | **Correction Factor** (L Chamber) |
|---|---|---|
| 0 | 1.00 | 1.00 |
| 300 | 1.00 | 1.05 |
| 600 | 1.00 | 1.09 |
| 900 | 1.00 | 1.14 |
| 1200 | 1.03 | 1.18 |
| 1500 | 1.09 | 1.22 |
| 1800 | 1.15 | 1.28 |
| 2100 | 1.21 | 1.33 |
| 2400 | 1.27 | 1.39 |

Table 5.3: Correction factors for the altitude [MIAM05].

The EIC are used also to measure the radon activity concentration in water. This method belongs to the general class of *de-emanation method* of measuring dissolved radon in water. A small water sample is placed in the bottom of a glass jar. An E-PERM suspended in the air phase above the water. The lid of the flask is closed and sealed to make it radon-tight. Radon reaches equilibrium between the water and air phase. At the end of the desired exposure period, the flask is opened and the E-PERM removed. The average radon concentration in the air phase is calculated using the equation 5.8. A calculation using this air concentration in conjunction with the other parameters gives the radon concentration of the water, $C_{water}$.

For sample bottles of 68 mL $C_{water}$ is given by:

$$C_{water} = C_{air} \times C_1 \times C_2 \tag{5.10}$$

where $C_1$ is given by:

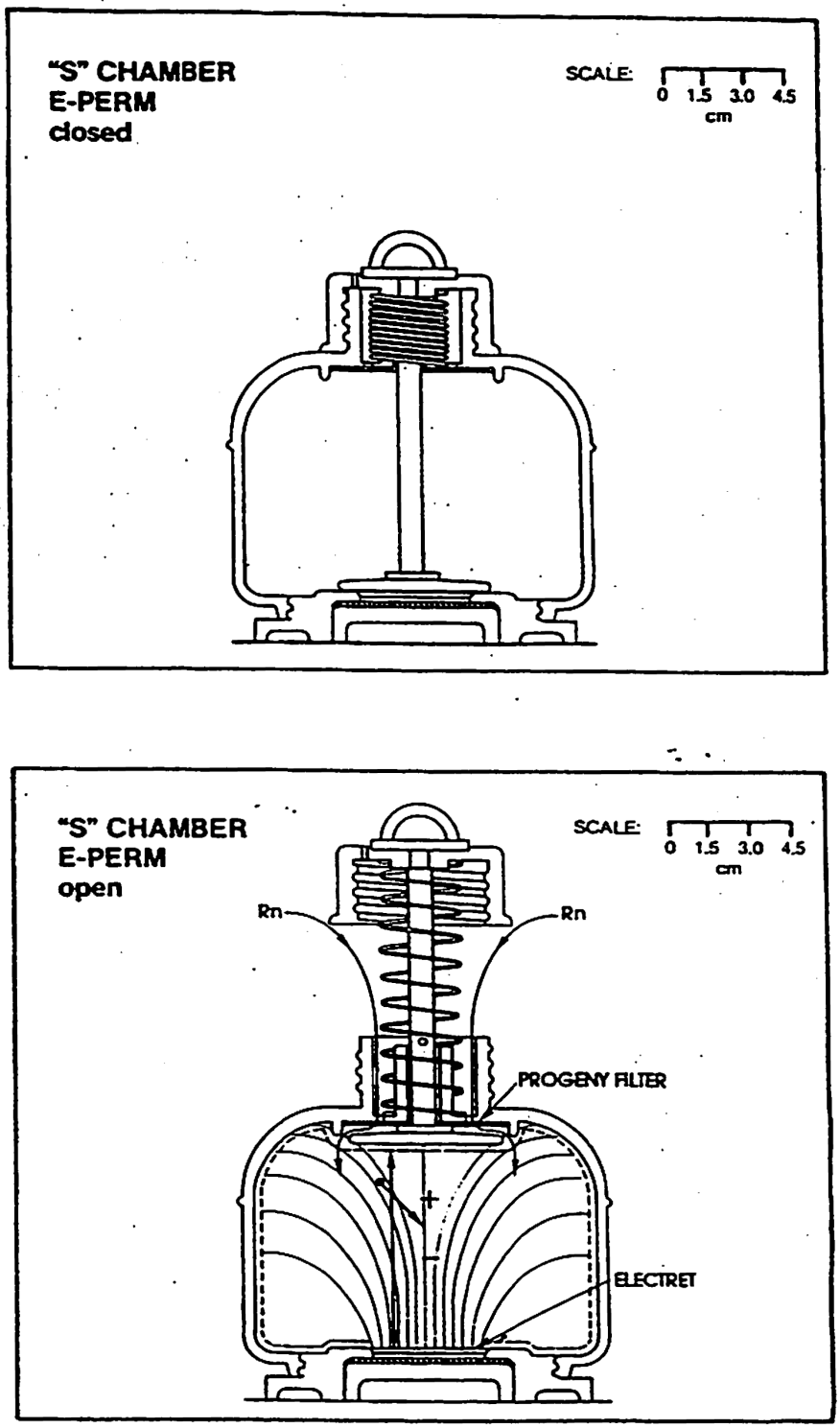


Figure 5.10: Schematic S Chamber E-PERM.

$$C_1 = e^{0.1814 \cdot t_{coll}}, \tag{5.11}$$

in which $t_{coll}$ (in days) is the time between the collection of the water sample and its placing in the chamber for the analysis; $C_2$ is given by:

$$C_2 = \frac{55.55 \times 0.1814 \times t_{exp}}{(1 - e^{-0.1814 \times t_{exp}})} \tag{5.12}$$

where $t_{exp}$ is the exposure time of the water sample.

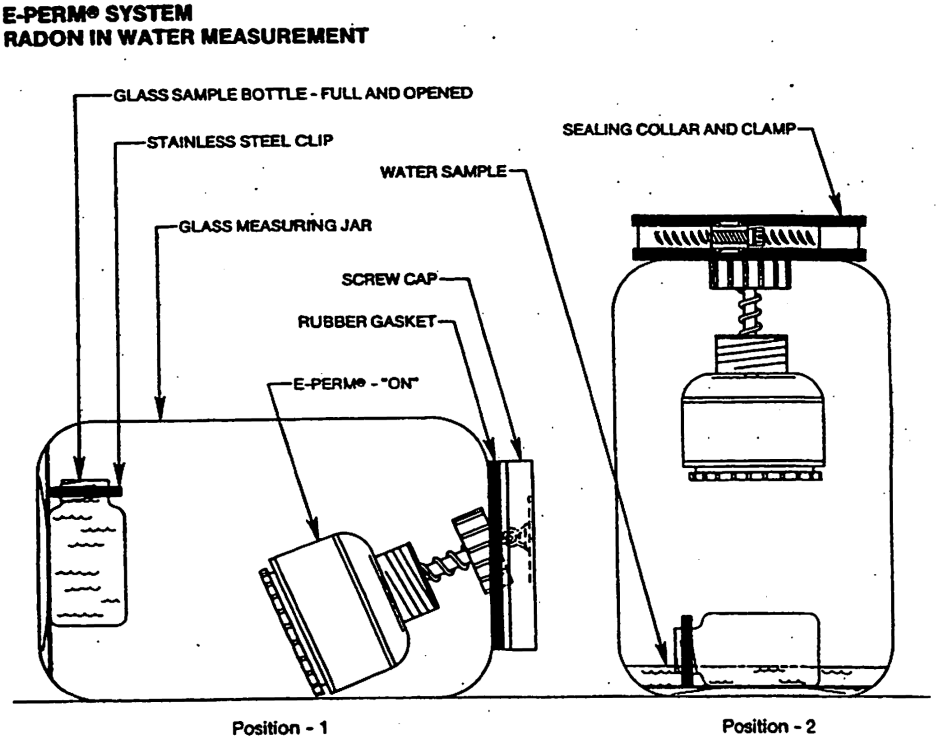


Figure 5.11: Schematic for measuring radon in water using E-PERM.

For sample bottle of 136 mL, the radon concentration in water is given by equation 5.10 divided by 2.

The results obtained from the measurements of radon activity concentration with the E-PERM system are consistent with the ones obtained with the RADH2O system only for great values of concentration ($\geq$ 25 Bq/L). In fact, for lower values, the errors are high and the result is not very reliable. So the measurements with the E-PERM system have been made only for samples collected at the springs, where radon concentration is higher.

| Detector | AC | AT | E-PERM | CRM |
|---|---|---|---|---|
| Features | Activated Charcoal | Alpha Track | Electret Ion Chambers | Continuous Radon Monitor |
| Short Term or Long Term | ST | LT | ST and LT | ST |
| True Integration | No | Yes | Yes | Yes |
| Hourly Readings | No | No | No | Yes |
| Temperature Correction | Required | No | No | No |
| Humidity Correction | Required | No | No | No |
| Elevation Correction | Not Known | Yes | Yes | May Require |
| Cost per Measurement | Low | Low | Low | High |
| Detector Cost | Low | Low | Low | High |
| Ruggedness | Good | Good | Good | Requires Careful Handling |
| Analysis Equipment | High | Very High | Low | High |

Table 5.4: Comparative features of different radon detectors [Kot00].

# Chapter 6

# Results and discussion

The Radon activity concentration data, acquired as reported in the previous chapter, have been arranged in relation to the fluvial level hierarchy and scale analysis: firstly, at segment scale, managing the data collected only from the main stations; secondly, at reach scale, including also the data from the complementary stations. Finally, as experimental support to improve the MBKS conceptual model, the results of the Radon activity concentration from the karst spring monitored have been explained and discussed.

Moreover an analysis of radon transfer from water to air has been made, applying two models taken from literature.

## 6.1 Segment scale analysis

The first river segment, the Middle Bussento Segment, starting from Old Mill Spring to Bussentino creek confluence gorge, comprises, from upstream, the following stations: BS15_S01_US (Upstream Old Mill Spring Station), BS15_S01_01, BS15_S01_02 and BS15_S01_03 (below Old Mill Spring Station), BS15_S01_DS (downstream Old Mill Spring Station).

The second river segment, the Middle-lower Bussento, starts from the above cited confluence gorge to the Bussento Hydropower Plant, comprising, from upstream, the following stations: BS13_US, BS13_03, BS13_02, BS13_01, BS13, BS13_DS, BS13_DS_Jundra_DS and BS12, with the numerous groundwater inflows from the bank and bed fracture along the uppermost segment reach. The groundwater inflows from the Cillito spring group are represented with the main springs codes BS13_S01 and BS13_S02. Tables 6.1 and 6.2 contain the average radon activity concentration data, related to the sampling campaigns from 2007 to 2009. In table 6.1 the BS25 (Bacuta Sinkhole Station) has been added to compare the Radon activity concentration in streamwater ingoing the MBKS, with the unique groundwater inflow into streamflow from the karst conduit Old Mill Spring (BS15_S01).

The average values for radon activity concentration are estimated according the periods of aquifer recharge (approximatively from autumn to spring) and aquifer recharge (approximatively from spring to autumn). These values vs. the topographic distance of the stations, monitored along the two segments, are graphically displayed in figures 6.1 and 6.2, highlighting the locations of the radon high-content inflows from the main spring stations.

As it can be seen from the figures, in the recharge periods the values of

| | BS25 | BS15_US | BS15_01 | BS15_02 | BS15_03 | BS15_DS |
|---|---|---|---|---|---|---|
| **Period** | $^{222}$Rn Conc. (Bq/L) | $^{222}$Rn Conc. (Bq/L) | $^{222}$Rn Conc. (Bq/L) | $^{222}$Rn Conc. (Bq/L) | $^{222}$Rn Conc. (Bq/L) | $^{222}$Rn Conc. (Bq/L) |
| Recharge 1 | 0.3 ± 0.1 | 2.9 ± 1.6 | 3.7 ± 0.4 | 0.8 ± 0.5 | 0.5 ± 0.3 | 0.2 ± 0.1 |
| Discharge 1 | 0.3 ± 0.2 | 3.8 ± 1.7 | 7 ± 2 | 1.5 ± 1.0 | 0.7 ± 0.4 | 0.5 ± 0.3 |
| Recharge 2 | 0.4 ± 0.1 | 4.0 ± 1.0 | 6.9 ± 0.5 | 0.9 ± 0.4 | 0.4 ± 0.2 | 0.5 ± 0.3 |
| Discharge 2 | 0.3 ± 0.1 | 5.8 ± 1.9 | 9.5 ± 2.5 | 1.2 ± 0.8 | 0.6 ± 0.3 | 0.3 ± 0.1 |

Table 6.1: Average values of radon activity concentration at the middle Bussento segment, estimated for the aquifer recharge and discharge periods.

| | BS13_US | BS13_02 | BS13_01 | BS13 | BS13_DS | BS12 |
|---|---|---|---|---|---|---|
| **Period** | $^{222}$Rn Conc. (Bq/L) | $^{222}$Rn Conc. (Bq/L) | $^{222}$Rn Conc. (Bq/L) | $^{222}$Rn Conc. (Bq/L) | $^{222}$Rn Conc. (Bq/L) | $^{222}$Rn Conc. (Bq/L) |
| Recharge 1 | 2.8 ± 1.6 | 7.0 ± 2.5 | 7.5 ± 2.5 | 4.5 ± 1.5 | 5.5 ± 2.0 | 0.8 ± 0.6 |
| Discharge 1 | 8.5 ± 2.0 | 10.5 ± 2.5 | 11.5 ± 4.5 | 7.5 ± 2.5 | 8 ± 3 | 0.4 ± 0.2 |
| Recharge 2 | 4.5 ± 0.3 | 8.9 ± 1.2 | 10 ± 2 | 5.4 ± 0.6 | 6.2 ± 1.1 | 0.6 ± 0.3 |
| Discharge 2 | 8 ± 3 | 12.2 ± 1.5 | 14.0 ± 1.5 | 6.8 ± 1.8 | 8 ± 2 | 0.5 ± 0.2 |
| Recharge 3 | 5.5 ± 1.3 | 9.2 ± 1.7 | 6.0 ± 1.5 | 7.0 ± 1.7 | 5.5 ± 1.1 | 0.6 ± 0.3 |

Table 6.2: Average values of radon activity concentration at the middle-lower Bussento segment, estimated for the aquifer recharge and discharge periods. Not all the stations of the segment are reported.

the activity concentration are lower than the ones of the discharge periods. In fact, during the recharge periods, the river flow increases and the contribution of the superficial waters (with a low radon content) is greater than the contribution of the baseflow, mainly due to groundwater (with a high radon content).

In the discharge periods the situation is the opposite. In fact, during the periods of river low flows, much of discharge is contributed by baseflow.

Data analysis at segment scale highlights the spatial variations of Radon activity concentration, detected along the middle and middle-lower Bussento river segments, and suggests the following considerations: i) the in-water variations of Radon activity concentration vs. the river long profile detect clearly the location of the surface-groundwater interactions, also where no discharge increments result from quantitative surveys (see BS15_S01_US and BS13_DS values); ii) define roughly the linear extension downstream of the groundwater influx, strictly related to the magnitude of the groundwater inflow and hydraulic condition of each reach; iii) prospect the approximate streamflow reference base value in the Radon activity concentration for the Bussento river, corresponding to the lower values detected from BS12 station

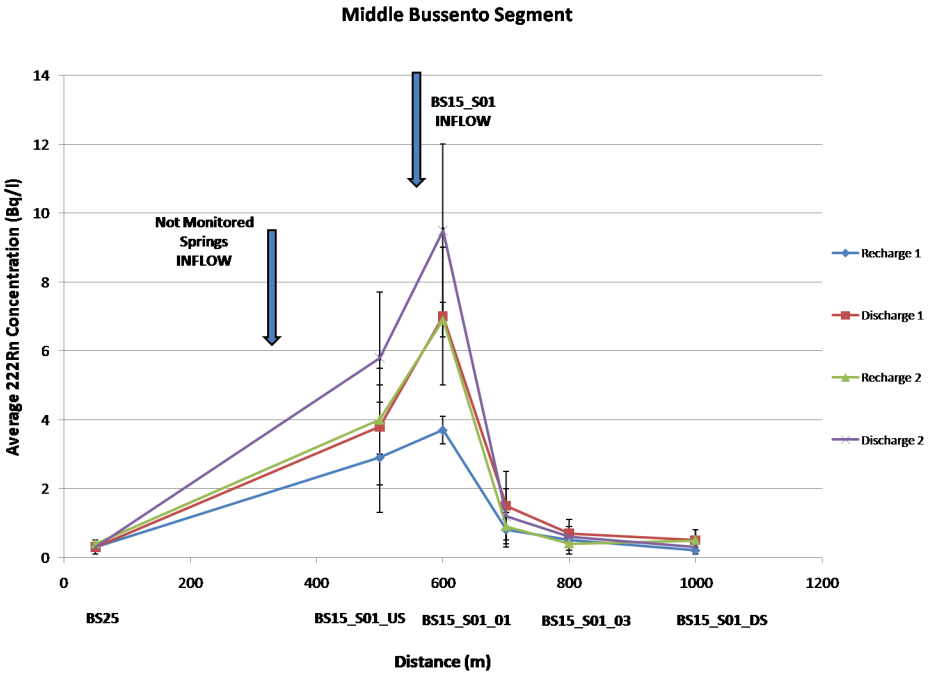


Figure 6.1: Average radon activity concentration values at the Middle Bussento segment. Data are divided according to the different seasonal periods (discharge, recharge). **Legend**: *Recharge Period 1 goes from September 07 to March 08; Discharge Period 1 goes from April 08 to June 08; Recharge Period 2 from October 08 to December 08; Discharge Period 2 goes from May 09 to October 09.*

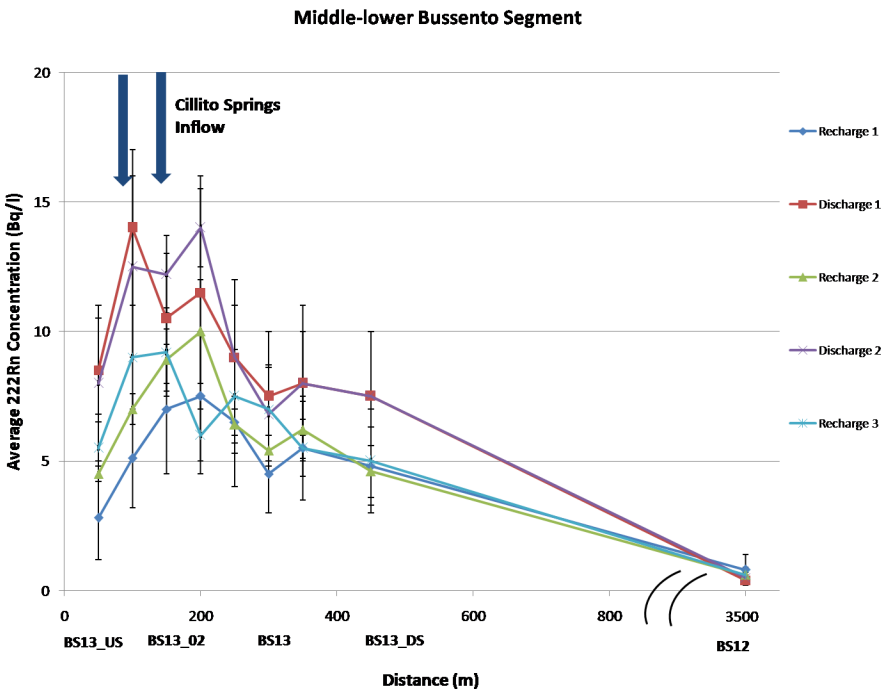


Figure 6.2: Average Radon activity concentration values measured along the Middle-lower Bussento segment. Data are divided according to the different seasonal periods (discharge, recharge). **Legend**: *Recharge Period 1 goes from September 07 to March 08; Discharge Period 1 goes from April 08 to June 08; Recharge Period 2 from October 08 to December 08; Discharge Period 2 goes from May 09 to October 09; Recharge Period 3 goes from November 09 to December 09.*

(mean value: 0.7 Bq/l) and BS25 station (mean value: 0.3 Bq/l).

For the middle Bussento segment (figure 6.1) the general trend obtained by the plot show an increase of radon concentration between the stations BS25 and BS15_S01_US, because of the presence of diffuse epikarst springs (not monitored). Then a greater increase can be seen between the station BS15_S01_US and BS15_S01_01, because of the inflow of the Old Watermill spring (BS15_S01), which is rich in radon (20-30 Bq/L). Finally the concentration decreases because of radon volatilization to the atmosphere and because there are no other spring inputs.

Analogously, at the middle-lower segment, fig 6.2 shows a great increase in radon concentration between the station BS13_US and the following three (BS13_03, BS13_02 and BS13_01) because of the inflow of the Cillito spring group (concentration between 30 and 50 Bq/L).

In order to correlate Radon data with other environmental parameters, table 6.3 reports the mean values of the physical-chemical parameter monitored by HI9828 multiparametric probe (Hanna Srl) along the segments of interest, during the 2007-2008 campaigns.

| **Station** | **T** (°C) | **pH** value | **DO** (%) | $\sigma$ ($\mu$S/cm) | $\rho$ (M$\Omega \cdot$ cm) | **TDS** (ppm) | **S** value |
|---|---|---|---|---|---|---|---|
| BS00 | 10.14 | 8.24 | 4.0 | 471 | 0.0021 | 236 | 0.23 |
| BS01 | 10.86 | 8.17 | 2.6 | 411 | 0.0024 | 206 | 0.20 |
| BS02 | 10.23 | 8.12 | 9.5 | 426 | 0.0023 | 213 | 0.21 |
| BS12 | 11.60 | 10.26 | 12.1 | 409 | 0.0024 | 205 | 0.20 |
| BS13 | 12.69 | 8.23 | 12.7 | 407 | 0.0025 | 204 | 0.20 |
| BS13_US | 12.77 | 8.43 | 14.7 | 412 | 0.0024 | 206 | 0.20 |
| BS15_US | 12.68 | 9.51 | 16.7 | 398 | 0.0025 | 199 | 0.19 |
| BS15_S01 | 12.92 | 7.73 | 12.9 | 409 | 0.0024 | 204 | 0.20 |
| BS15DS | 12.73 | 9.51 | 15.4 | 397 | 0.0025 | 198 | 0.19 |

Table 6.3: Mean values of the physical-chemical parameters monitored by Multiparametric Probe HI9828 (Hanna Srl) (2007-2008 campaigns). **Legend**: *1. T - Temperature; 2. pH; 3. DO - Dissolved Oxygen; 4. $\sigma$ - Conductivity; 5. $\rho$ - Resistivity; 6. TDS - Total Dissolved Solids; 7. S - Salinity.*

## 6.2 Reach scale analysis

The rate of spatial in-stream groundwater influx results differentiated for the two segments of interest, in relation to groundwater hydro-chemical type, discharge magnitude, and hydraulic river constraints, related to hydro-geomorphological typology of stream. In order to understand this differentiation, due to a different degassing rate of Radon from free surface of streamflow, an analysis at reach level and more detailed scale has been performed along the Sicilì Bridge reference reach and WWF Oasis reference reach. In the following, the results and data discussion for each reach are explained.

Their hydro-geomorphological characteristic, based on standardized geomorphic measurements [Nic07], allow to classify the first reach in the category "plane bed", *sensu* Montgomery & Buffington [Mot98] defined as an alluvial channel bed morphology type C, and the second, in the "step-pool"

category with a channel bed morphology type B. Figure 6.3 highlights the relations between the above reaches and their classification, *sensu* Montgomery & Buffington [Mot98] referring to the main hydraulics parameters (slope/gradient and Manning's $n$).

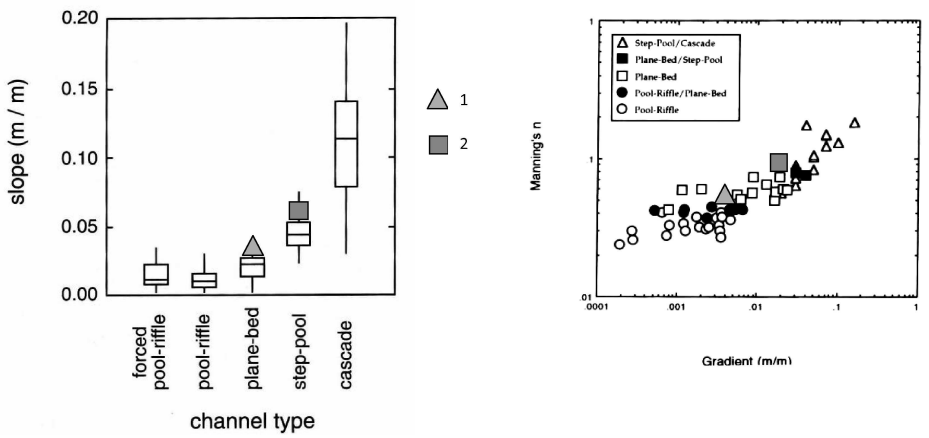


Figure 6.3: Classification of the Sicilì Bridge (1) and WWF Oasis reference reaches (2), in relation to: a) longitudinal slope and b) gradient vs. Manning's n. (modified from Montgomery D. R. and Buffington J. M., [Mot98]).

### 6.2.1 Sicilì Bridge reference reach

This reference reach is located uppermost the Middle-lower Bussento river segment (figure 4.5), identified by the reference main station BS13 (*Sicilì Bridge*).

| | **BS13_US** | **BS13_03** | **BS13_02** | **BS13_01** | **BS13_00** |
|---|---|---|---|---|---|
| **Measurement Campaign** | $^{222}$Rn Conc. (Bq/L) | $^{222}$Rn Conc. (Bq/L) | $^{222}$Rn Conc. (Bq/L) | $^{222}$Rn Conc. (Bq/L) | $^{222}$Rn Conc. (Bq/L) |
| January 08 | 4.3 ± 1.2 | 5.0 ± 0.6 | 6.5 ± 1.3 | 6.7 ± 0.6 | 5.3 ± 1.5 |
| February 08 | 3.2 ± 0.5 | 6.6 ± 1.0 | 7.7 ± 0.9 | 8.9 ± 0.9 | 7.9 ± 0.8 |
| March 08 | 0.9 ± 0.5 | 2.7 ± 0.5 | 3.4 ± 0.7 | 5.0 ± 0.5 | 1.9 ± 0.2 |
| April 08 | 7.6 ± 1.3 | 12.1 ± 0.8 | 12.1 ± 1.0 | 12.2 ± 1.8 | 9.4 ± 1.2 |
| May 08 | Not Av. | 19 ± 2 | 8.6 ± 0.7 | Not Av. | 7.9 ± 1.9 |
| June 08 | 8.8 ± 1.5 | 17.6 ± 1.7 | 19 ± 2 | 14 ± 4 | 9 ± 2 |
| October 08 | 9.0 ± 0.8 | 14 ± 2 | 11.5 ± 0.8 | 11.3 ± 1.5 | 9.4 ± 1.3 |
| December 08 | 4.5 ± 0.3 | 7.0 ± 0.6 | 8.9 ± 1.2 | 10 ± 2 | 6.4 ± 1.1 |
| May 09 | Not Av. | 17.6 ± 1.3 | Not Av. | Not Av. | 7.6 ± 1.4 |
| July 09 | 10 ± 3 | 14 ± 3 | 12.6 ± 0.5 | 12.5 ± 1.5 | 10.0 ± 1.2 |
| October 09 | 7.8 ± 0.7 | 7.6 ± 1.3 | 9.5 ± 1.4 | 14.3 ± 0.5 | 9.5 ± 1.1 |
| November 09 | 8.3 ± 1.1 | 11.0 ± 1.5 | 9.5 ± 1.5 | 13.0 ± 1.5 | 9.5 ± 1.5 |
| December 09 | 4.6 ± 0.7 | 6.5 ± 1.5 | 9.2 ± 0.8 | 5.5 ± 0.4 | 6.7 ± 1.0 |

Table 6.4: Sicilì Bridge - Upstream Monitoring Stations.

| | BS13 | BS13_DS | BS13_DS_J_DS |
|---|---|---|---|
| **Measurement Campaign** | $^{222}$Rn Conc. (Bq/L) | $^{222}$Rn Conc. (Bq/L) | $^{222}$Rn Conc. (Bq/L) |
| September 07 | 4.5 ± 0.8 | Not Available | Not Available |
| December 07 | 5.0 ± 0.8 | Not Available | Not Available |
| January 08 | 5.2 ± 1.1 | 7.0 ± 1.4 | 5.1 ± 0.5 |
| February 08 | 5.1 ± 0.6 | 7.2 ± 0.8 | 6.1 ± 0.9 |
| March 08 | 1.0 ± 0.5 | 1.2 ± 0.3 | 1.1 ± 0.4 |
| April 08 | 6.9 ± 0.6 | 8.0 ± 0.8 | 7.5 ± 0.9 |
| May 08 | 8.7 ± 1.7 | 9.1 ± 1.8 | 7.8 ± 1.6 |
| June 08 | 9.4 ± 1.2 | 8 ± 2 | 7.0 ± 1.4 |
| October 08 | 7.7 ± 1.0 | 7.6 ± 0.9 | 7.7 ± 0.8 |
| December 08 | 5.4 ± 0.6 | 6.2 ± 1.1 | 4.6 ± 1.0 |
| May 09 | 6.4 ± 1.2 | 3.6 ± 1.6 | 7 ± 2 |
| July 09 | 10.8 ± 1.3 | 7.8 ± 1.2 | 8.0 ± 0.6 |
| October 09 | 6.6 ± 0.3 | 8.9 ± 0.6 | 6.3 ± 1.2 |
| November 09 | 7.5 ± 0.9 | 6.5 ± 1.0 | 7 ± 2 |
| December 09 | 5.6 ± 1.5 | 5.2 ± 0.5 | 5.2 ± 0.5 |

Table 6.5: Sicilì Bridge - Downstream Monitoring Stations.

The station BS13_US has been chosen as an upstream monitoring station. It is placed upstream the Cillito springs group, emerging along the right bank, from enlarged fractures into Miocene calcarenites, overlaid by the marly-clayey formation regional aquiclude. Downstream, the first spring outlet of the Cillito group, four monitoring secondary stations (BS13_03, BS13_02, BS13_01, BS13_00) have been established in the river at a relative distance of 50 m, one from the other (figure 6.4).

Downstream the main station BS13, other two monitoring stations have been established: BS13_DS, and BS13_DS_Jundra_DS, this one downstream the superficial inflow from Jundra creek (figure 6.5).

The results of the measurement campaigns carried out from September 2007 to December 2007, as a procedure testing, and from January 2008 to December 2009, as experimental data acquisition, are reported in tables 6.4, 6.5 and 6.6, and the associated data are plotted in figure 6.6 for 2008 campaigns and figure 6.7 for 2009 campaigns.

These results show, as expected, that concentration measured at the group of 4 stations from BS13_03 to BS13_00 increases because of the inflow of the lateral springs, whose water is richer in radon. At the following stations there is a downstream decrease of radon concentration due to radon losses to the atmosphere, with the exception of the station BS13_DS, which shows a certain increase of concentration for almost all the measurement campaign.

The plot in figures 6.6 and 6.7 also show:

1. Homogeneity in the general trend of the curves: there is, in fact, an increase in Radon activity concentration values starting from the station BS13_03 and then a decrease from the station BS13 which is not influenced by the springs.

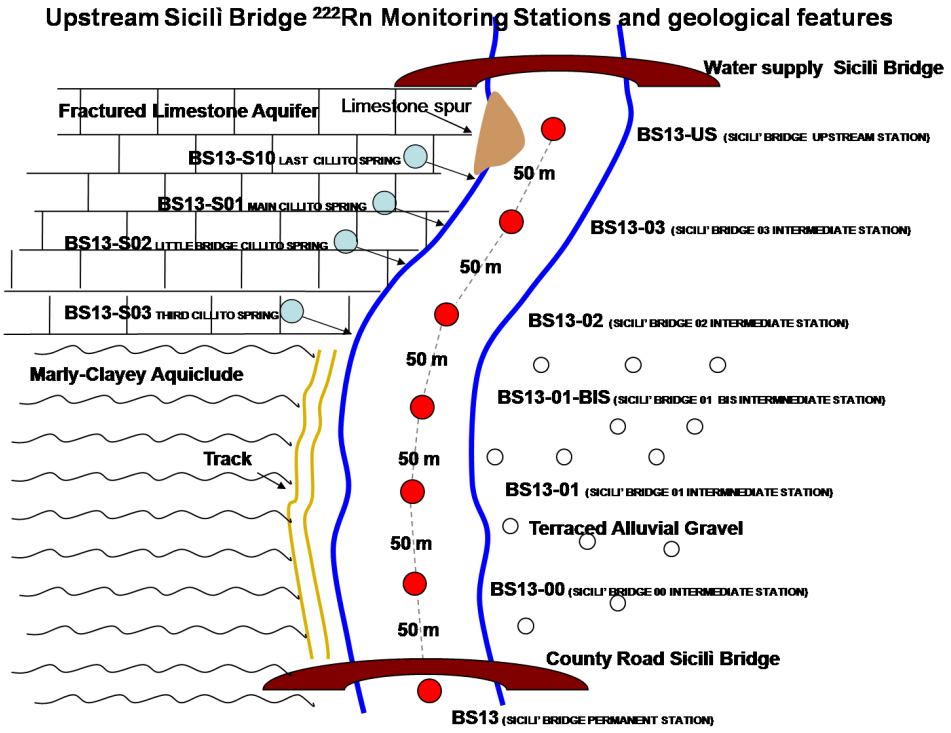


Figure 6.4: Upstream Sicilì Bridge Radon Monitoring Stations and geological features.

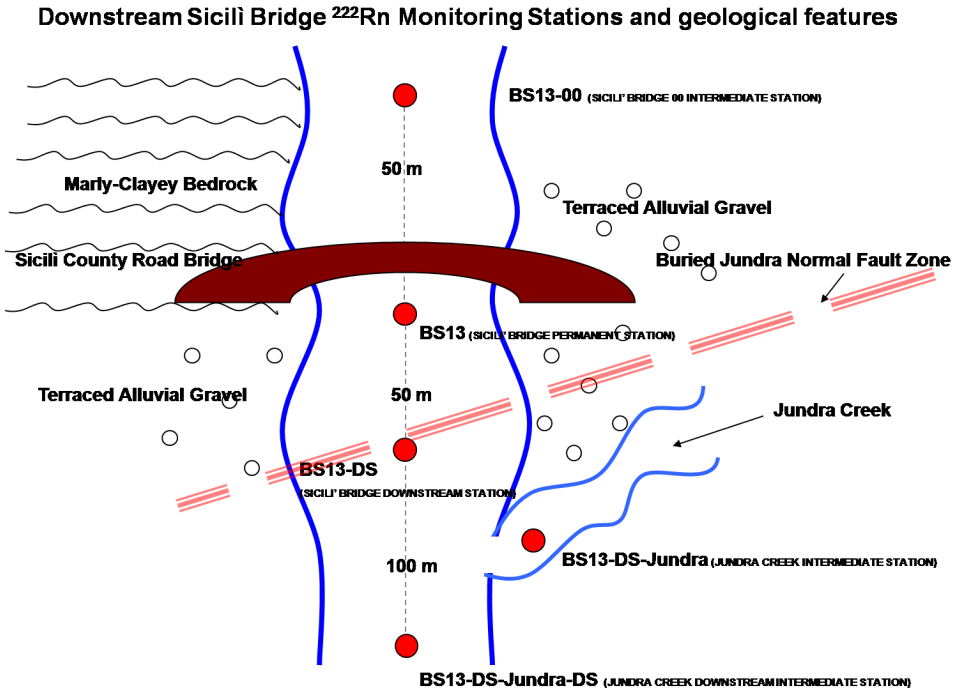


Figure 6.5: Downstream Sicilì Bridge Radon Monitoring Stations and geological features.

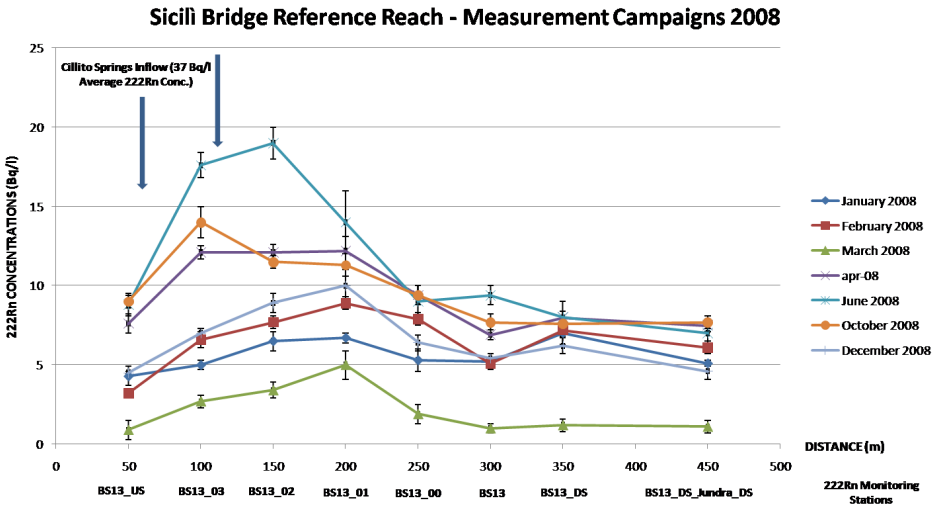


Figure 6.6: Radon activity concentration values measured (monthly base) at the Sicilì Bridge reference reach (2008 measurement campaigns).

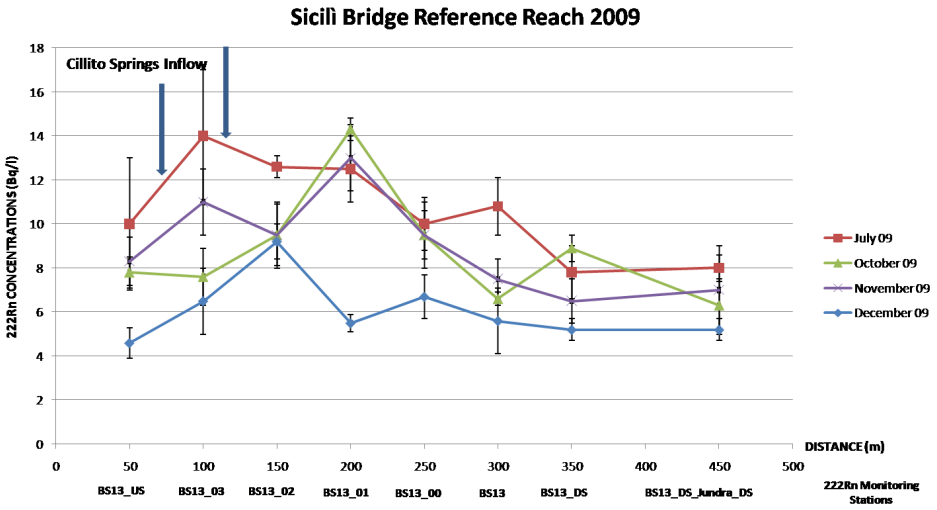


Figure 6.7: Radon activity concentration values measured (monthly base) at the Sicilì Bridge reference reach (2009 measurement campaigns).

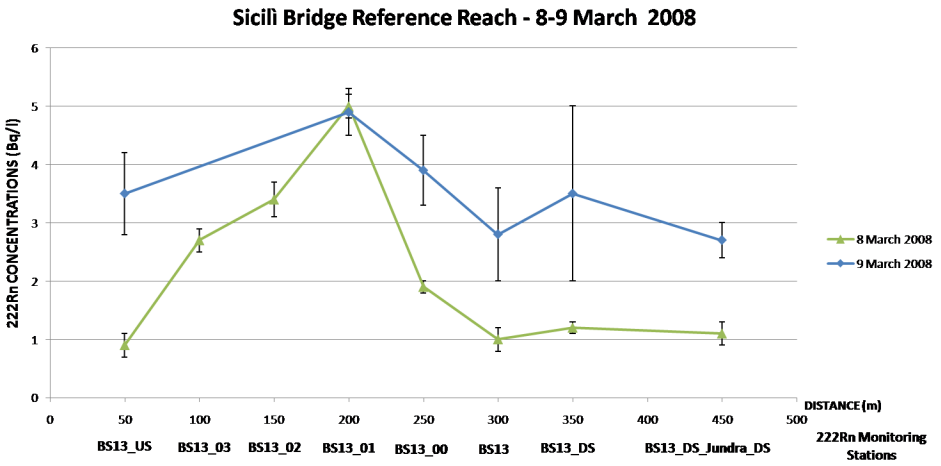


Figure 6.8: Radon activity concentration values measured at the Sicilì Bridge reference reach on the 8th (river in flood) and 9th March (after the flood) 2008. The green values obtained when the river was in flood are lower than the blue ones, which were measured the day after the flood.

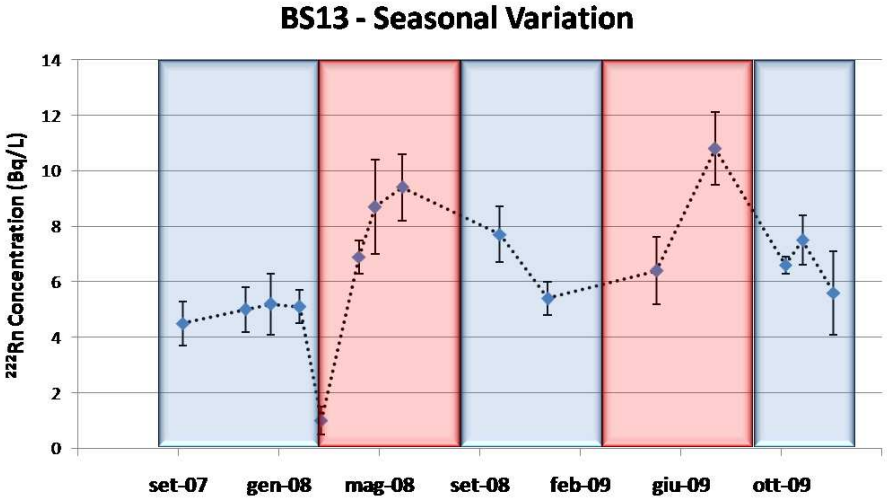


Figure 6.9: Radon activity concentration values measured at the Sicilì Bridge monitoring station (BS13) from 2007 to 2009. The blue color corresponds approximatively to the recharge period and the red color to the discharge period.

| | BS13_S01 | BS13_S02 |
|---|---|---|
| **Measurement Campaign** | $^{222}$Rn Conc. (Bq/L) | $^{222}$Rn Conc. (Bq/L) |
| September 07 | 28 ± 2 | Not Available |
| December 07 | 45 ± 8 | Not Available |
| January 08 | 35 ± 6 | 40 ± 8 |
| February 08 | 33.7 ± 1.2 | 36 ± 2 |
| March 08 | Not Available | Not Available |
| April 08 | 35.5 ± 7.5 | 39 ± 2 |
| May 08 | 37 ± 9 | 32.5 ± 5.5 |
| June 08 | Not Available | 36 ± 5 |
| October 08 | 35.5 ± 4.5 | 37 ± 3 |
| December 08 | 36.5 ± 3.5 | Not Available |
| May 09 | 33 ± 10 | 24 ± 8 |
| July 09 | 34 ± 2 | 31 ± 5 |
| October 09 | 35 ± 6 | Not Available |
| November 09 | 40.5 ± 6.5 | 37 ± 2 |
| December 09 | 39 ± 4 | Not Available |

Table 6.6: Cillito Springs Monitoring Stations.

2. Seasonality of radon relative concentrations, confirming in general that the measures made during the aquifer recharge period (Sep 07 - Mar 08) provide values of concentrations that are lower than the ones of the discharge period (Apr 08 - Oct 08). There is also an intermediate stripe of values corresponding to the first part of the new recharge period (Nov 08 - Dec 08) with a decrease in the Radon activity concentration. Also 2009 data confirm greater values of radon concentration during the aquifer discharge (July 09) and then a decrease (Oct 09 - Dec 09).

3. The March 2008 data are lower than the other ones because, on that day, the river was in flood, so there was a great quantity of superficial water, poor of radon. These values are shown in detail in figure 6.8 together with the values obtained from the sampling campaign of the day after the flood. In this plot it can be clearly observed an increase of radon activity concentration comparing the data from the two campaigns.

4. There is an anomalous increase in Radon concentration, for all the three periods considered, between the stations BS13 and BS13_DS, that is at the moment subject of further investigations in order to determine whether it can be attributed just to statistical fluctuations or not.

The seasonality of radon concentration is shown also in figure 6.9, where data obatined at the BS13 monitoring station are plotted. The trend obtained confirms that the values of radon concentration in the recharge period decrease going from autumn to winter, and then, in the discharge period, the values increase going from spring to summer. This is due, as mentioned

before, to the fact that in the discharge period, the presence of groundwater (richer in radon) is more predominant than in the recharge period.

### 6.2.2 WWF Oasis reference reach

This second case study concerns another reference reach of the Bussento river, located inside a World Wildlife Fund (WWF) oasis (figure 6.10), in which there is a main spring (BS15_S01 - Old Watermill Spring), where an average radon activity concentration with a range of values from 30 to 40 Bq/L has been measured.

| | **BS15_US** | **BS15_01** | **BS15_02** | **BS15_03** | **BS15_DS** |
|---|---|---|---|---|---|
| **Measurement Campaign** | $^{222}$Rn Conc. (Bq/L) | $^{222}$Rn Conc. (Bq/L) | $^{222}$Rn Conc. (Bq/L) | $^{222}$Rn Conc. (Bq/L) | $^{222}$Rn Conc. (Bq/L) |
| January 08 | 6.1 ± 1.6 | Not Av. | Not Av. | Not Av. | 2.0 ± 1.7 |
| February 08 | 0.9 ± 0.4 | 3.7 ± 0.4 | 0.8 ± 0.5 | 0.4 ± 0.2 | 0.2 ± 0.1 |
| March 08 | 0.6 ± 0.4 | 0.4 ± 0.1 | 1.1 ± 0.9 | 0.6 ± 0.3 | 0.8 ± 0.5 |
| April 08 | 1.6 ± 0.1 | 3.7 ± 0.9 | 0.8 ± 0.7 | 0.4 ± 0.3 | 0.8 ± 0.1 |
| May 08 | 1.7 ± 0.8 | 8.7 ± 0.8 | 1.7 ± 0.4 | 0.9 ± 0.5 | 0.6 ± 0.3 |
| June 08 | 6.5 ± 1.2 | 8.2 ± 1.4 | 1.6 ± 0.2 | 0.8 ± 0.3 | 0.3 ± 0.2 |
| October 08 | 6.3 ± 1.3 | Not Av. | 1.1 ± 0.8 | Not Av. | 0.2 ± 0.1 |
| December 08 | 4.0 ± 1.0 | 6.9 ± 0.5 | 0.9 ± 0.4 | 0.4 ± 0.4 | 0.5 ± 0.3 |
| May 09 | 5 ± 2 | Not Av. | 1.1 ± 0.7 | 0.5 ± 0.1 | 0.9 ± 0.7 |
| July 09 | 5.7 ± 0.5 | 15 ± 2 | 1.8 ± 0.7 | 0.9 ± 0.3 | 0.7 ± 0.4 |
| October 09 | 5.9 ± 0.4 | 8.8 ± 1.1 | 0.9 ± 0.5 | 0.8 ± 0.2 | 0.15 ± 0.15 |

Table 6.7: WWF Oasis - River Monitoring Stations.

| | **BS15_S01** |
|---|---|
| **Measurement Campaign** | $^{222}$Rn Conc. (Bq/L) |
| September 07 | 25 ± 2 |
| December 07 | 33 ± 3 |
| January 08 | 26.5 ± 6.5 |
| February 08 | 28 ± 3 |
| March 08 | 7 ± 6 |
| April 08 | 33.5 ± 6.5 |
| May 08 | 17.5 ± 3.5 |
| June 08 | 25.5 ± 3.5 |
| October 08 | 21.5 ± 5.0 |
| December 08 | 28 ± 5 |
| May 09 | 21.5 ± 6.5 |
| July 09 | 22 ± 7 |
| October 09 | 25.0 ± 4.5 |

Table 6.8: Old Watermill Spring Monitoring Station.

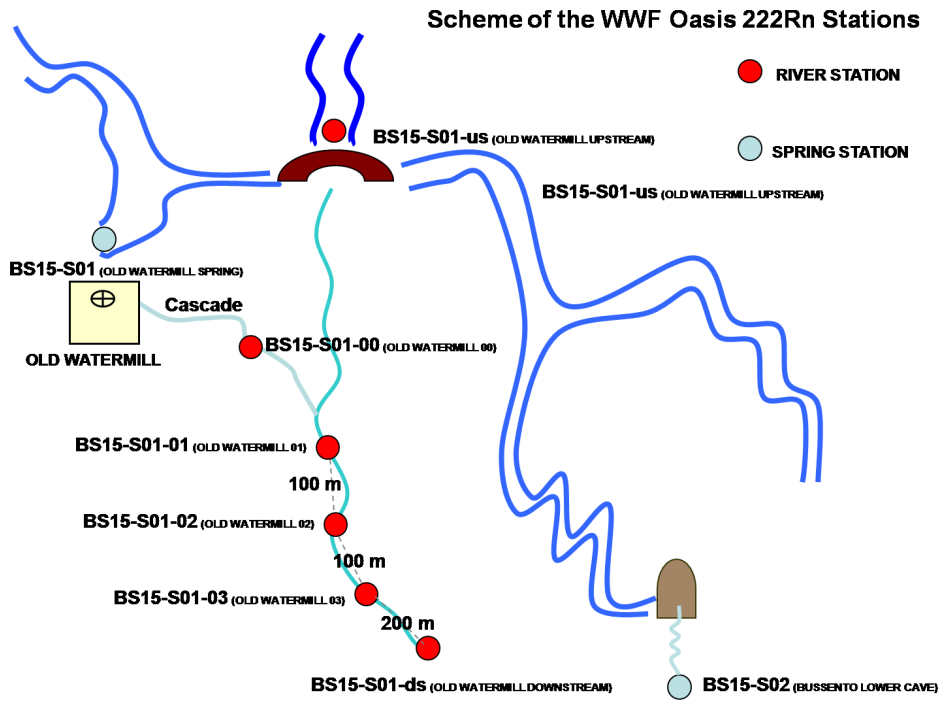


Figure 6.10: Radon Monitoring Stations and geological features at the WWF Oasis reference reach.

As in the previous case, a monitoring station (BS15_S01_US - Old Watermill Upstream) has been established above the inflow of the water coming from the spring, which, through a little cascade, falls into the river. Below the cascade and down the course of the river other 4 monitoring stations have been established. This part of the river is characterized by high turbulence, according to the step and pool stream typology, which surely can affects the Radon losses, increasing its degassing to the atmosphere. The results of the measurement campaigns, reported in tables 6.7 and 6.8 are plotted in figure 6.11 for the 2008 campaigns and in figure 6.12 for the 2009 campaigns.

It can be inferred a great increase in the Radon activity concentration in correspondence of the stations below the spring inflow, and then a quick decrease, which is due to the high turbulence of this reach, as mentioned above. In fact, the values obtained at the station BS15_S01_01 are always greater then the ones measured at the upstream station BS15_S01_US (except for March 2008 when the river was in flood).

Also for these two stations there is a seasonal trend, which is shown in figures 6.13 and 6.14. The values measured in the discharge period (approximatively from spring to summer) are greater than the ones obtained in the recharge one. For the station BS15_S01_01 this feature is more marked because of the direct influence of the water from the spring station (BS15_01).

Also in this case, data from the campaign of March 2008 are lower than the others and are approximatively homogeneous. This is due, as mentioned above, to the fact that the river was in flood, so radon concentration was affected by presence of superficial waters.

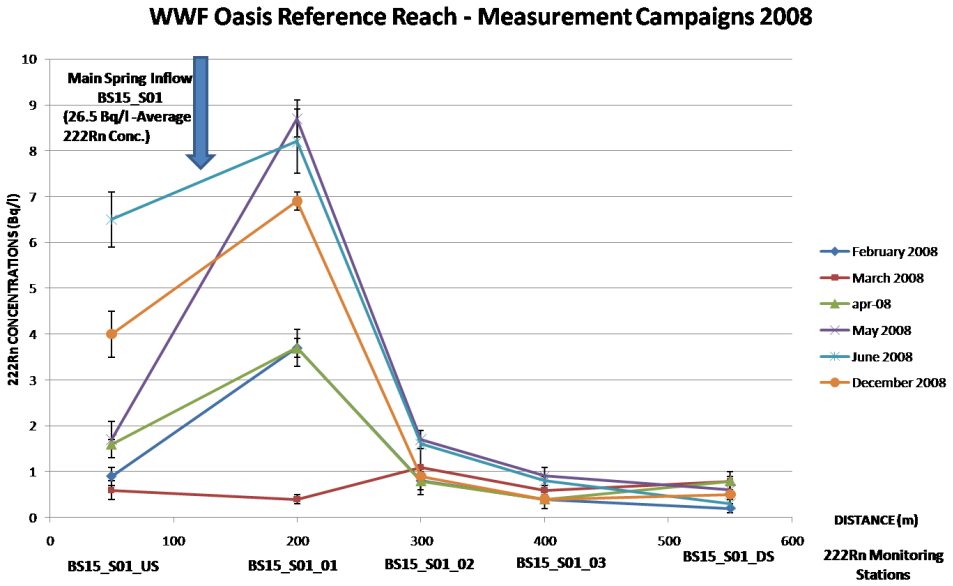


Figure 6.11: Radon activity concentration values measured at the WWF Oasis reference reach (only for 2008 measurement campaigns).

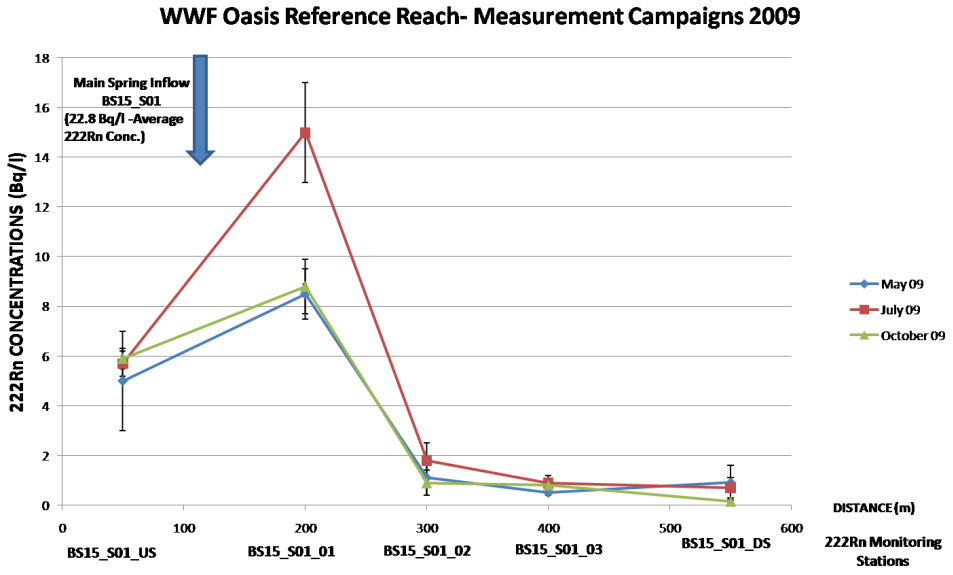


Figure 6.12: Radon activity concentration values measured at the WWF Oasis reference reach (only for 2009 measurement campaigns).

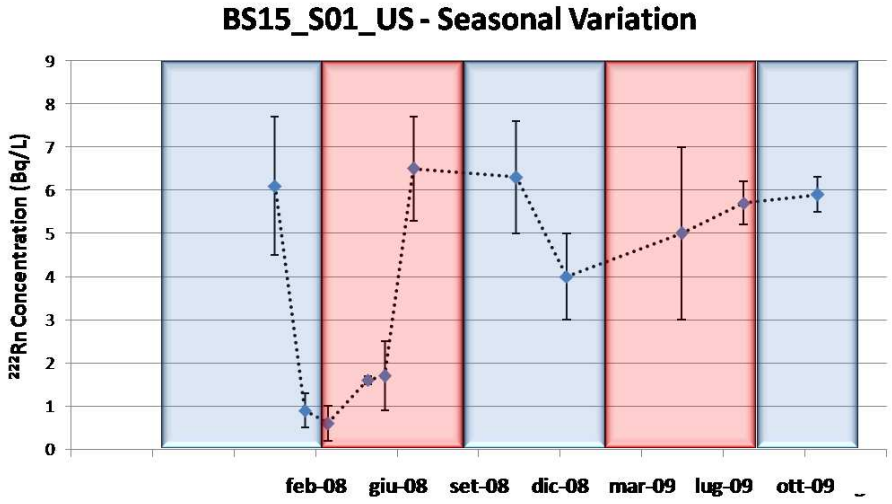


Figure 6.13: Radon activity concentration values measured at the WWF Oasis Upstream monitoring station (BS15_S01_US) from 2008 to 2009. The blue color corresponds approximatively to the recharge period and the red color to the discharge period.

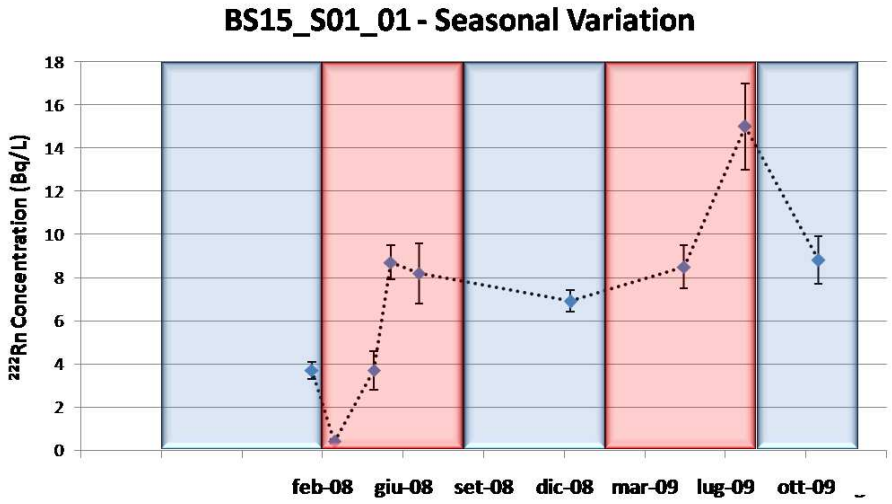


Figure 6.14: Radon activity concentration values measured at the WWF Oasis first monitoring station (BS15_S01_01), just below the inflow of the water from the spring (BS15_S01), from 2008 to 2009. The blue color corresponds approximatively to the recharge period and the red color to the discharge period.

## 6.3 Upper Bussento Segment

Another river segment that has been analyzed is the Upper Bussento segment. In this segment there are the upstream stations (BS22, BS21 and BS20) which have been established to estimate the radon concentration of the water (prevalently spring water) coming from the southern side of Mount Cervati and from the northern side of Mount Centaurino.

| **Measurement Campaign** | **BS18** $^{222}$Rn Conc. (Bq/L) | **BS19** $^{222}$Rn Conc. (Bq/L) | **BS20** $^{222}$Rn Conc. (Bq/L) | **BS21** $^{222}$Rn Conc. (Bq/L) | **BS22** $^{222}$Rn Conc. (Bq/L) |
|---|---|---|---|---|---|
| September 07 | 4.2 ± 0.6 | 0.5 ± 0.3 | Not Available | Not Available | Not Available |
| December 07 | 4.8 ± 0.8 | 0.4 ± 0.3 | Not Available | 2.5 ± 0.8 | Not Available |
| January 08 | 3.3 ± 0.9 | 0.2 ± 0.1 | 0.8 ± 0.4 | 0.7 ± 0.5 | 0.9 ± 0.3 |
| February 08 | 4.1 ± 0.8 | Not Available | Not Available | Not Available | Not Available |
| April 08 | 4.6 ± 0.8 | 0.9 ± 0.2 | 0.4 ± 0.2 | 0.4 ± 0.1 | 0.9 ± 0.4 |
| May 08 | 7.7 ± 1.0 | 0.3 ± 0.2 | Not Available | 0.2 ± 0.1 | 0.7 ± 0.4 |
| June 08 | 7.9 ± 0.9 | 0.5 ± 0.3 | 0.3 ± 0.1 | 0.4 ± 0.3 | 0.3 ± 0.2 |
| October 08 | Not Available | Not Available | 0.4 ± 0.3 | 0.7 ± 0.6 | 0.5 ± 0.3 |
| November 08 | 4.3 ± 0.9 | 0.5 ± 0.4 | 0.4 ± 0.3 | 0.2 ± 0.2 | 0.5 ± 0.2 |
| December 08 | 5.0 ± 0.4 | 0.3 ± 0.2 | 0.4 ± 0.1 | 0.3 ± 0.3 | 0.5 ± 0.3 |
| March 09 | Not Available | Not Available | 0.8 ± 0.2 | 0.9 ± 0.4 | 0.3 ± 0.2 |
| May 09 | 8.5 ± 2.5 | 0.2 ± 0.2 | 0.1 ± 0.1 | 0.3 ± 0.2 | 0.1 ± 0.1 |
| December 09 | 11.2 ± 1.3 | 4.2 ± 1.5 | 2.3 ± 0.8 | 1.8 ± 1.1 | Not Available |

Table 6.9: Upper Bussento Monitoring Stations.

The values of radon concentration obtained at these stations are low (between 0.2 and 0.9 Bq/L). This is due to the fact that the river depth is very low, the river course from the springs is long and there is also a middle turbulence, so most of radon outflows to the air.

There are other three stations downstream. The Farnetani Bridge Stations (BS19) has been established to estimate the radon concentration above the inflow of the Farnetani springs group and below all the inflows coming from the mountain creeks and the piedmont springs. The values of radon concentration at this station are a little higher than the ones obtained at the upstream stations, because of the influence of the piedmont springs.

Then there is the Acquevive Bridge Station (BS18), which is localized at the river dike, and has been established to estimate the radon concentration in the river water below the Farnetani springs group. The values measured at this station are higher than the previous ones (between 3 and 11 Bq/L), because of the presence of the Farnetani springs which contribute with an average radon concentration of about 30-35 Bq/L.

Another station has been established downstream the BS18, it corre-

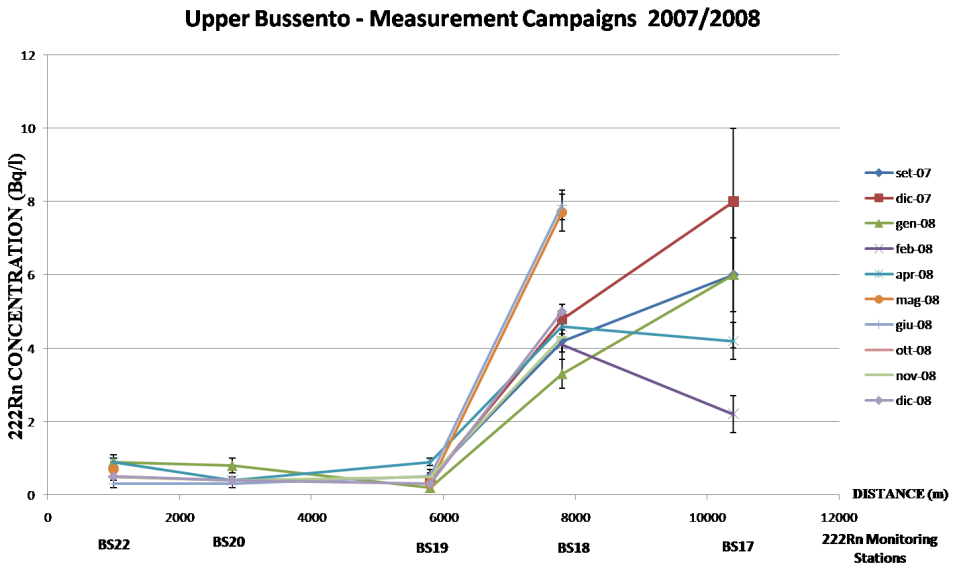


Figure 6.15: Upper Bussento measurement campaigns 2007/2008.

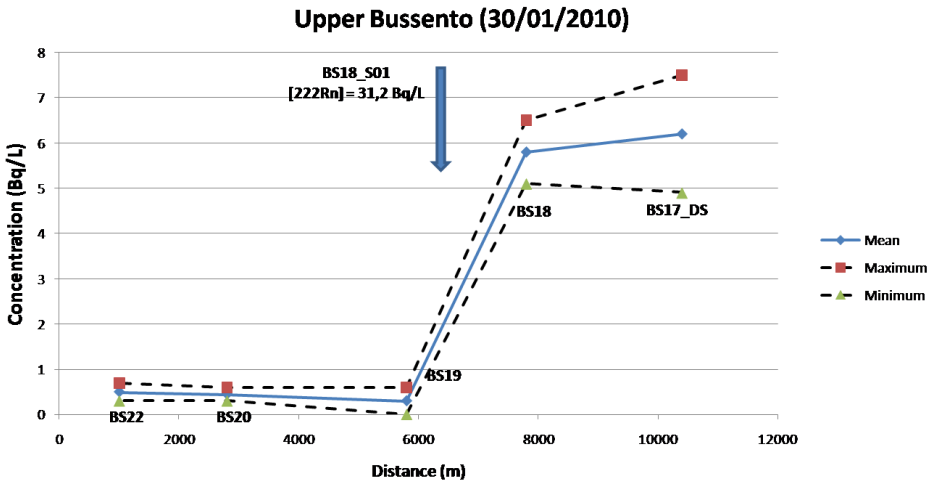


Figure 6.16: Measurements at the Upper Bussento segment on the 30th January 2010.

sponds to the Sabetta reservoir and it is localized at the right side of Bussento, in correspondence of the entrance of the hydropower plant. Some water samples have sometimes been collected at this monitoring station, but there is still uncertainty about their significance because the water collected could come from different inflows.

In tabel 6.9, data from 2007-2009 measurement campaigns are reported. Figure 6.15 shows the trend obtained for the data from the 2007-2008 campaigns: there is a flat trend (within the experimental errors) for the values measured from the station BS22 to BS19; then there is a great increase in radon concentration at the station BS18, and then this value stabilizes at the BS17 station.

Figure 6.16 shows the same trend of figure 6.15, it is related to a measurement camapign made on the 30th January 2010. In this campaign radon concentration is measured also at a significant spring of the Farnetani group and it is 31.2 Bq/L, which justifies the great increase of radon concentration between stations BS19 and BS18. This time an other water sample was collected at the station BS17_DS, which is downstream the BS17 (Sabetta reservoir) station. It is important because the value measured here can be considered as a reference value for the Middle Bussento segment before the influence of the spring inflows.

## 6.4 Radon gas exchange analysis

The radon content of river water is strongly affected by volatilization to the atmosphere, and this must be accounted for in using radon data to estimate a possible groundwater influx from subsurface water sources, important in river flow generation.

An important mechanism for radon removal from river water is the gas exchange. The model used to characterize the transfer of radon to the atmosphere is the stagnant film model.

This model assumes that the rate of exchange of gases between the water and the atmosphere is controlled by molecular diffusion through a stagnant film tens of microns thick at the air-water interface. Both the air above and the water below this film are assumed to constitute two well-mixed reservoirs with uniform vertical concentrations separated by the stagnant film of water. The thickness of the film is so dependent on the degree of agitation of the water surface caused by wind, waves and currents.

The transfer of the gases through the film is governed by Fick's law for diffusive flux which applied to the stagnant film model becomes:

$$F = -D\frac{C^{\alpha} - C^{w}}{z} \tag{6.1}$$

where $F$ is the transfer rate of gas per unit area and time, $D$ is the molecular diffusion coefficient for the gas, $C^{\alpha}$ is the concentration of the gas at the atmosphere-water interface (equal to the solubility times partial pressure), $C^{w}$ is the concentration of the gas at the bottom of the film, and $z$ is the stagnant film thickness (positive downward).

To apply equation 6.1 to $^{222}$Rn gas exchange, parameters $C^{\alpha}$ and $C^{w}$ should be measured; however, as Hammond et al. have shown [Ham77], the

concentration of $^{222}$Rn in equilibrium with the atmosphere ($C^{\alpha}$) is on the order of 0.02 to 0.05 dpm/liter, thus equation 6.1 simplifies to

$$F = D\frac{C^w}{z}. \tag{6.2}$$

The molecular diffusivity for radon has been determined to be (1.14 ± 0.07) × $10^{-5}$ cm$^2$/s at 18°C [Ron18]. Peng et al. [Pen74] developed an expression relating the molecular diffusion for radon in water as a function for temperature which can be used in our calculations requiring $D$:

$$-logD = (980/T) + 1.59 \tag{6.3}$$

The units of $D$ are cm$^2$/s and $T$ is the absolute temperature. From equation 6.2 the only parameters that are unknown are $F$ and $z$. The treatment used to determine the values of these unknowns varies with each system. In open ocean systems an estimate of the depth integrated deficiency of $^{222}$Rn at the near surface is used for the transfer rate ($F$) and film thickness ($z$) values are calculated. Emerson [Eme75] developed an empirical relationship of film thickness to wind speed and Hammond et al. [Ham77] used this relationship to determine film thickness in the Hudson river estuary and Hammond and Fuller [Ham79] used it in San Francisco Bay. After estimating the film thickness, an evasion rate was calculated.

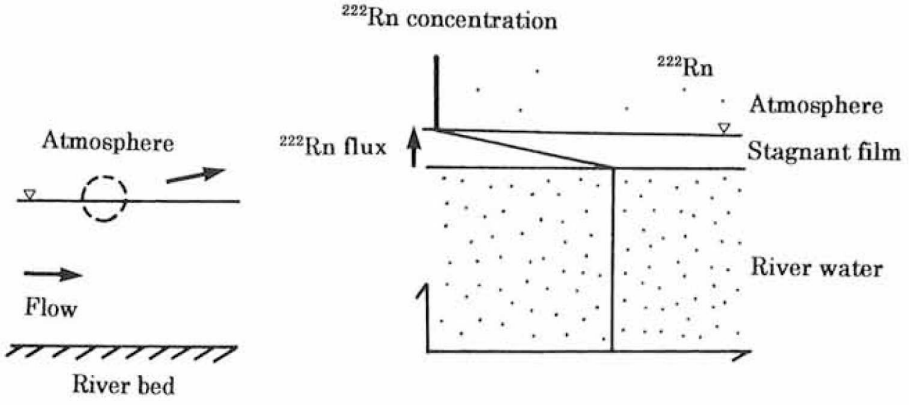


Figure 6.17: Stagnant film [Had99].

The behavior of $^{222}$Rn in a river can be approximated with the following equation:

$$\frac{dC}{ct} = V\frac{dC}{dx} - (\frac{dC}{dt})_{EV} \tag{6.4}$$

where $C$ is the concentration of $^{222}$Rn, $V$ is the velocity of water and $EV$ is the radon lost by evasion to the atmosphere.

The evasion component is related to the flux, $F$, in equation 6.2 by:

$$(\frac{dC}{dt})_{EV} = \frac{F}{h} = -D\frac{C^w}{zh} \tag{6.5}$$

where $h$ is the mean depth of the river.

Combining equations 6.4 and 6.5, the following equation can be obtained:

$$\frac{dC}{dt} = V\frac{dC}{dx} - \frac{D}{zh}C^w \tag{6.6}$$

and at $\frac{dC}{dt} = 0$:

$$C^w = C^{x=0}e^{-(D/zhV)x}. \tag{6.7}$$

Taking the ln of equation 6.7 produces the equation of a line,

$$ln\frac{C^w}{C^{x=0}} = -(D/zhV)x \tag{6.8}$$

with a slope of $D/zhV$.

The thicker the boundary layer, the more slowly that $^{222}$Rn is transferred from surface water to the atmosphere. For example, in a surface water system where radioactive decay is the dominant mechanism of $^{222}$Rn loss, the stagnant film model considers the stagnant film layer to be exceedingly thick such that $^{222}$Rn loss via molecular diffusion to the atmosphere is prohibited. The thickness of the stagnant film, z, is estimated (6.9) by comparing upstream and downstream $^{222}$Rn concentrations in a section of the stream where it can be assumed that there is no groundwater contribution to stream flow:

$$z = \frac{xD}{ln\left(C_0/C_T^n\right)h\nu}. \tag{6.9}$$

In the equation 6.9 z is the thickness of the stagnant film, x is the distance between the sampling stations, $D$ is the molecular diffusivity of $^{222}$Rn (1.2 $\times$ $10^{-9}$ $m^2$ $s^{-1}$ at 23°C), $C^0$ is the $^{222}$Rn activity concentration upstream (Bq/L), $C^n{}_T$ is the $^{222}$Rn activity concentration downstream (Bq/L), $h$ is the average depth of the stream (m) and $v$ is the velocity of the stream water.

Elsinger and Moore [Els83] found values for $z$ in a range from 19$\mu$m to 48$\mu$m in the Pee Dee river (USA). Their values fall within the range that Peng et al. [Pen74] determined for the North Pacific Ocean (9$\mu$m to 56$\mu$m) where the thickness was related to the wind speed. If wind controls the exchange, one might expect $z$ thickness to be larger as Emerson and Broecker [Eme73] found in the experimental lakes in Ontario, which have low wind velocity (1-2 m/s): they obtained a range of $z$ between 500 and 700 $\mu$m.

An analysis of the Radon diffusion phenomenon from water to atmosphere has been made for the Sicilì Bridge and for the WWF Oasis reaches, at which two stations were chosen as significant stations for an upstream, $C_{US}$, and a downstream, $C_{DS}$, concentration. Then the trend of the radon concentration in the river section considered has been analyzed, for the various campaigns obtaining different results for the two reaches.

At the Sicilì Bridge reach the upstream reference station was the BS13_02 and the downstream reference station was the BS13_DS_Jundra_DS. The distance between the two stations is 350 m. According to a numerical analysis of the radon concentration data, an exponential decay law can be assumed as a good approximation, thus fixing with the stagnant film equation. The exponential coefficient $\alpha$ and the thickness of the stagnant film, $z$, have been

estimated for the different measurement campaigns and are reported in table 6.11. As it can be seen from the table, most of the values estimated for $z$ are within a range from 5 to 15 $\mu$m.

| **Measurement Campaign** | **Degassing Coefficient** $\alpha$ ($m^{-1} \cdot 10^{-3}$) | **Stagnant Film Thickness** $z$ ($\mu$m) |
|---|---|---|
| January 08 | 0.8 ± 0.1 | 15 ± 2 |
| February 08 | 0.8 ± 0.1 | 15 ± 2 |
| March 08 | 3.8 ± 1.1 | 3.2 ± 1.0 |
| April 08 | 1.4 ± 0.2 | 9.0 ± 1.0 |
| June 08 | 3.3 ± 6 | 3.6 ± 0.7 |
| October 08 | 1.7 ± 0.3 | 7.0 ± 1.1 |
| December 08 | 2.2 ± 0.5 | 5.5 ± 1.1 |
| May 09 | 2.6 ± 1.0 | 4.6 ± 1.8 |
| July 09 | 1.6 ± 0.5 | 7.5 ± 2.5 |
| October 09 | 1.4 ± 0.5 | 9 ± 3 |
| November 09 | 1.3 ± 0.6 | 9 ± 4 |
| December 09 | 1.9 ± 0.4 | 6.5 ± 1.5 |

Table 6.10: Radon degassing coefficient $\alpha$ and stagnant film thickness $z$ estimated at the Sicilì Bridge reference reach for different measurement campaigns.

| **Measurement Campaign** | **Degassing Coefficient** $\alpha$ ($m^{-1} \cdot 10^{-3}$) | **Stagnant Film Thickness** $z$ ($\mu$m) |
|---|---|---|
| February 08 | 8 ± 5 | 1.4 ± 0.8 |
| March 08 | 1.3 ± 0.8 | 9 ± 6 |
| April 08 | 4 ± 1 | 2.7 ± 0.7 |
| May 08 | 7.6 ± 1.8 | 1.6 ± 0.4 |
| December 08 | 7.5 ± 2.0 | 1.6 ± 0.4 |
| May 09 | 6 ± 4 | 2.0 ± 1.5 |
| July 09 | 9 ± 6 | 1.4 ± 1.0 |
| October 09 | 12 ± 10 | 1.2 ± 1.0 |

Table 6.11: Radon degassing coefficient $\alpha$ and stagnant film thickness $z$ estimated at the WWF Oasis reference reach for different measurement campaigns.

Also for the WWF Oasis reach the values of $\alpha$ and $z$ have been estimated and are reported in table 6.12. In this case, the two reference stations, chosen to evaluate $\alpha$, are the station BS15_S01_01 (as upstream station), which, being just below the spring inflow, has the highest values of radon concentration, and the station BS15_S01_DS (as downstream station). The distance between them is 350 m, in which there is no other groundwater contribution. The values of the stagnant film thickness,$z$, obtained for this reach are within a range from $\sim$ 1.5 to 9 $\mu$m.

For the WWF Oasis an other mathematical modeling has also been carried on. In fact, because of the high turbulence of the water, a very sudden and sharp decrease of radon activity concentration has been observed. So, from a numerical analysis, the best fit curve for the degassing model has turned out to be a power law as shown in figures 6.18 and 6.19.

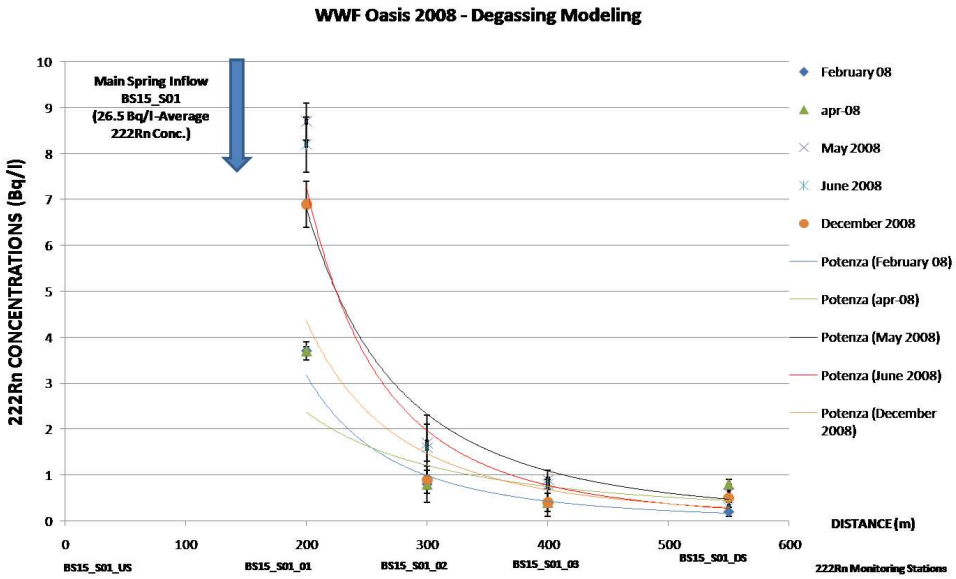


Figure 6.18: Radon degassing modeling for the data from the WWF Oasis reference reach (2008 measurement campaigns).

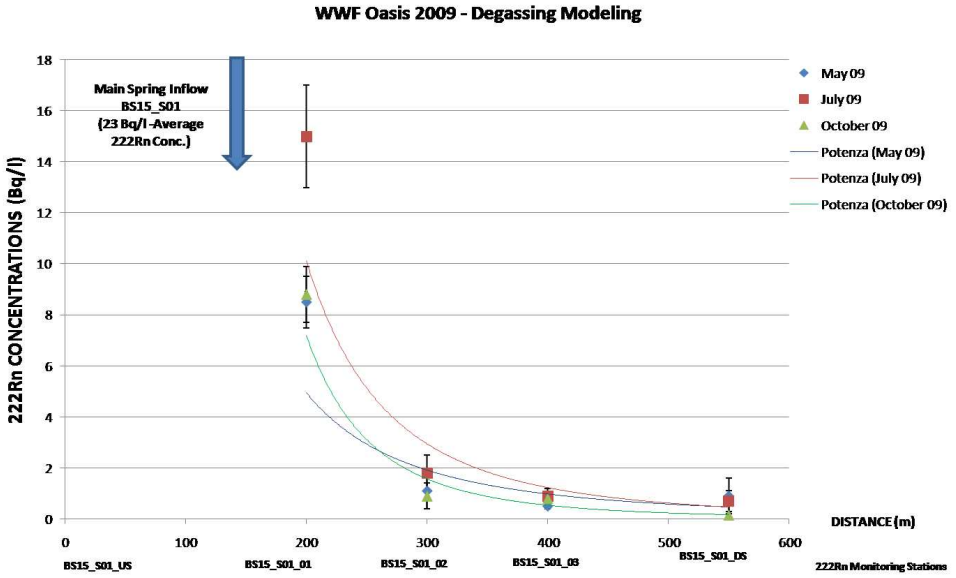


Figure 6.19: Radon degassing modeling for the data from the WWF Oasis reference reach (2009 measurement campaigns).

The highest point in the plot, corresponding to the BS15_S01_01 monitoring station, and the lowest one, corresponding to the BS15_S01_DS monitoring station, have been considered as the two significant stations also in this case, obtaining an equation:

$$y = K\ x^{-\delta} \tag{6.10}$$

where $\delta$ is a coefficient that is indicative of the radon degassing rate. This coefficient has been estimated for 5 campaigns of 2008 and for 3 campaigns of 2009, and the results are shown in table 6.12. As it can be seen, the values obtained are mainly included in the range between 2.5 and 3.5, that shows a certain homogeneity in the trend.

| **Measurement Campaign** | **K** | $\delta$ | **$R^2$ Curve Fitting** |
|---|---|---|---|
| February 08 | $10^7$ | 2.87 | 0.979 |
| April 08 | $1.6 \cdot 10^4$ | 1.66 | 0.578 |
| May 08 | $9 \cdot 10^6$ | 2.65 | 0.938 |
| June 08 | $2 \cdot 10^8$ | 3.22 | 0.989 |
| December 08 | $7 \cdot 10^6$ | 2.69 | 0.795 |
| May 09 | $10^6$ | 2.35 | 0.673 |
| July 09 | $10^8$ | 3.04 | 0.886 |
| October 09 | $3 \cdot 10^9$ | 3.76 | 0.938 |

Table 6.12: Radon degassing rate coefficient, $\delta$, at the WWF Oasis reference reach.

An other way to estimate the radon volatilization to the atmosphere is given by a simple one-dimensional mass-balance model by Kies [Kie05]. This model considers a given length, $\Delta$x, of a river and two sampling sites at the upstream and downstream ends, and gives the following equation:

$$Q_{DS}C_{DS} = Q_{US}C_{US} + q\Delta xC_q - k\tau Q_{avg}C_{avg} \tag{6.11}$$

where Q ($m^3/s$) is the river discharge, the subscripts US and DS designate the upstream and downstream ends, q ($m^3s^{-1}m^{-1}$) the inflow rate per unit of river length, $\tau$ the travel time, $k$ a radon degassing rate constant; $Q_{avg}$ and $C_{avg}$ are the mean river discharge and the mean radon concentration in the stream.

This model has been applied to the Sicilì Bridge reference reach for three measurement campaigns of 2009 to get an estimation of this coefficient $k$, which gives information on the radon degassing rate per unit of time the considered length of the river.

During these campaigns the river discharge was measured at the upstream station, BS13_US, at the downstream station, BS13_DS and at the inflow from springs (Cillito group). The discharge at the reference station BS13 was considered as the average, $Q_{avg}$.

The travel time, $\tau$, was given from the mean velocity, which was measured during the three campaigns. As the travel time is very short, a loss of radon due to decay is negligible, and the primary mechanism of radon removal is gas exchange.

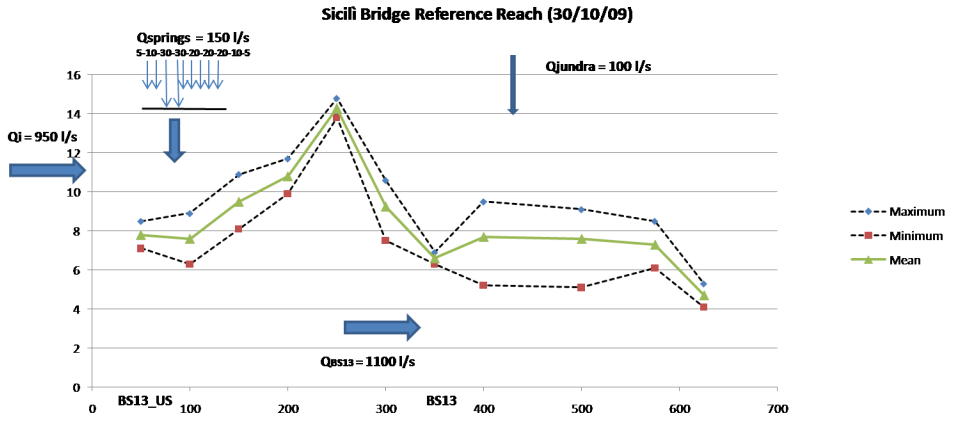


Figure 6.20: Radon activity concentration measured at the Sicilì Bridge reference reach in October 2009. In this case two more downstream stations have been monitored, in order to get more information about the downstream part.

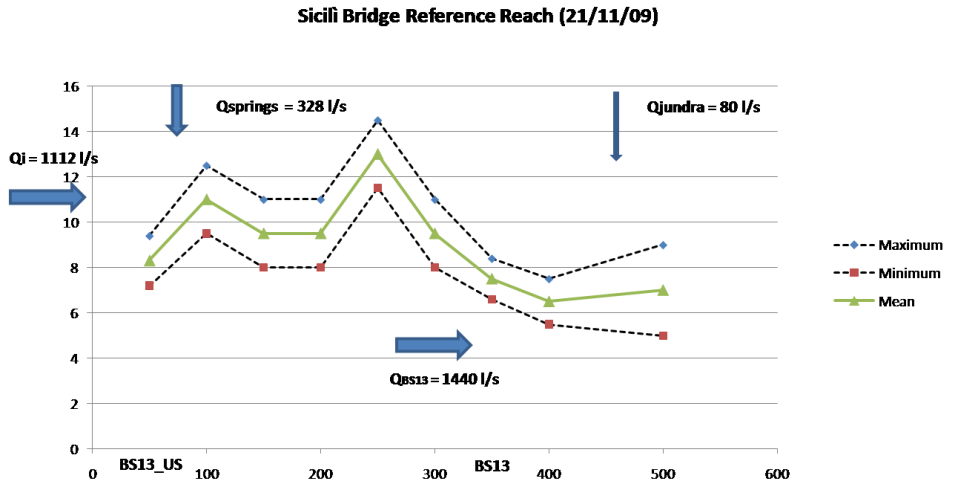


Figure 6.21: Radon activity concentration measured at the Sicilì Bridge reference reach in November 2009.

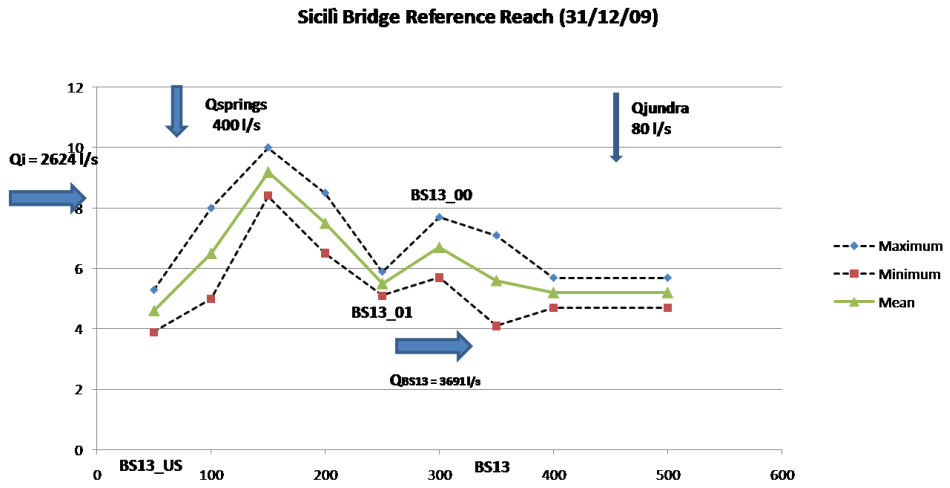


Figure 6.22: Radon activity concentration measured at the Sicilì Bridge reference reach in December 2009.

Figures 6.20, 6.21 and 6.22 show the data obtained from the three campaigns mentioned above. The trend is the same of the one observed during the 2008 campaigns, and there is also, for the October campaign the increase of radon concentration between the stations BS13 and BS13_DS like in some 2008 campaigns.

The value of the discharges, of the mean velocity of the stream and the estimations of $k$ are reported in table 6.13.

| **Measurement Campaign** | $\mathbf{Q}_{US}$ (l/s) | $\mathbf{Q}_{BS13}$ (l/s) | $\mathbf{q}_{springs}$ (l/s) | **Mean Stream Velocity** (m/s) | **k** ($s^{-1}$) |
|---|---|---|---|---|---|
| October 09 | 950 | 1100 | 150 | 0.5 | $(5 \pm 2) \cdot 10^{-4}$ |
| November 09 | 1100 | 1450 | 300 | 0.5 | $(12 \pm 4) \cdot 10^{-4}$ |
| December 09 | 2600 | 3700 | 400 | 0.7 | $(6 \pm 2) \cdot 10^{-4}$ |

Table 6.13: Radon degassing rate coefficient per unit of time, $k$, at the Sicilì Bridge reference reach.

## 6.5 Karst spring analysis

Some karst springs along the Bussento river basin have been, also, monitored. Their importance is due to their content in radon, which is responsible of the radon activity concentration increase in the surface water. According to the results from the various sampling campaigns, three "families",corresponding to the typologies of karst springs assumed in the conceptual model, have been identified, as shown in table 6.14 where data are grouped according to the seasonal period of river discharge (approximatively from spring to summer) and river recharge (approximatively from autumn to winter).

The three typologies of karst springs are:

1. Fracture basal springs (i.e., B13_S01 and BS13_S02), with high values of Radon activity concentration (mostly in the range from 30 to 40 Bq/L);

2. Conduit springs (i.e., BS15_S01) with very variable values (between 17.5 Bq/l (min) and 33.5 Bq/L (max)), with a main range from 20 to 30 Bq/L;

3. Cave resurgence springs with lower values (between 0.5 Bq/L (min) and 6.5 Bq/L (max)), that are not higher than 10 Bq/L.

The three families of springs can be seen in figure 6.23, where data obtained from the various sampling campaigns are reported.

Unlike the data obtained for the river monitoring stations, the radon activity concentrations measured at the spring stations do not show a marked seasonal variability, as it can be seen in figure 6.24.

The two basal springs of the Cillito group do not show any relevant difference in Radon concentration during the year, except for the second discharge period at the station BS13_S02 which shows an average decrease below 30 Bq/L (29 Bq/l average).

At the conduit spring (BS15_S01), more varying values have been obtained: they are a little higher in the recharge period (average value: 25.5 Bq/L) than in the discharge one (average value: 21.5 Bq/L). Anyway the averages are always in the range from 20 to 30 Bq/L.

For the resurgence spring some higher values (6.5 Bq/L) have been obtained during the second discharge period, while in the other months there are data with little variability.

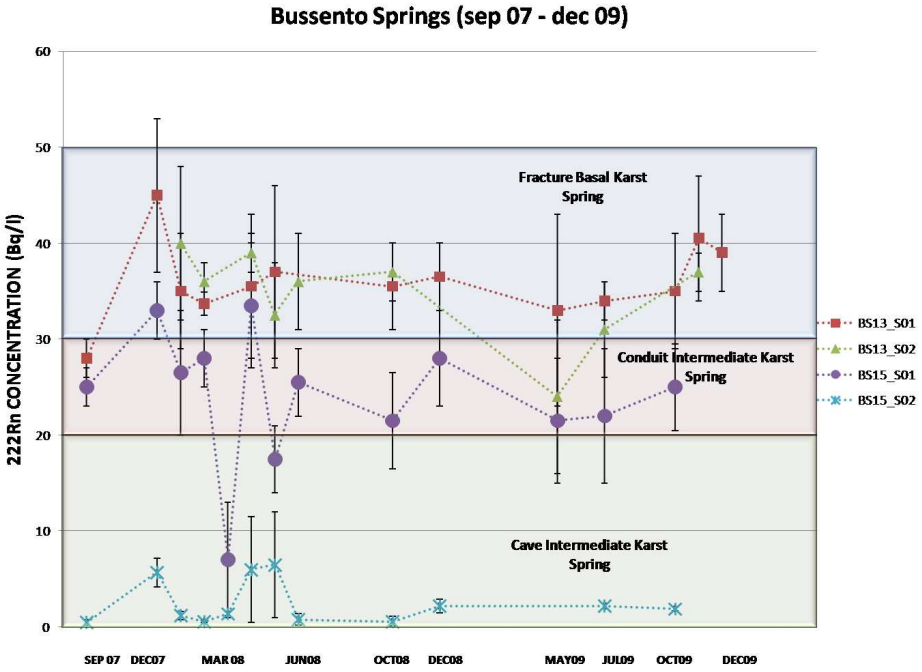


Figure 6.23: Radon activity concentration measured at the three *families* of Bussento karst springs. **Legend**: *The fracture basal springs (BS13_S01 and BS13_S02 from the Cillito group) belong to the upper blue box, with concentration values from 30 to 50 Bq/L. The conduit spring (BS15_S01) belongs to the central red box, with concentration values from 20 to 30 Bq/L. The cave resurgence spring (BS15_S02) belongs to the lower green box, with concentration values lower than 20 Bq/L.*

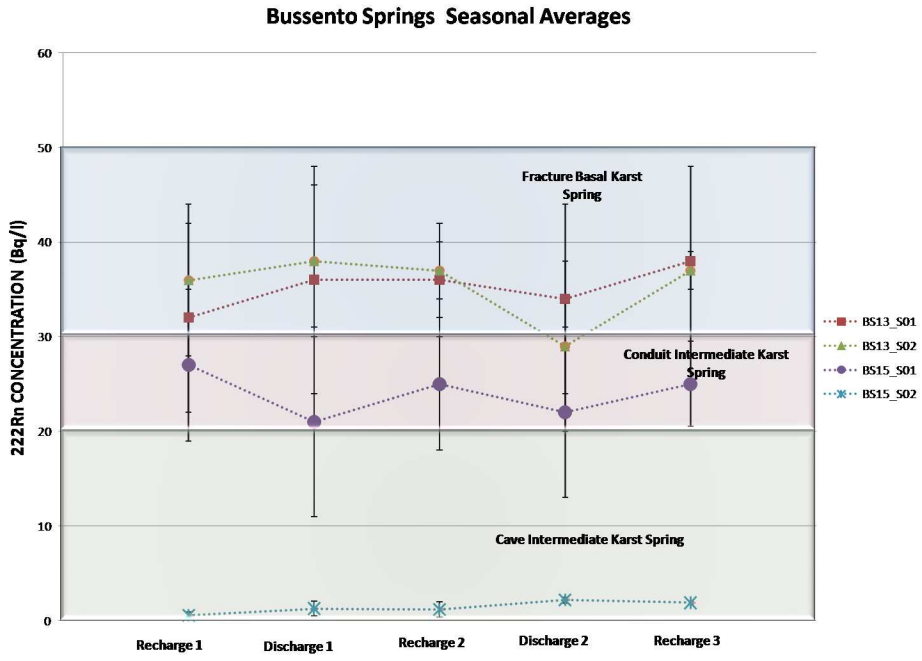


Figure 6.24: Seasonal variability of the three *families* of Radon concentration in the Bussento karst springs. The values reported are the seasonal averages (table 6.14) estimated for the five periods considered.

| **Measurement Campaign** | **BS13_S01** $^{222}$Rn Conc. (Bq/L) | **BS13_S02** $^{222}$Rn Conc. (Bq/L) | **BS15_S01** $^{222}$Rn Conc. (Bq/L) | **BS15_S02** $^{222}$Rn Conc. (Bq/L) |
|---|---|---|---|---|
| September 07 | 28 ± 2 | Not Av. | 25 ± 2 | 0.5 ± 0.3 |
| December 07 | 45 ± 8 | Not Av. | 33 ± 3 | 5.7 ± 1.5 |
| January 08 | 35 ± 6 | 40 ± 8 | 26.5 ± 6.5 | 1.2 ± 0.4 |
| February 08 | 33.7 ± 1.2 | 36 ± 2 | 28 ± 3 | 0.6 ± 0.1 |
| **Recharge Period 1** (Average) | **32 ± 10** | **36 ± 8** | **27 ± 8** | **0.6 ± 0.3** |
| March 08 | Not Av. | Not Av. | 7 ± 6 | 1.4 ± 0.2 |
| April 08 | 35.5 ± 7.5 | 39 ± 2 | 33.5 ± 6.5 | 6.0 ± 5.5 |
| May 08 | 37 ± 9 | 32.5 ± 5.5 | 17.5 ± 3.5 | 6.5 ± 5.5 |
| June 08 | Not Av. | 36 ± 5 | 25.5 ± 3.5 | 0.8 ± 0.6 |
| **Discharge Period 1** (Average) | **36 ± 12** | **38 ± 8** | **21 ± 10** | **1.3 ± 0.8** |
| October 08 | 35.5 ± 4.5 | 37 ± 3 | 21.5 ± 5.0 | 0.6 ± 0.5 |
| December 08 | 36.5 ± 3.5 | Not Av. | 28 ± 5 | 2.2 ± 0.7 |
| May 09 | 33 ± 10 | 24 ± 8 | 21.5 ± 6.5 | Not Av. |
| July 09 | 34 ± 2 | 31 ± 5 | 22 ± 7 | 2.2 ± 0.3 |
| **Discharge Period 2** (Average) | **34 ± 10** | **29 ± 9** | **22 ± 9** | **2.2 ± 0.3** |
| October 09 | 35 ± 6 | Not Av. | 25.0 ± 4.5 | 1.9 ± 0.2 |
| November 09 | 40.5 ± 6.5 | 37 ± 2 | Not Av. | Not Av. |
| December 09 | 39 ± 4 | Not Av. | Not Av. | Not Av. |
| **Recharge Period 3** (Average) | **38 ± 10** | **37 ± 2** | **25.0 ± 4.5** | **1.9 ± 0.2** |

Table 6.14: Data of radon activity concentration obtained at the three *families* of karst spring and their seasonal averages.

# Conclusions

This thesis work comes at the end of a two years and a half experimentation and investigation about the surface and groundwater bodies in the Bussento river basin.

The implementation of the radon measurement techniques has confirmed the perspective of using these methodologies in a karst Mediterranean environment to investigate the complex interactions and exchanges between streamflow and groundwater.

Experimental data about radon concentrations, in addition to physical-chemical data and streamflow rate, have been acquired during monthly measurement campaigns.

Different measurement techniques have been tested and compared allowing to determine a precise protocol for sample collection and for laboratory measurements.

From the data analysis, it has been established the possibility of localizing groundwater influx in riverbed. In fact, superficial waters have been shown to have a markedly different radon content from groundwater, the latter differing in radon concentrations if originating from different karst typologies. In order to provide a physical scheme of the complex recharge, storage and routing system of the river karst area, a preliminary, physically-based, conceptual model has been built-up.

The data have also enabled to individuate a spatial and temporal variability of the radon activity concentration along the river, and to identify, as mentioned above, three typologies of karst springs assumed in the conceptual model. It has been experimentally verified the possibility of making the hydrograph separation both on a seasonal scale and referring to a flood event.

Moreover, a preliminary investigation and modeling of radon diffusion from water to the atmosphere have been made along two selected segments of the river. In fact, analyzing the radon concentration gradients determined during different sampling campaigns, radon exchange rates according to three different models have been estimated.

The future aim of this research program is to continue and improve these studies using, together with radon, also radium in order to carry on a deeper investigation of the problem using a greater data set.

Together with the acquisition of a greater number of data, more precise analytical models can be implemented for the future studies in order to deepen the subject of radon losses from river water.

Finally, according to the RAD_CAMPANIA research program, these studies will be extended to other karst Mediterranean environments in the Campania Region, as well as to some submarine groundwater discharges

emerging in the Policastro gulf in order to study and assess them.

# Appendix A

# The recoil flux of alpha daughters to solution

This appendix shows the derivation of the explicit relations for the relative supply rates of U and Th series nuclides to groundwaters by recoil following their production in the aquifer solids by alpha decay. The chemical properties of the daughter nuclides should not affect their recoil supply rates because recoil is purely a physical process. The recoil flux of a daughter nuclide does, however, depend on the distribution of the parent nuclide in the solid, the recoil range of the daughter nuclide, the size of the solid particles, and their rate of dissolution. Accurate information on many of these parameters is not available, so we will consider a simplified rock-groundwater system to evaluate relative recoil fluxes. Related aspects of the recoil supply of daughter nuclides to solution have recently discussed by Key te al. [Key79] and Torgerson [Tor80].

The model is based on the following assumptions:

1. $^{238}$U and $^{232}$Th are distributed homogeneously in the solid phase.
2. The distribution of the daughter nuclides of $^{238}$U and $^{232}$Th in the solid are governed only by their production, radioactive decay abd recoil loss, i.e. there is no diffusion or dissolution.
3. Steady state conditions prevail.
4. The alpha recoil ranges of all daughter nuclides in the aquifer are the same.
5. The crystal-solution interface is flat and of infinite extent. Both the crystal and solution thicknesses are greater than that of the alpha recoil range. The coordinates are fixed with respect to the crystal lattice, and the crystal-solution interface does not move; there is no solution or precipitation.

## A.1 Spatial distribution of alpha recoil daughters

Consider a point source of parent nuclides in a crystal at some distance $x_0$ from the crystal-solution interface. The daughter atoms produced by the alpha decay of this parent source will be uniformly distributed over the

surface of a sphere with its center at the parent source, at depth $x_0$, and with a radius of $r$, the alpha recoil range (figure A.1).

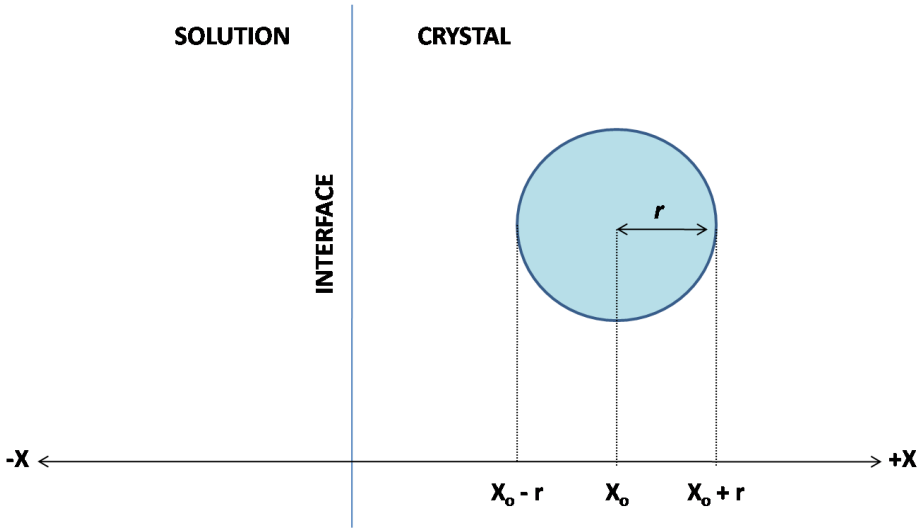


Figure A.1: Coordinate system used for the calculation of relative alpha recoil flux of various daughters in a decay series. The crystal-solution interface is at depth 0; the positive axis extends into the crystal. The daughters produced by the decay of a parent at depth $x_0$ are distributed uniformly over the area of a sphere of radius $r$, the recoil range.

The concentration of the daughters in the interval $dx$ within a recoil range of the source is equal to the fraction of the surface area of the sphere lying within the interval $dx$:

$$B_1(x) = \frac{B_0}{2r}dx \qquad [x_0 - r, x_0 + r] \tag{A.1}$$

where $B_0$ is the activity of parent, $B_1$ is the activity of first daughter.

The activity of the daughter at depths more than a recoil distance from the source will be 0:

$$B_1(x) = 0 \qquad (-\infty, x_0 - r) \tag{A.2}$$

and

$$B_1(x) = 0 \qquad (x_0 + r, \infty)\,. \tag{A.3}$$

Let us now consider a crystal with the parent nuclide distributed throughout its volume. The daughter atoms formed by the alpha decay of the parent at depth $x_0$ are uniformly distributed over the depth interval [$x_0$ - r, $x_0$ + r]. The activity $\rho_1(x)$ of the daughter nuclide at depth $x_1$ in the crystal depends upon the activity of the parent over the interval [$x_1$ - r, $x_1$ + r] and is given by the integral:

$$\rho_1(x_1) = \int_{x_1 - r}^{x_1 + r} (1/2r)\rho_0(x)dx \tag{A.4}$$

where $\rho_0$ and $\rho_1$ are the concentrations of parent and daughter nuclides, respectively, in decays per time per volume. If the activity of the parent has

a uniform value $A$ throughout the crystal and is zero in solution, then the activity of the daughter as a function of depth $x$ is given by, if:

$$\rho_0(x) = 0 \qquad (-\infty, 0) \tag{A.5}$$

and

$$\rho_0(x) = A \qquad (0, \infty) \tag{A.6}$$

then

$$\rho_1(x) = 0 \qquad (-\infty, -r) \tag{A.7}$$

and

$$\rho_1(x) = \frac{x + r}{2r} A \qquad [-r, r] \tag{A.8}$$

and

$$\rho_1(x) = A \qquad (r, \infty)\,. \tag{A.9}$$

## A.2 Flux of daughters to solution

The integral of the daughter nuclide activity in solution equals the recoil flux $F_1{}^c$ from the crystal:

$$F_1^c = \int_{-\infty}^{0} \rho_1(x) dx = \frac{1}{4} Ar \tag{A.10}$$

where $F_1{}^c$ is the flux of the first daughter in atoms per area per time. If the daughter nuclide behaves conservatively, then $F_1{}^c$ will be the activity inventory (activity per area). Elements such as radon, which are not adsorbed and have half-lives that are short with respect to the residence time of water in the aquifer, are expected to behave conservatively, and their activities in water are a direct measure of the recoil supply to solution.

## A.3 Effect of surface adsorption

The fate of the first daughter $D_1$ after injection into the aqueous phase will determine the activity profile of the second daughter $D_2$ in the solid phase and its recoil flux $F_2{}^c$ to solution. Similarly, the aquatic behavior of $D_2$ will govern the distribution and flux of the third daughter $D_3$. Let us assume that some fraction $f_1$ of the first daughter is adsorbed as a monolayer on the surface and that the remaining fraction (1-$f_1$) is dispersed in the aqueous phase. The activity of $D_1$ in the aqueous phase is small compared to that in solids, and its contribution to the activity profile of $D_2$ in the solid phase can be neglected. Since we assume steady state, we may define the activity of the first daughter on the surface as $\sigma_1$:

$$\sigma_1 = F_1^c f_1 \qquad activity\ \ area^{-1}. \tag{A.11}$$

The decay products of this adsorbed surface layer will be uniformly distributed over the depth interval [-r, r]. If $\rho_2^c$(x) represents the activity of second daughter due to decay of adsorbed first daughter:

$$\rho_2^c(x) = 0 \qquad (-\infty, -r) \tag{A.12}$$

and

$$\rho_2^c(x) = \frac{1}{2r}\sigma_1 \qquad [-r, r] \tag{A.13}$$

and

$$\rho_2^c(x) = 0 \qquad (r, \infty)\,. \tag{A.14}$$

The activity of the nth daughter as a function of depth in the crystal $x$ is given by:

$$\rho_n(x) = \rho_n^c(x) + \int_{x_1-r}^{x_1+r} (1/2r)\rho_{n-1}(z)dz. \tag{A.15}$$

The deficiency of the daughter activity in the solid phase relative to the activity of the parent is equal to the recoil loss of the daughter to the solution.

## A.4 Relative recoil fluxes

If the daughters recoiled into solution are not adsorbed, then the activity of successive daughters near the surface of the crystal is depleted and their recoil supply decreases. If the daughters in solution are adsorbed, then the surface and near-surface region of the crystal is enriched in successive daughters and their recoil flux increases, as shown in table A.1.

| | **Decay Series** | | $\epsilon$ Recoil Supply Relative to $^{222}$Rn | |
|---|---|---|---|---|
| Daughter Number | $^{238}$U | $^{232}$Th | $f_i = 0$, No Adsorption | $f_i = 1$, Total Adsorption |
| 1 | $^{234}$Th | $^{228}$Ra | 2.14 | 0.769 |
| 2 | $^{230}$Th | $^{224}$Ra | 1.43 | 0.897 |
| 3 | $^{226}$Ra | $^{220}$Rn | 1.16 | 0.961 |
| 4 | $^{222}$Rn | $^{216}$Po | = 1.000 | = 1.000 |

Table A.1: Recoil supply [Kri82].

# Bibliography


[Ads08] Abreu de Souza T. (2008). Isótopos de rádio como uma ferramenta para o estudo de mistura de águas no estuário do Rio Paraíba do Sul. PhD thesis, Pontifícia Universidade Católica do Rio de Janeiro, Brazil (in Portuguese).

[Ake90] Akerblöm G., Petterson B. and Rosén B. (1990). *Handbook on Investigation of the Radon Situation in Areas Before Building*. The Swedish Council for Building Research and the Swedish National Board for Physical Planning and Building, Report **R88:1988**, Revised edition 1990, 1-160.

[Ake97] Akerblöm G. and Mellander H. (1997). Geology and Radon. In *Radon Measurements by etched track detectors. Applications in Radiation Protection, Earth Sciences and the Environment*, Durrani S.A. and Ilić R. (Eds.), World Scientific Publishing, ISBN: 981-02-2666-7.

[All76] Allen J.W. (1976). Development of a portable radon detection system. *Bendix fieldengineering corp.*, Grand Junction, Colorado, GBJX-50.

[Alt63] Altshuler B. and Pasternack B. (1963). Statistical Measures of the Lower Limit of Detection in a Radioactivity Counter. *Health Physics*, **9**, 293-298.

[And83] Andersson P., Clavensjo B. and Akerblom G. (1983). The effect of the ground on the concentration of radon and gamma radiation indoors. *Swedish Council for Building Research*, Report **9**, 1-442.

[Ans72] Andrews J.N. and Woods D.F. (1972). Mechanism of radon release in rock matrices and into groundwaters. *Trans. Inst. Min. Metall. Sec.*, **B81**, 198-209.

[Ans89] Andrews J. N., Davis S. N., Fabryka-Martin J., Fontes J.-Ch., Lehmann B. E., Loosli H. H., Michelot J.-L., Moser H., Smith B. and Wolf M. (1989). The in situ production of radioisotopes in rock matrices with particular reference to the Stripa granite. *Geochimica et Cosmochimica Acta*, **53**, 1803-1815.

[App96] Appelo C.A.J. and Postma D. (1996). Geochemistry, groundwater and pollution. A. A. Balkema, Rotterdam, Netherlands.

[Apt07] Appleton J.D. (2007). Radon: sources, health risks, and hazard mapping. *Ambio*, **36**, 85-89.

[ARP08] Adamo N., Della Rocca M.R., Guida D., Guida M., Lino R., Sicignano E., Cuomo A., Guadagnuolo D. and Siervo V. (2008). Radioattività. In *Agenti Fisici - Il monitoraggio in Campania 2003-2007*, **III**, 169-206. Agenzia Regionale Protezione Ambientale in Campania (Regione Campania POR 2000-2006). ISBN: 978-88-902451-8-3 (in Italian).

[Aul76] Aulenbach D. B. and Davis R. E. (1976). Long-term consumption of mineral water containing natural Ra-226. *Proceedings of the Tenth Midyear Topical Symposium* Health Physics Society. Rensselaer Polytechnic Institute, Troy, New York.

[Bak95] Bacalowicz M. (1995). The inflitration zone of karst aquifers. *Hydrogeologie*, **4**, 3-21.

[Bar05] Barbieri M., Boschetti T., Petitta M. and Tallini M. (2005). Stable isotopes ($^{2}H$, $^{18}O$ and $^{87}Sr/^{86}Sr$) and hydrochemistry monitoring for groundwater hydrodynamics analysis in a karst aquifer (Gran Sasso, Central Italy). *Applied Geochemistry*, **20(11)**, 2063-2081.

[Bat75] Baretto P.M.C. *et al.* (1975). Physical characteristics of $^{222}Rn$ emanation from rocks, soils and minerals: relation to temperature and alpha dose. In *Natural Radiation Environment* (Symposium 1972), Houston.

[Ben90] Benes P. (1990). Radium in (continental) surface water. In: *The environmental behavior of radium*, **1**, IAEA, Vienna, 373-418.

[Bev89] Beven K.J. (1989). Changing ideas in hydrology - The case of physically based models. *J. Hydrol.*, **105**, 157-172.

[Bev00] Beven K.J. (2000). Uniqueness of place and process representations in hydrological modelling. *Hydrol. Earth Syst. Sci.*, **4**, 203-213.

[Bev01] Beven K.J. (2001). How far can we go in distributed hydrological modelling? *Hydrol. Earth Syst. Sci.*, **5**, 1-12.

[Bis96] Bisci C. et al. (1996). In *Landslide Recognition*, 150-160.

[Bol93] Bollinger M.S. and Moore W.S. (1993). Evaluation of salt marsh hydrology using radium as a tracer. *Geochim. Cosmochim. Acta*, **57**, 2203-2212.

[Bon88] Bonardi G., D'Argenio B. and Perrone V. (1988). La Carta Geologica dell'Appennino Meridionale. *Mem. Soc. Geol. It.*, **41**. Congress of Italian Geological Society, Sorrento, Italy, 1988.

[Bou03] Bourdon B., Turner S., Henderson G.M. and Lundstrom C.C. (2003). Introduction to U-series Geochemistry. *Reviews in Mineralogy and Geochemistry*, **52**, 1-21.

[Bra88] Brahana J.V. and Hollyday E.F. (1988). Dry stream reaches in carbonate terranes - Surface indicators of ground-water reservoirs. *American Water Resources Association Bulletin*, **24(3)**, 577-580.

[Brg91] Brager G.S. and Rezvan K.L. (1991). Transport and deposition of indoor radon decay products - II. Influence of environmental conditions. *Atmosph. Environment*, **25B**, 3, 343-358.

[Bru81] Brutsaert W.F., Norton S.A., Hess C.T. and Williams J.S. (1981). Geologic and hydrologic factors controlling radon-222 in ground water in Maine. *Ground Water*, **19**, 407-417.

[Bub01] Burbank D.W. and Anderson R.S. (2001). Tectonic Geomorphology, Malden, MA. Blackwell Publishing.

[Bun96] Bugna G.C., Chanton J.P., Cable J.E., Burnett W.C. and Cable P.H. (1996). The importance of ground water discharge to the methane budgets of near shore and continental shelf waters of the northeastern Gulf of Mexico. *Geochim. Cosmochim. Acta*, **60**, 4735-4746.

[Bur00] Burnett W.C., Kim G. and Lane-Smith D. (2000). A continuous monitor for assessment of $^{222}$Rn in the coastal ocean. *Journal of Radioanalytical and Nuclear Chemistry*, **249**, 167-172.

[Bur01] Burnett W.C., Taniguchi M. and Oberdorfer J. (2001). Measurement and significance of the direct discharge of groundwater into the coastal zone. *J. Sea Res.*, **46**, 109-116.

[Bur03] Burnett W.C. and Dulaiova H. (2003). Estimating the dynamics of groundwater input into the coastal zone via continuous radon-222 measurement. *Journal of Environmental Radioactivity*, **69**, 21-35.

[Bur06] Burnett W.C. and Dulaiova H. (2006). Radon as a tracer of submarine groundwater discharge into a boat basin in Donnalucata, Sicily. *Continental Shelf Research*, **26**, 862-873.

[But07] Buttafuoco G., Tallarico A. and Falcone G. (2007). Mapping soil gas radon concentration: a comparative study of geostatistical methods. *Environmental Monitoring and Assessment*, **131**, 135-151.

[Bro80] Broecker W.S., Peng T.-H., Mathieu G., Hesslein R. and Torgensen T. (1980). Gas exchange measurements in natural systems. *Radiocarbon*, **22**, 676-683.

[Bro82] Broecker W.S. and Peng T.-H. (1982). Tracers in the sea. Elgidio Press, Palisades, NY.

[Bru97] Brunke M. and Gonser T. (1997). The ecological significance of exchange processes between rivers and groundwater. *Freshwater Biology*, **37**, 1-33.

[Cab96] Cable J.E., Bugna G.C., Burnett W.C. and Chanton J.P. (1996). Application of $^{222}$Rn and $CH_4$ for assessment of ground water discharge to the coastal ocean. *Limnol. Oceanogr.*, **41**, 1347-1353.

[Cab97] Cable J.E., Burnett W.C. and Chanton J.P. (1997). Magnitude and variations of groundwater seepage along a Florida marine shoreline. *Biogeochemistry*, **38**, 189-205.

[Cam00] Cammarosano A., Danna M., De Rienzo F., Martelli L., Miele F. and Nardi G. (2000). Il substrato del Gruppo del Cilento tra il M. Vesalo e il M. Sacro (CIlento, Appennino Meridionale). *Bollettino della Società Geologica Italiana*, **119** (2), 395-405 (in Italian).

[Cam04] Cammarosano A., Cavuoto G., Danna M., De Capoa P., De Rienzo F., Di Staso A., Giardino S., Martelli L., Nardi G., Sgrosso A., Toccacelli R.M. and Valente A. (2004). Nuovi dati sui flysch del Cilento (Appennino Meridionale, Italia). *Bollettino della Società Geologica Italiana*, **123** (2), 253-273 (in Italian).

[Cel78] Celico P.B. (1978). Schema idrogeologico dell'Appennino Meridionale. *Memorie e Note Istituto di Geologia Applicata*, **19**, Napoli (in Italian).

[Cel83] Celico P.B. (1983). Idrogeologia dell'Italia Meridionale. *Quaderni della Cassa per il Mezzogiorno*, **4** (2), Roma (in Italian).

[Civ97] Civita M. and De Maio M. (1997). SINTACS Un sistema parametrico per la valutazione e la cartografia della vulnerabilità degli acquiferi all'inquinamento. *Metodologia & Automatizzazione*, **60**, Pitagora Editrice, Bologna (in Italian).

[Cla93] Claps P., Rossi F. and Vitale C. (1993). Conceptual-stochastic modeling of seasonal runoff using autoregressive moving average models at different scales of aggregation. *Water Resources and Research*, **29** (8), 2545-2559.

[Cle74] Clements W.E. and Wilkening M.H. (1974). Atmospheric pressure effects on $^{222}$Rn transport across the earth-air interface. *J. Geophys. Res.*, **79**, 5025-5029.

[Cor00] Corbett D.R., Dillon K., Burnett W.C. and Chanton J. (2000). Estimating the groundwater contribution into Florida Bay via natural tracers $^{222}$Rn and $CH_4$. *Limnol. Oceanogr.*, **45**, 1546-1557.

[Cot87] Cothern C.R., Smith J.E.Jr., Crawford-Brown D.J., Michel J. and Eichholz G.G. (1987). Environmental Radon. *Environmental Science Research*, **35**, Plenum Press, New York, NY, USA. ISBN: 0-306-42707-9.

[Cou78] Countess R.J. (1978). Measurement of $^{222}$Rn in water. *Health Physics*, **34**, 390-391.

[Cut86] Cuttell J.C., Lloyd J.W., Ivanovich M. (1986). A study of uranium and thorium series isotopes in Chalk groundwaters of Lincolnshire. *UK. Journal of Hydrology*, **86**, 343-365.

[Dar73] D'Argenio B., Pescatore T. and Scandone P. (1973). Schema geologico dell'Appennino meridionale (Campania-Lucania). Atti del Convegno: *Moderne vedute sulla geologia dell'Appennino.* Ac. Naz.Lincei, Quad., **183**.

[Das03] Dassonville L. and Fé d'Ostiani L. (2003). Mediterranean watershed management: overcoming water crisis in the Mediterranean. *Watershed Management: Water Resources for the Future*, Conference Proceedings (Porto Cervo, Sassari, Sardinia, Italy, October 22-24 2003).

[Dav90] Davis R.M. and Watson J.R. (1990). Influence of $^{226}$Ra concentration in surrounding rock on $^{222}$Rn concentration in ground water. *Health Physics*, **58**, 369-371.

[Del87] D'Elia G., Guida M. and Terranova C. (1987). Osservazioni sui fenomeni di deformazione gravitativa profonda nel bacino del fiume Bussento, Campania. *Bollettino Società Geologica Italiana*, **106** (in Italian).

[Dim07] Dimova N., Burnett W.C., Horwitz E.P. and Lane-Smith D. (2007). Automated measurement of $^{224}$Ra and $^{226}$Ra in water. *Applied Radiation and Isotopes*, **65**, 428-434.

[Dob79] Dobrovolsky I.P., Zubkov S.I. and Miachkin V.I. (1979). Estimation of the size of earthquake preparation zones. *Pure Appl. Geophys.*, **117**, 1025-1044.

[Dul06] Dulaiova H., Burnett W.C., Chanton J.P., Moore W.S., Bokuniewicz H.J., Charette M.A. and Sholkovitz E. (2006). Assessment of groundwater discharges into West Neck Bay, New York, via natural tracers. *Continental Shelf Research*, **26**, 1971-1983.

[Dum92] Dumenil L. and Todini E. (1992). A rainfall-runoff scheme for use in the Hamburger climate model. *European Geophysical Society Series on Hydrological Sciences*, **1**.

[Dur97] Durrani S.A. and Ilić R. (1997). Radon Measurements by etched track detectors. Applications in Radiation Protection, Earth Sciences and the Environment. World Scientific Publishing, ISBN: 981-02-2666-7.

[DUR09a] DURRIDGE (2009). RAD7 RADON DETECTOR. Owner's Manual, Bedford, MA, USA.

[DUR09b] DURRIDGE (2009). RAD7 RADH2O Radon in Water Accessory. Owner's Manual, Bedford, MA, USA.

[Ebe07] Ebert C. (2007). Untersuchung neuer Verfahren zur Radonextraktion aus Wasser. PhD thesis, Fakultät für Physik und Astronomie Ruprecht-Karls-Universität Heidelberg (in German).

[Eik01] Eikenberg J., Tricca A., Vezzu G., Stille P., Bajo S., Ruethi M. (2001). $^{228}$Ra/$^{226}$Ra/$^{224}$Ra and $^{87}$Sr/$^{86}$Sr isotope relationships for determining interactions between ground and river water in the upper Rhine valley. *Journal of Environmental Radioactivity*, **54**, 133-162.

[Eis95] Eisenlohr L. and Surbeck H. (1995). Radon as a natural tracer to study transport processes in a karst system; an example from the Swiss Jura. *C. R. Acad. Sci. Paris*, **321**, II, 761-767.

[Eks95] Ek J. and Ek B.M. (1995). Radium and uranium concentrations in two eskers with enhanced radon emission. *Environment International*.

[Ell90] Ellins Kelly K., Roman-Mas A. and Lee R. (1990). Using $^{222}$Rn to examine groundwater/surface discharge interaction in the Rio Grande de Manati, Puerto Rico. *Journal of Hydrology*, **115**, 319-341.

[Els83] Elsinger R.J. and Moore W. (1983). Gas exchange in the Pee Dee river based on $^{222}$Rn evasion. *Geophysical Research Letters*, **10**, 443-446.

[Emb03] Emblanch C., Zuppi G.M., Mudry J., Blavoux B. and Batiot C. (2003). Carbon-13 of TDIC to quantify the role of the unsaturated zone: the example of the Vaucluse karst systems, Southeastern France. *Journal of Hydrology*, **279**, 262-274.

[Eme73] Emerson S. and Broecker W.S. (1973). Gas exchange rates in a small lake as determined by the radon method. *J. Fish. Res. Board Can.*, **30**, 1475-1484.

[Eme75] Emerson S. (1975). Gas exchange rates in small Canadian shield lakes. *Limnol. Oceanogr.*, **20**, 754-761.

[Eva69] Evans R.D. (1969). Engineers' guide to the elementary behavior of radon daughters. *Health Phys.*, **17**, 229-252.

[EWF00] The EU Water Framework Directive (EWFD) (2000). Directive 2000/60/EC of the European Parliament and of the Council, October 23, 2000.

[Fan82] Fanning K., Breland J.A. and Byrne R.H. (1982). Radium-226 and Radon-222 in the coastal waters of West Florida: high concentrations and atmospheric degassing. *Science*, **215**, 667-670.

[FAO86] FAO (1986). Strategies, approaches and systems in integrated watershed management. Conservation Guide No. 14. Rome.

[FAO98] FAO (1998). Developing participatory and integrated watershed management. Community Forestry Case Study Series No. 13. Rome.

[Fau54] Faul H. (1954), *Nuclear Geology*, John Wiley and Sons, New York.

[Fle80] Fleischer R.L. (1980) Isotopic disequilibrium of uranium: Alpha-recoil damage and preferential solution effects. *Science* **207**, 979-981.

[Fle81] Fleischer R.L. (1981). Dislocation model for radon response to distant earthquakes. *Geophys. Res. Lett.*, **8**, 477-480.

[Fle82] Fleischer R.L. (1982). Alpha-recoil damage and solution effects in minerals: Isotopic disequilibrium and radon release. *Geochim. Cosmochim.*, **46**, 2191-2201.

[Fle84] Fleischer R.L. and Turner L.G. (1984). Correlations of radon and carbon isotopic measurements with petroleum and natural gas at Cement, Oklahoma. *Geophysics*, **49**, 810-817.

[Fle88] Fleischer R.L. (1988). Radon in the environment - opportunities and hazards. *Nucl. Tracks Radiat. Meas.* **14**, 421-435.

[Fle92] Fleischer R.L. (1992). Permeability of caulking compounds to $^{222}$Rn. *Health Phys.* **62**, 91-95.

[Fle97] Fleischer R.L. (1997). Radon: Overview of Properties, Origin and Transport. In *Radon Measurements by etched track detectors. Applications in Radiation Protection, Earth Sciences and the Environment*, Durrani S.A. and Ilić R. (Eds.), World Scientific Publishing, ISBN: 981-02-2666-7.

[Fre79] Freeze R.A. and Cherry J.A. (1979). Groundwater, Prentice-Hall Inc., Englewood Cliffs, NJ.

[For89] Ford D.C. and Williams P.W. (1989). Karst geomorphology and hydrology. London, Unwin Hyman.

[For07] Ford D.C. and Williams, P.W. (2007). Karst Hydrogeology and Geomorphology. (Reprint with corrections of the 1989 title *Karst geomorphology and hydrology*). J. Wiley and Sons Ltd, Chichester.

[Fra96] Franchini M., Wendling J., Obled C. and Todini E. (1996). Physical interpretation and sensitivity analysis of the TOPMODEL. *Journal of Hydrology*, **175**, 293-338.

[Fre97] Freyer K., Treutler H.C., Dehnert J. and Nestler W. (1997). Sampling and measurement of radon-222 in water. *Journal of Environmental Radioactivity*, **37**, 327-337.

[Fuk85] Fukui M. (1985). $^{222}$Rn concentrations and variations in unconfined groundwater. *Journal of Hydrology*, **79**, 83-94.

[Gai07] Gainon F., Goldscheider N. and Surbeck H. (2007). Conceptual model for the origin of high radon levels in spring waters - the example of the St. Placidus spring, Grisons, Swiss AlpsSwiss. *J. Geosci.*, **100**, 251-262.

[Gal95] Gall I.K., Ritzi R.W., Baldwin A.D., Pushkar P.D., Carney C.K. and Talnagi J.F. (1995). The correlation between bedrock uranium and dissolved radon in ground water of a fractured carbonate aquifer in Southwestern Ohio. **Ground Water**, **33**, 197-206.

[Gan07] Gandy C.J., Smith J.W.N. and Jarvis A.P. (2007). Attenuation of mining-derived pollutants in the hyporheic zone: a review. *Science of the Total Environment*, **373**, 435-446.

[Gen90] Genereaux D.P. and Hemond H.F. (1990). Naturally occurring radon-222 as a tracer for streamflow generation: steady state methodology and field example. **Water Resources and Resources**, **26** (12), 3065-3075.

[Gen93] Genereaux D.P., Hemond H.F. and Mulholland P.J. (1993). Use of radon-222 and calcium as tracers in a three-end-member mixing model

for streamflow generation on the wet fork of Walker Branch watershed. *J. Hydrol.*, **142**, 167-211.

[Gib90] Giblin A.E. and Gaines A.G. (1990). Nitrogen inputs to a marine embayment: the importance of ground water. *Biogeochem.*, **10**, 309-328.

[Goc14] Gockel A. (1914). Die Radioactivität von Boden und Quellen, Friedr. Vieweg & Sohn, Braunschweig, Germany.

[Gol07] Goldscheider N. and Drew D. (2007). Methods in Karst Hydrogeology. Taylor & Francis Group, London, UK.

[Gra07] Grath J., Ward R. and Quevauviller P. (Leaders) (2007). Common Implementation Strategy for the WATER FRAMEWORK DIRECTIVE (2000/60/EC). Guidance Document No. 15 - Guidance on Groundwater Monitoring. Publications of the European Community, Luxembourg ISBN 92-79-04558-X - ISSN 1725-1087.

[Grv88] Graves B. (1988). Radon in groundwater, Lewis Publishers, Chelsea, MI.

[Gud92] Gudzenko V. (1992). Radon in subsurface water studies. In *Isotopes of Noble Gases as Tracers in Environmental Studies*. Proceedings of a Consultants Meeting, International Atomic Energy Agency, Vienna, 249-261.

[Gui80] Guida D., Guida M., Luise D., Salzano G.and Vallario A. (1980). Idrogeologia del Cilento (Campania). *Geologica Romana*,**XIX**, 349-369.

[Gui88] Guida D., Iaccarino G. and Perrone V. (1988). Nuovi dati sulla successione del Flysch del Cilento nell'area di M.te Centaurino: Relazioni fra Unità Litostratigrafiche, Unità Litotecniche e principali Sistemi Franosi. *Memorie Società Geologica Italiana*, **41** (in Italian).

[Gui06] Guida D., Longobardi A., Ragone G. and Villani P. (2006). Hydrogeological and hydrological modelling for water resources management in karstic landscape at the basin scale. A case study: the Bussento river basin. *3rd EGU General Assembly*, Vienna, Austria, April 02-07 2006.

[Gui08] Guida D., Guida M., Cuomo A., Siervo V. and Guadagnuolo D. (2008). Radon-prone Areas Assessment in Campania Region. Applications of a Hierarchical and Multi-scale Approach to the Environmental Planning. *Journal of Technical & Environmental Geology*, **XVI** (2), 38-62.

[Gum07a] Guida M. and Guida D. (2007). SGDCILERAD Submarine Groundwater Discharge assessment on the interregional coastal areas of Cilento, southern Italy, with measurements of natural isotopic tracers like Radon-222. Programme *PEOPLE* - Call FP7-PEOPLE-2007-4-2-IIF - Proposal No.221278.

[Gum07b] Guida M., Guadagnuolo D., Guida D., Longobardi A. and Villani P. (2007). Submarine Groundwater Discharge assessment of river springs and development and application of innovative continuous

Radon-monitoring measurements for the Bussento river and the Policastro gulf. NREVIII, 8thInternational Symposium on the Natural Radiation Environment, Buzios, Brazil, October 7-12 2007.

[Gun89] Gundersen L. C. S. (1989). Anomalously high radon in shear zones. In Proceedings: *The 1988 Symposium on Radon and Radon Reduction Technology* - vol. 1. Symposium Oral Papers, Washington, DC. U. S. Environmental Protection Agency, EPA/600/9-89/006a.

[Hak97] Hakl J., Hunyadi I., Csige I., Geczy G., Lenart L. and Varhegyi A. (1997). Radon transport phenomena studied in karst caves: International experiences on radon levels and exposures. *International Conference on Nuclear Tracks in Solids* No. 18, (Cairo , Egypte, September 1 1996) **28** (1-6), 675-684.

[Had99] Hamada H. (1999). Analysis of the Interaction between Surface Water and Groundwater Using Radon-222. *Japan Agricultural Research Quarterly*, **33**, 261-265.

[Had00] Hamada H. (2000). Estimation of groundwater flow rate using the decay of 222Rn in a well. *Journal of Environmental Radioactivity*, **47**, 1-13.

[Ham77] Hammond D.E., Simpson H.J. and Mathieu G. (1977). $^{222}$Rn distribution and transport across the sediment-water interface in the Hudson river estuary. *J. Geophys. Res.*, **82**, 3913-3920.

[Ham79] Hammond D.E. and Fuller C. (1979). The use of $^{222}$Rn to estimate benthic exchange and atmospheric exchange rates in San Francisco Bay. In *San Francisco Bay: The Urbanized Estuary*, Pacific Division AAAS, California Academy of Science, San Francisco, 213-230.

[Ham88] Hammond D.E., Zukin J.G. and Ku T.L. (1988). The kinetics of radioisotope exchange between brine and rock in a gepthermal system. *J. Geophys. Res.*, **93**, 13175-13186.

[Her88] Herczeg A.L., Simpson H.J., Anderson R.F., Trier R.M., Mathieu G.G. and Deck B.L. (1988). Uranium and radium mobility in groundwaters and brines within the Delaware Basin, southeastern New Mexico, U.S.A., *Chemical Geology* (Isotope Geoscience Section), **72**, 181-196.

[Hig95] Hightower J.H. and Watson J.E. (1995). 222Rn in water: A study of two sample collection methods, effects of mailing samples, and temporal variation of concentrations in North Carolina groundwater. *Health Physics*, **69**, 219-226.

[Hid83] Hildingson O. (1983). Radon emitted from gravel and aggregate; Testing method and consistencies for indoor environment. Swedish National Testing Institute. Technical Report **28**, 1-45 (in Swedish).

[Hil97] Hillaire-Marcel C. and Ghaleb B. (1997). Thermal ionization mass spectrometry measurements of 226Ra and U-isotopes in surface and groundwaters - porewater/matrix interactions revisited and potential

dating implications, *Isotope Techniques in the Study of Past and Current Environmental Changes in the Hydrosphere and Atmosphere*, IAEA Symposium 349, April, 1997, Vienna.

[Hoe04] Hoehener P. and Surbeck H. (2004). $^{222}$Rn as a tracer for non-aqueous phase liquid in the vadose zone: experiments and analytical method. *Vadose Zone Journal*, **3**, 1276-1285.

[Hon89] Hoehn E. and Gunten H. R. (1989). Radon in groundwater: a tool to assess infiltration from surface waters to aquifers, *Water Resources Research*, **28**, 1795-1803.

[Hon91] Hoehn E., Willme U., Hollerung R., Schulte-Ebbert U. and Gunten H. R. (1992). Application of the 222Rn technique for estimating the residence times of artificially recharged groundwater,*Isotope in Water Resources Development*. IAEA Symposium 319, March 1991, Vienna, 712-714.

[Hoo06] Hood J.L., Roy J.W. and Hayashi M. (2006). Importance of groundwater in the water balance of an alpine headwater lake. *Geophysical Research Letters*, **33**, L13405, doi:10.1029/2006GL026611.

[Hop86] Hooper R.P. and Shoemaker C.A. (1986). A comparison of chemical and isotopic streamflow separation. *Water Resour. Res.*, **22** (10), 1444-1454.

[Hu06] Hu C., Muller-Karger F.E. and Swarzenski P.W. (2006). Hurricanes, submarine groundwater discharge, and Florida's red tides. *Geophys. Res. Lett.*, **33**.

[Iac87] Iaccarino G. (1987). Analisi idrogeologica del base flow annuo del medio Bussento. Motivazioni idrogeologiche. *Boll. Museo Storia Naturale Lunigiana*, Aulla, 6-7 (in Italian).

[Iac88] Iaccarino G., Guida D. and Basso C. (1988). Caratteristiche idrogeologiche della struttura carbonatica di Morigerati (Cilento Meridionale). *Memorie Società Geologica Italiana*, **41**, 1065-1077 (in Italian).

[IAEA02] IAEA - Rickwood P. (2002). IAEA Bulletin 44/1/2002, 21-24.

[Iel02] Ielsch G., Ferry C., Tymen G. and Robé M. C. (2002). Study of a predictive methodology for quantification and mapping of the Radon-222 exhalation rate. *Journal of Environmental Radioactivity*, **63** (1), 15-33.

[Ili97] Ilić R. and Šutej T. (1997). Radon Monitoring Devices Based on Etched Track Detectors. In *Radon Measurements by etched track detectors. Applications in Radiation Protection, Earth Sciences and the Environment*, Durrani S.A. and Ilić R. (Eds.), World Scientific Publishing, ISBN: 981-02-2666-7.

[Iva92] Ivanovich M., Latham A.G., Longworth G. and Gascoyne M. (1992). Applications to radioactive water disposal studies. In *Uranium-series disequilibrium*, Ivanovich M. and Harmon R.S. (eds), Clarendon Press, Oxford, 583-630.

[Jac93] Jacobi W. (1993). The history of the radon problem in mines and homes. *Ann ICRP*, **23**, 39-45.

[Kaf01] Kafri U. (2001). Radon in Groundwater as a tracer to assess flow velocities: two test cases from Israel. *Environmental Geology*, **40** (3), 392-398.

[Kar87] Karanth K. (1987). Groundwater assessment. Development and management. Tata McGraw-Hill,New Delhi. Cambridge.

[Ken98] Kendall C. and McDonnell J.J. (Eds) (1998). Isotope Tracers in Catchment Hydrology. Elsevier Science. Amsterdam.

[Key79] Key R.M., Guinasso N.L.Jr. and Schink D.R. (1979). Emanation of radon-222 from marine sediments. *Mar. Chem.*, **7**, 221-250.

[Kie05] Kies A., Hofmann H., Tosheva Z., Hoffmann L. and Pfister L. (2005). Using $^{222}$Rn for hydrograph separation in a micro basin (Luxembourg). *Annals of Geophysics*, **48**(1), 101-107.

[Kig71] Kigoshi K. (1971). Alpha-recoil $^{234}$Th: Dissolution into water and the $^{234}$U/$^{238}$U disequilibrium in nature. *Science* **173**, 47-48.

[Kil85] Kilpatrick F.A. and Cobb E.D. (1985). Measurement of discharge using tracers. *U.S. Geol. Surv.*, Techniques of Water-Resources Investigations, Book 3, Chapter A-16.

[Klu07] Kluge T., Ilmberger J., von Rohden C. and Aeschbach-Hertig W. (2007). Tracing and quantifying groundwater inflow into lakes using a simple method for radon-222 analysis. *Hydrology and Earth System Sciences*, **11**, 1621-1631.

[Kog71] Kogan R.M., Nazarov I.M. and Fridman S.D. (1971). Gamma Spectrometry of Natural Environments and Formations, *Israel program for scientific translations*, Jerusalem, 1-337.

[Kot89] Kotrappa P., Dempsey J.C., Hickey J.R. and Stieff L.R. (1989). An electret passive environmental radon monitor based on ionization measurement. *Health Physics*, **54**, 47-56.

[Kot90] Kotrappa P., Dempsey J.C., Stieff L.R. and Ramsey R.W. (1990). A practical electret passive environmental radon monitor for indoor radon measurements. *Health Physics*, **58**, 461-467.

[Kot93] Kotrappa P. and Jester W.A. (1993). Electret ion chamber radon monitors measure radon in water. *Health Physics*, **64**, 397-405.

[Kot96] Kotrappa P., Stieff L.R. and Bigu J. (1996). Passive Rad Elec Inc., E-PERM radon flux monitors for measuring undisturbed radon flux from the ground. *International Radon Symposium II*, 1996.

[Kot00] Kotrappa P. (2000). Review of E-PERM passive integrating electret ionization chambers for measuring radon in air, thoron in air, radon in water and radon flux from surfaces and mill tailings. *International Radon Symposium*, 2000.

[Kra98] Kraemer T.F. and Genereux D.P. (1998). Applications of Uranium- and Thorium-Series Radionuclides in Catchment Hydrology Studies. In *Isotope Tracers in Catchment Hydrology* (Kendall C. and McDonnell J.J. (Eds.)). Elsevier, Amsterdam, 679-722.

[Kra05] Kraemer T.F. (2005). Radium isotopes in Cayuga Lake, New York: Indicators of inflow and mixing processes. *Limnol. Oceanogr.*, **50**, 158-168.

[Kre00] Krest J.M., Moore W.S., Gardner L.R. and Morris J.T. (2000). Marsh nutrient export supplied by ground water discharge: Evidence from radium measurements. *Global Biogeochem. Cycles*, **14**, 167-176.

[Kri82] Krishnaswami S., Graustein W.S., Turekian K.K. and Dowd J.F. (1982). Radium, thorium and radioactive lead isotopes in groundwaters: application to the in situ determination of absorption-desorption rate constants and retardation factors. *Water Resources Research*, **18**, 1633-1675.

[Kri91] Krishnaswami S., Bhushan R. and Baskaran M. (1991). Radium isotopes and $^{222}$Rn in shallow brines, Kharaghoda (India). *Chem. Geol.* (Isot. Geosci.), **87**, 125-136.

[Ku92] Ku T.L., Luo S., Leslie B.W. and Hammond D.E. (1992). Decay-series disequilibria applied to the study of rock-water interaction and geothermal systems. In *Uranium-series disequilibrium*, Ivanovich M. and Harmon R.S. (eds), Clarendon Press, Oxford, 631-668.

[Lak96] Lakey B. and Krothes N. C. (1996). Stable isotopic variation of storm discharge from a perennial karst spring, Indiana. *Water Resources Research*, **32**, 721-731.

[Lam03] Lambert M.J. and Burnett W.C. (2003). Submarine groundwater discharge estimates at a Florida coastal site based on continuous radon measurements. *Biogeochemistry*, **66**, 55-73.

[Lan85] Langmuir D. and Reise A.C. (1985). The thermodynamic properties of radium. *Geochim. Cosmochim. Acta*, **49**, 1593-1601.

[Las80] Lambiase S. and Ruggiero A. (1980). La forra del Torano (Matese Centrale): un caso di convergenza fra morfogenesi carsica e fluviale. *Atti della Società Toscana di Scienze Naturali - Memorie*, Serie A Vol. LXXXVII, 171-192 (in Italian).

[Law05] Lawrence C. (2005). Measurement of $^{222}$Rn exhalation rates and $^{210}$Pb deposition rates in a tropical environment. *School of Physical and Chemical Sciences*, Queensland University of Technology, Brisbane, QLD.

[Lee87] Lee R. and Hollyday E.F. (1987). Radon measurement in streams to determine location and magnitude of ground-water seepage. In *Radon, radium, and other radioactivity in groundwater* (Graves B. (Ed.)), 241-249. Lewis Publishers, Inc. (Chelsea, Mich.).

[Lee91] Lee R. and Hollyday E.F. (1991). Use of radon measurements in Carters Creek, Maury County, Tennessee, to determine location and magnitude of groundwater seepage. In *Field studies of radon in rocks, soils and water*. (Gundersen, L.C. and Wanty, R.B. (Eds.)), 237-242, U. S. Geological Survey Bulletin.

[Lee06] Lee J.-M. and Kim G. (2006). A simple and rapid method for analyzing radon in coastal and ground waters using a radon-in-air monitor. *Journal of Environmental Radioactivity*, **89**, 219-228.

[Leo74] Leopold Luna B. (1974). Water: A Primer, San Francisco, W.H Freeman Co.

[Lev71] Levêque P.S., Maurin C., Severac I. (1971). Le $^{222}$Rn traceur naturel complementaire en hydrologie souterranie. *C. R. Hebd. Seances Acad. Sci.*, **272** (18), 2290.

[Lew24] Lewis W.K. and Whitman W.C. (1924). Principles of gas absorption. *Ind.Eng.Chem.*, **17**, 1215-1220.

[Lid63] Lindhard J., Scharff M. and Schiott H.E. (1963). Range concepts and heavy ion ranges. *Mat. Fys. Medd. Dan. Vid. Selsk.*, **33**, 14, 1-42.

[Lin08] Lindsay R., Newman R.T. and Speelman W.J. (2008). Astudy of airborne radon levels in Paarl Houses (South Africa) and associated source terms, using electret ion-chambers and gamma-ray spectrometry. *App. Radiat. Isotopes*.

[Lon08] Longobardi A. and Villani P. (2008). Baseflow index regionalization analysis in a Mediterranean environment and data scarcity context: role of the catchment permeability index. *Journal of Hydrology*, **355**, 63-75.

[Lou99] Loucks D. and Gladwell J. (1999). Sustainability criteria for water resource systems. Cambridge University Press.

[Lov08] Loveless A.M., Oldham C.E., Hancock G.J. (2008). Radium isotopes reveal seasonal groundwater inputs to Cockburn Sound, a marine embayment in Western Australia. *Journal of Hydrology*, **351**, 203-217.

[Low96a] Low R. (1996). Radon as a natural groundwater tracer in the Chalk aquifer, *UK Environment International*, **22**, S333-S338.

[Low96b] Low R. (1996). Radon in the groundwater in the Chalk of East Anglia. PhD Thesis, University of East Anglia, Norwich.

[Mag00] Margat J. and Vallée D. (2000). Water Resources and Uses in the Mediterranean Countries. Figures and Facts. *The Mediterranean in Figures. Blue Plan for the Mediterranean*. Regional Activity Centre, Sophia-Antipolis, France, 224 pp.

[Mah91] Mahoney J.J. and Langmuir D. (1991). Adsorption of Sr on kaolinite, illite, and montmorillonite at high ionic strengths. *Radiochim. Acta*, **54**, 139-144.

[Mal01] Malli G.L. (2001). Relativistic all-electron Dirac ± Fock calculations on $RnF_6$ and its ions. *J. Mol. Struct.*, **537**, 71-77.

[Man81] Manheim F.T. and Paull C.K. (1981). Patterns of ground water salinity changes in a deep continental-oceanic transect off the south-eastern Atlantic coast of the U.S.A. *J. Hydrol.*, **54**, 95-105.

[Mar79] Marine I.W. (1979). The use of naturally occurring helium to estimate groundwater velocities for studies of geologic storage of radioactive waste. *Water Resources and Research*, **15**, 1130-1136.

[Mak92] Markkanen M. and Arvela H. (1992). Radon emanation from soils. *Radiat. Prot. Dosim.*, **45**, 269-272.

[Mat88] Mathieu G.G., Biscaye P.E., Lupton R.A. and Hammond D.E. (1988). System for measurement of $^{222}$Rn at low levels in natural waters. *Health Physics*, **55**, 989-992.

[Mcd03] McDonnell I.J. (2003). Where does water go when it rains? Moving beyond the variable source area concept of rainfall-runoff response. *Hydrological Processes*, **17**, 1869-1875.

[Meg74] Megumi K. and Mamuri T. (1974). Emanation and exhalation of radon and thoron gases from soil particles. *J. Geophysical Res.*, **79**, 3357-3360.

[Men03] Menéndez M. and Pinero M.J. (Leaders) (2003). COMMON IMPLEMENTATION STRATEGY FOR THE WATER FRAMEWORK DIRECTIVE (2000/60/EC) - Guidance Document No 11 - Planning Processes Produced by Working Group 2.9 - Planning Processes, Office for Official Publications of the European Communities, Luxembourg: 2003 - ISBN 92-894-5614-0 - ISSN 1725-1087.

[MIAM05] MI.AM s.r.l. (2005). RAD ELEC E-PERM, Sistema per la Misura del Gas Radon, Manuale d'Uso. Via Borsa 17, Monza (MI), Italy (in Italian).

[Min83] Minell H. (1983). Gamma radiation and contents of K, U and Th in Swedish soils. *Geological Survey of Sweden*, Report **IRAP 83051**.

[Min90] Minell H. (1990). Natural radioactivity from different ground types, *Quaternary Economic Geology in the Nordic Countries*, Uppsala, **29**, 73-78.

[Mog77] Mogro-Campero A. and Fleischer R.L. (1977). Subterrestrial fluid convection: A hypothesis for long-distance migration of radon within the earth. *Earth Planet. Sci. Lett.*, **34**, 321-325.

[Moi00] Moise T., Starinsky A., Katz A. and Kolodny Y. (2000). Ra isotopes and Rn in brines and ground waters of the Jordan-Dead Sea Rift Valley: enrichment, retardation, and mixing. *Geochim. Cosmochim. Acta*, **64**, 2371-2388.

[Mon94] Monnin M., Morin J.P., Pane M.B., Seidel J.L. (1994). Radon-222 measurements in a fractured karst aquifer. In *Proc. of the Montpellier-Millau workshop*, European Commission, DC Science, Research and Development, Brussels, 81-91.

[Mon97] Monnin M. and Seidel J.L. (1997). Radon Measurement Techniques. In *Radon Measurements by etched track detectors. Applications in Radiation Protection, Earth Sciences and the Environment*, Durrani S.A. and Ilić R. (Eds.), World Scientific Publishing, ISBN: 981-02-2666-7.

[Mon98] Monnin M. (1998). A multidisciplinary global approach of groundwater flows in karstic areas and its consequences for water resources and environmental studies. Rept. ERB-CHRX-CT94-0567 European Commission DGXII- Brussels.

[Mon02] Monnin M. and Seidel J.-L. (2002). Radon concentrations in karstic aquifers. *Geofísica Internacional*, **41** (3), 265-270.

[Moo96] Moore W.S. (1996). Large ground water inputs to coastal waters revealed by $^{226}$Ra enrichments. *Nature*, **380**, 612-614.

[Moo98] Moore W.S. and Shaw T.J. (1998). Chemical signals from submarine fluid advection onto the continental shelf. *J. Geophys. Res.*, **103**, 21543-21552.

[Moo00] Moore W.S. (2000). Determining coastal mixing rates using radium isotopes. *Cont. Shelf Res.*, **20**, 1995-2007.

[Moo08] Moore W.S., Sarmiento J.L. and Key R.M. (2008). Submarine Groundwater Discharge Revealed by $^{228}$Ra Distribution in the Upper Atlantic Ocean. *Nature Geoscience*, **1**, 309-311.

[Mot98] Montgomery D.R. and Buffington J.M. (1998). Channel processes, classification, and response. In *River Ecology and Management* (Naiman R.J. and Bilby R.E., Eds.), Springer Verlag.

[Mud08] Mudd G.M. (2008). Radon sources and impacts: a review of mining and non-mining issues. *Rev. Environ. Sci. Biotechnol.*, **7**, 325-353.

[Mul07] Mullinger N.J., Binley A.M., Pates J.M. and Crook N.P. (2007). Radon in Chalk streams: Spatial and temporal variation of groundwater sources in the Pang and Lambourn catchments,UK. *Journal of Hydrology*, **339**, 172-182.

[Mut57] Muth H., Schraub A., Aurand K. and Hantke H.H. (1957). Measurements of normal radium burdens. *Br.J.Radiol.*, **7**, (suppl.)

[Nag94] Nagda N.L. (1994). Radon: prevalence, measurements, health risks and control. American Society for Testing and Materials, Philadelphia, PA, ISBN: 0-8031-2057-5.

[Nak08] Nakayama T. and Watanabe M. (2008). Missing role of groundwater in water and nutrient cycles in the shallow eutrophic Lake Kasumigaura, Japan. *Hydrological Processes*, **22**, 1150-1172.

[NAS99] NAS (1999). Health effects of exposure to radon (BEIR VI). National Academy Press, Washington DC, USA.

[NCRP87] National Council on Radiation Protection and Measurements (1987). Ionizing Radiation Exposure of the Population of the United States. NCRP Report **93**, Bethesda, MD.

[Ner89] Nero A. (1989). Earth, Air, Radon and Home. *Physics Today*, **42** (2), 32-39.

[Nic07] Nickolotsky A. and Pavlowsky R. (2007). Morphology of step-pools in a wilderness headwater stream: The importance of standardizing geomorphic measurements. *Geomorphology*, **83**, 294-306.

[Osm92] Osmond J.K. and Cowart J.B. (1992). Groundwater. In *Uranium-Series Disequilibrium: Applications to Earth, Marine and Environmental Sciences* (Ivanovich, M. and Harmon, R.S. (Eds.)). Clarendon Press, Oxford, 290-333.

[Pan95] Pane M.B. (1995). Le radon, traceur des circulations en milieu karstique. *C.R. Acad. Sci. Paris*, **340** (4), 37-45.

[Pan94] Pane M. B., Seidel J.-L., Monnin M. and Morin J.-P. (1994). Radon as a tracer of fluids motion in fractured aquifers. *Environ. Geochem. & Health*, **16**, suppl., 325-334.

[Par90] Parsa B. and Horton T. (1990). Radon-222 in drinking water: An NJDEP-EERF collaborative study. *Health Physics*, **58**, 209-212.

[Pat87] Patrick R., Ford E. and Quarles J. (1987). Groundwater contamination in the United States, University of Pennsylvania Press.

[Pay53] Payot R. (1953). Distribution de la radioactivité en Suisse. PhD thesis, University of Neuchâtel, Switzerland.

[Pen74] Peng T.-H., Takahashi T. and Broecker W.S. (1974). Surface radon measurements in the north Pacific Ocean station Papa. *J. Geophys. Res.*, **79**, 1772-1780.

[Per18] Perret H. (1918). Radioactivité des eaux neuchâteloises et Seelandaises. PhD thesis, University of Neuchâtel, Switzerland.

[Poh79] Pohl-Ruling J. and Fischer P. (1979). The dose-effect relationship of chromosome aberrations to alpha and gamma radioactivity. *Radiat. Res.*, **80**, 61-81.

[Por03] Porcelli D. and Swarzenski P.W. (2003). The Behavior of U- and Th-series Nuclides in Groundwater. *Reviews in Mineralogy and Geochemistry*, **52**, 317-361.

[Pos84] Porstendörfer J. (1984). Behavior of radon daughters products in indoor air. *Radiat. Prot. Dosim.*, **7**, 1-4, 107-113.

[Prc05] Pritchard J.L. (2005). Dynamics of stream and groundwater exchange using environmental tracers. PhD thesis, School of Chemistry, Physics and Earth Sciences, Faculty of Science and Engineering, Flinders University of South Australia.

[Pri77] Prichard H.M. and Gesell T.F. (1977). Rapid measurements of $^{222}$Rn concentrations in water with a commercial liquid scintillation counter. *Health Physics*, **33**, 577-581.

[Que05] Quevauviller Ph. (2005). Groundwater monitoring in the context of EU legislation: reality and integration needs. *J. Environ. Monit.*, **7**, 89-102, The Royal Society of Chemistry.

[Ram84] Rama and Moore W. S. (1984). Mechanism of transport of U-Th series radioisotopes from solids into ground water. *Geochim. Cosmochim. Acta*, **48**, 395-399.

[Ran92] Rank D., Volkl G., Maloszewski P. and Stichler W. (1992). Flow dynamics in an alpine karst massif studied by means of environmental isotopes. *Isotope Techniques in Water Resources Development*, IAEA Symposium 319, March 1991, Vienna, 327-343.

[Rea92] Reay W.G., Gallagher D.L. and Simmons G.M. (1992). Ground water discharge and its impact on surface water quality in a Chesapeake Bay inlet. *Water Res. Bull.*, **28**, 1121-1134.

[Ren80] Renoux A., Tymen G., Le Gac J. and Madeleine G. (1980). Study of the $^{222}$Rn short-lived daughters disequilibrium in mixed maritime and continental atmosphere near granitic soils. *Health Physics*, **39**, 291-298.

[Rob95] Robé M.C. and Labed V. (1995). Explaining the variation in soil radon concentrations: a study of the influence of some intrinsic properties of a rock matrix on the radon emission factor. In *Gas Chemistry* (ed. C. Dubois), *Science Reviews*, 535-542.

[Rog58] Rogers A. (1958). Physical behavior and geologic control of radon in mountain streams. *U.S. Geological Survey Bulletin*, **1052**-E.

[Ros94] Rosgen D.L. (1994). A Classification of Natural Rivers. *Catena*, **22**, 169-199.

[Ros96] Rosgen D.L. (1996). Applied River Morphology. *Wildland Hydrology*, Pagosa Springs, Colorado.

[Ros98] Rosgen D.L. (1998). Stream Classification Stream Guide. *Wildland Hydrology*, Pagosa Springs, Colorado.

[Ron18] Rona E. (1918). Diffusiongrösse and Atomdurchmesser der Radiumemanation. *Z. Physik Chem.* (Leipzig), **92**, 213-218.

[Rut83] Ruth P., Ford E. and Quarles J. (1983). Groundwater Contamination in the United States. University of Pennsylvania Press., Philadelphia, PA, USA. ISBN: 0-8122-8079-2.

[Sal03] Salih I. M. Musa (2003). Radon in Natural Waters. Analytical Methods; Correlation to Environmental Parameters; Radiation Dose Estimation; and GIS Applications. PhD thesis, Faculty of Health Sciences, Linköping University, Sweden.

[Scd60] Scheidegger A.E. (1960). *The Physics of Flow Through Porous Media*. University of Toronto Press, Toronto.

[Sch06] Schubert M., Buerkin W., Peña P., Lopez A.E., Balcázar M. (2006). On-site determination of the radon concentration in water samples: Methodical background and results from laboratory studies and a field-scale test. *Radiation Measurements*, **41**, 492-497.

[Sch07] Schubert M., Paschke A., Lau S., Geyer W. and Knöller K. (2007). Radon as a naturally occurring tracer for the assessment of residual NAPL contamination of aquifers. *Environmental Pollution*, **145**, 920-927.

[Sch08] Schubert M., Schmidt A., Paschke A., Lopez A. and Balcázar M. (2008). In situ determination of radon in surface water bodies by means of a hydrophobic membrane tubing. *Radiation Measurements*, **43**, 111-120.

[Scm07] Schmidt A. and Schubert M. (2007). Using radon-222 for tracing groundwater discharge into an open-pit mining lake - a case study. *Isotopes in Environmental and Health Studies*, **43** (4), 387-400.

[Scm08] Schmidt A., Stringer C.E., Haferkorn U. and Schubert M. (2008). Quantification of groundwater discharge into lakes using radon-222 as naturally occurring tracer. *Environmental Geology*, **56** (5), 855-863.

[Scr89] Schery S.D. and Whittlestone S. (1989). Desorption of radon at the earth's surface. *J. Geophys. Res.*, **94**, 297-303.

[Scw03] Schwartz M.C. (2003). Significant groundwater input to a coastal plain estuary: assessment from excess radon. *Estuarine Coastal and Shelf Science*, **56**, 31-42.

[Seg07] Segovia N., Gaso M.I. and Armienta M.A. (2007). Environmental radon studies in Mexico. *Environ. Geochem. Health*, **29**, 143-153.

[Sem87] Semprini L. (1987). Radon-222 concentration in groundwater from a test zone of a shallow alluvial aquifer in the Santa Clara Valley, California. In *Radon in Groundwater*, (Graves B., (Ed.)), Lewis Publishers, Chelsea, MI, 205-218.

[Sem00] Semprini L., Hopkins O.S. and Tasker B.R. (2000). Laboratory, Field and Modeling Studies of Radon-222 as a Natural Tracer for Monitoring NAPL Contamination. *Transport in Porous Media*, textbf38, 223-240.

[Sha01] Shah T., Molden D., Sahthiradelvel and Seckler D. (2001). The global situation of groundwater: overview of opportunities and challenges. *International Water Management Institute*.

[Shp84] Shapiro M.H., Rice A., Mendenhall M.H., Melvin D. and Tombrello T.A. (1984). Recognition of environmentally caused variations in radon time series. *Pure and Appl. Geophys.*, **122**, 309-326.

[Sim98] Simonovic S. (1998). Water resources engineering and sustainable development. *Proceedings of the XXVI Congress of Hydraulics* (Catania, Italy, 1998).

[Smi04] Smith L.A. (2004). Using Radon-222 as a tracer of mixing between surface and ground water in the Santa Fe river sink/rise system. Thesis presented to the graduate school of the University of Florida.

[Sol93] Solomon D.K., Schiff S.L., Poreda R.J. and Clarke W.B. (1993). A validation of the $^3H/^3He$ method for determining groundwater recharge. *Water Resources and Research*, **29** (9), 2851-2962.

[Sol95] Solomon D.K., Poreda R.J., Cook P.G. and Hunt A. (1995). Site characterization using $^3H/^3He$ groundwater ages (Cape Cod, MA.). *Ground Water*, **33**, 988-996.

[Sol97] Solomon D.K., Cook P.G. and Sanford W.E. (1997). Dissolved Gases in Subsurface Hydrology. In *Isotope Tracers in Catchment Hydrology* (Kendall C. and McDonnell J.J. (Eds.)), Elsevier, 291-318.

[Sop02] Sophocleous M. (2002). Interactions between groundwater and surface water: the state of the science. *Hydrogeology Journal*, **10**, 52-67.

[Sul71] Sultankhodzhaev A.N., Spiridonov A.I. and Tyminsij V. G. (1971). Underground water's radiogenic and radioactive gas ratios (He/Rn and Xe/Rn) in groundwaters and their utilization for groundwater age estimation. *Uzbek Geol. J.*, **5**, 41.

[Sur91] Surbeck H. and Medici F. (1991). Rn-222 transport from soil to karst caves by percolating water. In *Proc 22$^{nd}$ Congress of the IAH*, Aug.27-Sept.1, Lausanne, Switzerland. *Int. Ass. Of Hydrogeologists Memoires*, **XXII**, part 1, 348-355.

[Sur92] Surbeck H. (1992). Nature and extent of a 226Ra anomaly in the western Swiss Jura Mountains. In *Proc. 1992 Int. Symp. On Radon and Radon Reduction Technology*, EPA-Report EPA-600/R-93-0836, NTIS PB93-296202, U.S.EPA, Washington D.C., 8-19.

[Sur93] Surbeck H. (1993). Radon monitoring in soils and water. *Nucl. Tracks Radiat. Meas.*, **22**, 463-468.

[Sur94] Surbeck H. and Eisenlohr L. (1993). Radon as a tracer in hydrogeology: a case study. In *Gas geochemistry*, Dubois C. (Ed.), supplement to vol.16 of *Environmental Geochemistry and Health*, Science Review, Northwood, GB, 91-100.

[Sur96] Surbeck H. (1996). A radon-in-water monitor based on fast gas transport membranes. In *Proc. Int. Conf. Technologically enhanced natural radioactivity (TENR) caused by non-uranium mining*, October 16-19, Szczyrk, Poland.

[Sur00] Surbeck H. (2000). Alpha spectrometry sample preparation using selectively adsorbing thin films. *Applied Radiation and Isotopes*, **53**, 97-100.

[Sur05] Surbeck H. (2005). Dissolved gases as natural tracers in karst hydrology; radon and beyond. *UNESCO chair "Erdélyi Mihály School of Advanced Hydrogeology*, Budapest, Hungary, August 22-27, 2005.

[Stu01] Sturchio N.C., Banner J.L., Binz C.M., Heraty L.B. and Musgrove M. (2001). Radium chemistry of ground waters in Palaeozoic carbonate aquifers, mid-continent, USA. *Appl. Geochem.*, **16**, 109-122.

[Swa03] Swarzenski P.W., Porcelli D., Andersson P.S. and Smoak J.M. (2003). The behavior of U- and Th- series nuclides in the estuarine environment. *Rev. Mineral Geochem.*, **52**, 577-606.

[Tag06] Taniguchi M., Burnett W.C., Dulaiova H., Kontar E.A., Povinec P.P. and Moore W.S. (2006). Submarine groundwater discharge measured by seepage meters in sicilian coastal waters. *Continental Shelf Research*, **26**, 835-842.

[Tan64] Tanner A.B. (1964). Radon migration in the ground: A review. In Adams J.A.S. and Lowder W.M. (Eds.), *Proceedings of the International Symposium on the Natural Radiation Environment*, University of Chicago Press, Chicago, Il, USA, 161-190.

[Tan80] Tanner A.B. (1980). Radon migration in the ground: A supplementary review, *The Natural Radiation Environment III*, National Technical Information Service, Springfield, VA. CONF-780422, 5-56.

[Tan91] Tanner A.B. (1991). Error in measuring radon in soil gas by means of passive detectors. *Nucl. Geophys.*, **5**, 25-30.

[Tod96] Todini E. (1996). The ARNO rainfall-runoff model. *Journal of Hydrology*, **175**, 339-382.

[Tol69] Tolstikhin I.N. and Kamensky I.L. (1969). Determination of groundwater age by the T-$^3$He method. *Geochem. Int.*, **6**, 810-811.

[Tog90] Torgensen T., Benoit J. and Mackie D. (1990). Controls on groundwater Rn-222 concentrations in fractured rocks. *Geophys. Res. Lett.*, **17** (6), 845-848.

[Tor80] Torgerson T. (1980). Controls on pore-fluid concentration of $^4$He and $^{222}$Rn and the calculation of $^4$He/$^{222}$Rn ages. *J. Geochem. Explor.*, **13**, 57-75.

[Tul05] Tulipano L., Fidelibus D. and Panagopoulos A. (2005). COST Action 621 Groundwater management of coastal karstic aquifers, Final report.

[Tri00] Tricca A., Porcelli D. and Wasserburg G.J. (2000). Factors controlling the ground water transport of U, Th, Ra and Rn. *Proc. Indian Natl. Acad. Sci.*, **109**, 95-108.

[Tse08] Tse K.C. and Jiao J.J. (2008). Estimation of submarine groundwater discharge in Plover Cove, Tolo Harbour, Hong Kong by $^{222}$Rn. *Marine Chemistry*, **111**, 160-170.

[Tuc05] Tuccimei P., Salvati R., Capelli G., Delitala M.C. and Primavera P. (2005). Groundwater fluxes into a submerged sinkhole area, Central Italy, using radon and water chemistry. *Applied Geochemistry*, **20**, 1831-1847.

[Tuc08] Tuccimei P. and Soligo M. (2008). Correcting for $CO_2$ interference in soil radon flux measurements. *Radiation Measurements*, **43**, 102-105.

[UNS82] UNSCEAR (1982). Ionizing radiation: Sources and effects Annex D. *United Nations Scientific Committee on the Effect of Atomic Radiation.* United Nations publications.

[UNS94] UNSCEAR (1958-1994). A series of reports concerning the sources, effects and risks of ionizing radiation. *United Nations Scientific Committee on the Effects of Atomic Radiation reports to the General Assembly of the United Nations with annexes.* United Nations, New York

[UNS00] UNSCEAR (2000). Sources and effects of ionizing radiation. United Nations Scientific Committee on the effects of atomic radiation, New York, USA, UN Publication.

[Uzi81] Uzinov I., Steinhausler F., and Pohl E. (1981). Carcinogenic risk of exposure to radon daughters. *Health Phys.*, **41**, 807-813.

[Vee98] Veeger A.I. and Ruderman N.C. (1998). Hydrogeologic controls on radon-222 in a buried valleyfractured bedrock aquifer system. *Ground Water*, **36**, 596-604.

[Ver91] Vervier P. and Gibert J. (1991). Dynamics of surface water/groundwater ecotones in a karstic aquifer. *Freshwater Biol.*, **26** (2), 241-250.

[Ver92] Vervier P., Gibert J., Marmonier P. and Dole-Olivier M.J. (1992). Perspective on the permeability of the surface freshwater-groundwater ecotone. *J. No. Amer. Benth. Soc.*, **11** (1), 93-102.

[Ver93] Vervier P., Dobson M. and Pinay G. (1993). Role of interaction zones between surface and groundwaters in DOC transport and processing: Considerations for river restoration. *Freshwater Biol.*, **29** (2), 275-284.

[Vit91] Vitz E. (1991). Toward a standard method for determining waterborne radon. *Health Physics*, 60, 817-829.

[Vog92] Vogel R. M. and Kroll C.N. (1992). Regional geohydrologic-geomorphic relationships for the estimation of low-flow statistics, *Water Resources and Research*, **28** (9), 2451-2458.

[Von96] Von Gunten H.R., Surbeck H. and Rössler E. (1996). Uranium series disequilibrium and high thorium and radium enrichments in karst formations. *Environ. Sci. and Technol.*, **30**, 1268-1274.

[Wan90] Wanninkhof R., Mulholland P.J. and Elwood J.W. (1990). Gas-exchange rates for a 1st-order stream determined with deliberate and natural tracers. *Water Resources and Research*, **26** (7), 1621-1630.

[War77] Ward W.J., Fleischer R.L. and Mogro-Campero A. (1977). Barrier technique for separate measurement of radon isotopes. *Rev. Sci. Instr.* **48**, 1440-1441.

[Wei78] Weigel F. (1978). Radon. *Chemiker-Zeitung*, **102**, 287-299.

[Wel02] Weltner A., Mäleläinen I. and Arvela H. (2002). Radon Mapping Strategy in Finland. *International Congress Series*, **1225**, 63-69.

[Whi69] White W.B. (1969). Conceptual models for limestone aquifers. *Groundwater*, **7** (3), 15-21.

[Whi77] White W.B. (1977). Conceptual models for carbonate aquifers: revised. In *Hydrologic Problems in Karst Terrain* (Dilamarter, R. R. and Casallany, S. C. (Eds)), Western Kentucky University, Bowling Green, KY, 176-187.

[Whi88] White W.B. (1988). Geomorphology and hydrology of karst terrains. Oxford University Press, Oxford.

[Whi03] White W.B. (2003). Conceptual models for karstic aquifers. *Karst Modeling*,Special Publication **5**, (Palmer A.N., Palmer M.V., and Sasowsky I.D. (Eds.)), The Karst Waters Institute, Charles Town, West Virginia (USA), 11-16.

[Win95] Winter T. (1995). Management of groundwater and surface water. *Review of Geophysics*,Supplement, **33**.

[Win98] Winter T.C., Harvey J.W., Franke O.L. and Alley W.M. (1998). Ground Water and Surface Water: A Single Resource. *U.S. Geol. Surv.*, Circular **1139**.

[Woo04] Wood W.W., Kraemer T.F. and Shapiro A. (2004). Radon ($^{222}$Rn) in groundwater of fractured rocks: A diffusion/ion exchange model. *Ground Water*, **42**, 552-567.

[Wu04] Wu Y., Wen X. and Zhang Y. (2004). Analysis of the exchange of groundwater and river water by using Radon-222 in the middle Heihe Basin of northwestern China. *Environmental Geology*, **45**, 647-653.

[Yon91] Yoneda M., Inoue Y. and Takine N. (1991). Location of groundwater seepage points into a river by measurement of $^{222}$Rn concentration in water using activated charcoal passive collectors. *Journal of Hydrology*, **124**, 307-316.

[Yu02] Yu K.N., Koo V.S.Y., Guan Z.J. (2002). A simple and versatile $^{222}Rn/^{220}Rn$ exposure chamber. *Nuclear Instruments and Methods in Physics Research A*, **481**, 749-755.

[Zek05] Zekster S., Loáiciga H.A., Wolf J.T. (2005). Environmental impacts of groundwater overdraft: selected case studies in the southwestern United States. *Environmental Geology*, **47**, 396-404.

[Zuk87] Zukin J.G., Hammond D.E., Ku T.L. and Elders W.A. (1987). Uranium-thorium series radionuclides in brines and reservoir rocks from two deep geothermal boreholes in the Salton Sea Geothermal Field, southeastern California. *Geochim. Cosmochim. Acta*, **51**, 2719-2731.